EPSRC
Engineering and Physical Sciences Research Council

The University of Nottingham
UNITED KINGDOM · CHINA · MALAYSIA

THE DEVELOPMENT OF AN APOFERRITIN-BASED ARTIFICIAL METALLOENZYME FOR CATALYSIS OF SULFIDE OXIDATION

CAMILLE HOTEIT

Thesis submitted to the University of Nottingham

For the degree of Master of Philosophy in Biotechnology,

January 2018

TABLE OF CONTENTS

1. ABSTRACT

The development of artificial metalloenzymes is an expanding field, involving various protein scaffolds and incorporating a wide range of transition-metal catalysts. Due to its pH-dependent disassembling properties, apoferritin has been used extensively for various purposes. However, very few studies reported its use as a scaffold for the design of artificial metalloenzymes.

This study investigated the development of an apoferritin-based artificial metalloenzyme, based on covalent conjugation with a manganese-salen complex, applied to the catalysis of sulphide oxidation.

A mouse recombinant heavy-chain apoferritin mutant, containing a unique and reactive cysteine, in position 68, pointing towards its hollow core, was expressed and purified. A manganese-salen bearing a maleimide linker was synthesised and covalently linked to apoferritin's cysteine 68, via a Michael addition reaction.

The catalytic activity towards the enantioselective oxidation of thioanisole was assessed in both organic and aqueous media and has resulted in pH-dependent activity and enantioselectivity, with up to 69 % conversion and 17 % *ee*, due to the reassembling of the conjugated apoferritin nanocapsule.

However, background reactions exhibited high yields in certain conditions and the stability of the apoferritin-based artificial metalloenzyme was extremely relative at pH ranges where native apoferritin was supposed to be stable. Therefore, further research is recommended to improve three key features of this catalyst: stability, enantioselectivity and reactivity.

2. ACKNOWLEDGMENTS

I would like to express my gratitude to Dr. Anca Pordea and Prof. Neil R. Thomas for their supervision, their patience, and their wise advices during the realisation of this project over the past years.

I am grateful to Dr. Lei Zhang, Mr. Mick Cooper and Dr. Jed Long for the technical help and assistance they provided at different stages of this project.

I would like to thank Dr. Simone Morra, for being a mentor, and for all the interesting scientific discussions we had together. I also thank all the past and present members of the Pordea's group, Alanna, Mattias, Tim, Ricardo, Nafees and Floriane, also known as "Anca's boys", for the countless hours spent together in the lab, helping one another and for the constant mutual cheer up.

I am also grateful to all the members from the BECT group, especially Luca, Charlotte, and Andy, for all their help as well as for becoming a great group of friends.

I would like to address my special thanks to Juliana, for our constant discussions and drinks together and for her constant joviality, which made her become one of my greatest friends.

My thanks and love go to all my family, as despite being scattered between four countries, we always managed to stay a close team and to bring support to each other, as well as some of the most cultured discussions ever. In the same way, I would like to thank my second family, the "Ter-ter", Aurèle, Jérôme, Thiziri, Elsa and many more, for their friendship, their honesty, and their support.

I express all my gratitude to FIP, which brought the best music background I ever needed, always matching my mood and which revealed perfect to accompany any moments of my days and my nights.

I cannot finish without expressing all my gratitude, my love and my thanks to Zoe, for the unlimited support and care she brought me in these past years. I am looking forward to our next adventures together.

This thesis is dedicated to the memory of Ms Justine Moulin (1992-2015).

3. LIST OF ABBREVIATIONS

Aft	Apoferritin
BINOL	1,1'-bi-2-naphthol
BSA	Bovine serum albumin
CD	Circular dichroism
DCC	Dicyclohexylcarbodiimide
DIC	Diisopropylcarbodiimide
DIPEA	Diisopropylethylamine
DMAP	Dimethylaminopyridine
DMF	Dimethylformamide
DMSO	Dimethyl sulfoxide
DNA	Deoxyribonucleic acid
DTNB	5,5'-dithio-*bis*-(2-nitrobenzoic acid)
DTT	Dithiothreitol
EC	Enzyme classification
EDC	1-Ethyl-3-(3-dimethylaminopropyl)carbodiimide
EDTA	Ethylenediaminetetraacetic acid
ee	Enantiomeric excess
ESI	Electrospray ionization
GFP	Green fluorescent protein
H-chain	Heavy-chain
HOBt	Hydroxybenzotriazole

HPLC	High-performance liquid chromatography
HSA	Human serum albumin
ICP	Inductively coupled plasma
IMAC	Immobilized metal ion affinity chromatography
IPTG	Isopropyl β-D-1-thiogalactopyranoside
IR	Infrared
K_a	Association constant
K_M	Michaelis constant
LB	Lysogeny broth
LC	Liquid chromatography
L-chain	Light-chain
M	Metal
MALDI-TOF	Matrix assisted laser desorption ionisation - time of flight
min.	Minute
MRI	Magnetic resonance imaging
MS	Mass spectrometry
nbd	Norbornadiene
NHS	*N*-Hydroxysuccinimide
NMR	Nuclear magnetic resonance
OD	Optical density
PAGE	Polyacrylamide gel electrophoresis
PDB	Protein data bank
PMS	Phenyl methyl sulfide (thioanisole)

PMSO	Phenyl methyl sulfoxide
$PMSO_2$	Phenyl methyl sulfone
Sav	Streptavidin
SDS	Sodium dodecyl sulfate
SOC	Super optimal broth
TBHP	*tert*-butyl hydroperoxide
TCEP	*Tris*(2-carboxyethyl)phosphine
TFA	Trifluoroacetic acid
Tfr1	Transferrin 1
TNB	2-Nitro-5-thiobenzoic acid
TOF	Turnover frequency
t	Time of retention
UV	Ultraviolet
UV-Vis	Ultraviolet-visible
v/v	Volume/volume ratio
WT	Wild-type

4. INTRODUCTION

4.1 Artificial metalloenzymes

4.1.1 General concept

The term “enzyme” was coined in 1876 by Wilhelm Friedrich Kühne[10]. At the time, enzymes were thought to be a class of non-living organisms participating in chemical reactions, notably in the process of fermentation. Since then, the real characteristics, biological roles and structures of enzymes have been intensively studied. It is now understood that enzymes are protein biopolymers with a significant role in the catalysis of key reactions essential to create and sustain life. Despite the large scope of reactions enzymes are known to catalyse, many valuable catalytic transformations discovered by chemists are not covered by any known enzymes [8]. On the other hand, homogenous catalysis, based on transition-metal catalysts, has developed extensively in the past century, as an efficient approach to perform a wide range of synthetic reactions with high rates and selectivity. Similarly, the field of enzymatic catalysis has also progressed in the past two decades, albeit with a narrower application scope than organometallics catalysts. The two catalysis fields combined in recent years, leading to the creation of the field of artificial metalloenzymes.

Organometallic catalysts usually use a transition metal as catalyst, surrounded by an organic ligand which tune the rate of conversion and selectivity of the reaction catalysed. Transition metal catalysis covers a broad range of reactions and substrates thanks to the large variety of metal and ligands now available[11]. However, many of these reactions are performed in harsh conditions, often using non-sustainable organic solvents, which become less acceptable as the industry is increasingly following the path of a more sustainable society[12]. Nevertheless, exploring the versatility of organometallic catalysts towards more efficient reactions and environmentally friendly conditions has always been a driving force in the field. It is common to swap a transition metal for another, as well as to modify a ligand to tune the electronic configuration or the steric hindrance of a catalyst and thus enhance the selectivity of the reaction catalysed. However, given the relatively small size of ligands, only a limited amount of modification can be made. Moreover, these modifications were substrate-dependent and similar for a range of different transformations. This means that the range of modification available to improve activity and selectivity is relatively limited.

As opposed to organometallic catalysts, enzymes have evolved towards the catalysis of specific reactions. This evolution led to high conversions and high selectivity, but limited synthetic scope[13]. It is estimated that up to half of the known enzymes require a metal to catalyse reactions, although the range of transition metals utilized by enzymes is narrower than that of synthetic catalysts, as it is based on the abundance and availability of metal ions in biological environments[14]. Enzymes possess an active site which binds the substrate, modifies it according to the reaction process and then releases the product. This active site consists of a complex three dimensional environment made by the arrangement of residues, often from different chains and secondary structures, all precisely oriented via hydrogen bonds, hydrophobic and electrostatic interactions as well as steric hindrance, in order to bind a narrow range of substrate, as well as stabilizing the rate determining the transition state of the reaction catalysed[15]. As a result, the control over the reaction outcome is very tight. The downside of this scaffold is that enzymes are difficult to modify, as even a single mutation can lead to the partial or complete loss of protein structure and function. Furthermore, redesigning an enzyme to catalyse a reaction that is not naturally performed has often proven a massive challenge.

The concept of artificial metalloenzymes aims to “bring the best of two worlds”: the high specificity and high selectivity of enzymes with the large scope of substrate and reactions covered by organometallic catalysts[16].

The two main components of an artificial metalloenzyme scaffold are the first and second coordination sphere (Scheme 1). The first coordination sphere is composed of the atoms bound to the transition metal centre[17]. Depending on the scaffold, the first coordination sphere can be made of amino acid side chains from the apoenzyme, synthetic ligands, or solvent molecules. The first coordination sphere is responsible for the reactivity of the transition metal centre for a specific substrate and reaction, regardless the conditions of reactions[18]. A change in the atoms coordinated with the metal will tune its electronic properties, and thus will impact the activity and, on a lesser extent, the selectivity of a reaction.

The second coordination sphere defines the components of the ligands and any functionalities that interacts with the first coordination sphere and, preferentially, with the

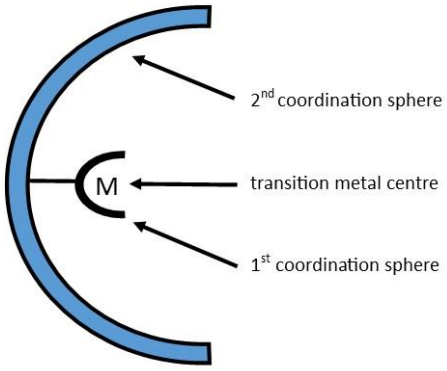

Scheme 1: Graphic representation of an artificial metalloenzyme. The transition-metal centre is directly coordinated with the first coordination sphere which tunes the metal reactivity. The second coordination sphere envelops the first and has a key role in the specificity and orientation of substrates, thus the selectivity of a reaction.

substrate rather than directly with the metal[19]. Second coordination sphere components can be different substituents of a ligand or additives and solvents present in the reaction, which will influence the selectivity of a reaction due to their tailoring of the spatial and functional arrangement around the catalytic site. In the case of artificial metalloenzymes, the second coordination sphere is provided by the protein scaffold surrounding the metal and ligand. The role of a protein scaffold as a second coordination sphere will be to create an environment which favours the reactivity of the transition-metal centre by controlling the hydrophobicity of the environment as well as orienting the substrate in the best way that would increase the reaction selectivity[17]. Protein active sites are highly interesting as second coordination spheres given the three-dimensional structure that characterizes them. With the assistance of structural knowledge, protein active sites can be modified to bind specific substrates and provide enantioselectivity to a specific range of reactions through mutagenesis.[20].

4.1.2 Types of second coordination spheres

To build artificial metalloenzymes, the first consideration is the selection of the biomolecular scaffold to use as a second coordination sphere. Generally, two types of scaffold have been used, either a protein or a nucleotide scaffold, the so-called “DNA-zymes” [8].

4.1.2.1 Oligonucleotides as second coordination sphere

Oligonucleotides are an attractive biomolecule for the building of artificial metalloenzymes. The deoxyribose-phosphate backbone is chiral and therefore brings selectivity to the reaction. Moreover, as DNA is composed of only four different nucleotides, engineering oligonucleotides has revealed to be less of a challenge than for proteins[21] and can mimic a protein active site. One of the primary examples was given by Roelfes *et al.* in 2005[1] where a salmon testes DNA strand was assembled with a non-chiral bidentate ligand coordinated to a Cu^{2+} centre to catalyse the Diels-Alder cycloaddition between azachalone and cyclopentadiene (Scheme 2). The enantioselectivity depended on the substrate but reached up to 90 % *ee*.

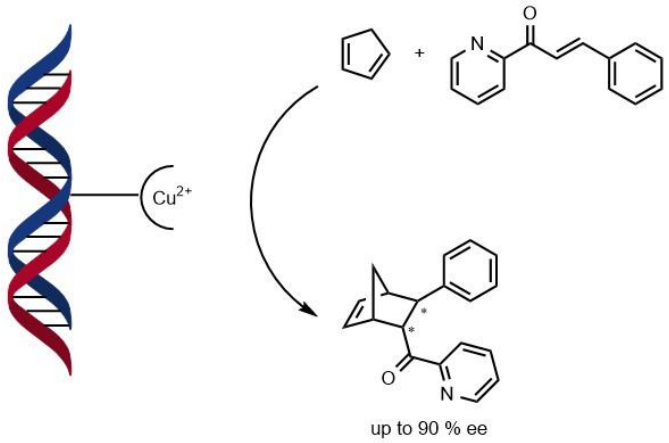

Scheme 2: Copper(II) DNA-based catalyst for the asymmetric Diels-Alder reaction as demonstrated by Roelfes et al.[1]

This work was later extended to several other asymmetric reactions, such as Michael addition[22], Friedel-crafts alkylation[23] and *syn* hydration[24]. Since then, the design of artificial metalloenzymes based on DNA scaffolds has become a growing field in biocatalysis[25]. Many examples can be cited, such as the incorporation of a bipyridine-Cu^{2+} catalyst in a DNA quadruplex scaffold for the asymmetric oxidation of sulfides[26]. A recent study described the incorporation of a heterobimetallic complex coordinated to Pt^{2+} and Cu^{2+} centres for the catalysed 1,3-dipolar cyclopropanation of azomethine ylides and maleimides[27]. DNA-based helical nanotubes coordinating various metals were shown to catalyse asymmetric Diels-Alder reaction, with high enantioselectivity (up to 91 % enantiomeric excess) [28]. These examples have proven that the enantioselectivity can be efficiently brought by a DNA strand, from single fragment to a helical nanotube. Whilst oligonucleotide-based artificial metalloenzymes

are out of the scope of this thesis, they are interesting competitors to protein-based artificial metalloenzymes, and an expanding fields, as RNA-zymes have also been reported[29].

4.1.2.2 Peptides and proteins as second coordination sphere

Peptides have also been used as a chassis for the creation of artificial metalloenzymes. Hayashi *et al*. reported the design of a diphosphine moiety bound to a single modified leucine to obtain a chiral palladium-diphosphine ligand for the catalysed asymmetric allylation of 2-acetylcyclohexanone, yielding an enantioselectivity of up to 52 % *ee*[30].

Since then, longer peptides have been used to bind transition-metal catalysts, mainly pioneered by Gilbertson's group [31], which exploits the different characteristics of protein secondary structure to create a three-dimensional environment, favouring selectivity and reactivity of the transition-metal centre, supplementing the chiral-inducing effect of residues. These were applied to the catalysis of asymmetric hydrogenation[31c] and allylic substitution[31b] (Scheme 3).

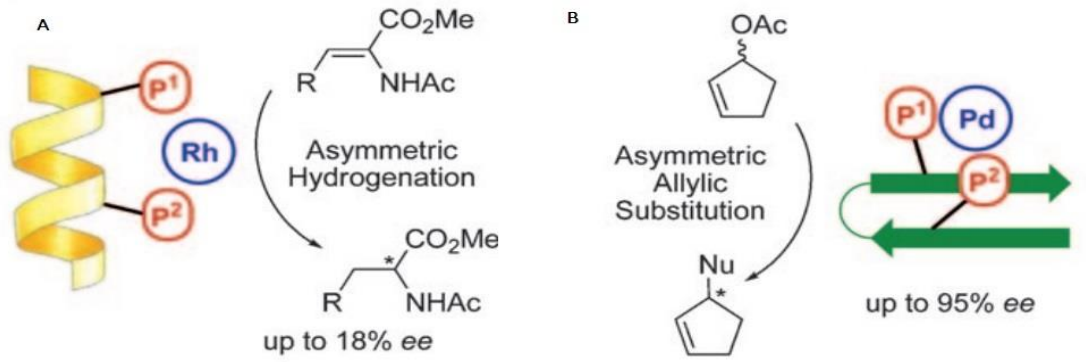

Scheme 3: Design of peptide-based organometallic catalyst. **A**. Use of an α-helix structure of the peptide to build a rhodium-artificial metalloenzymes for asymmetric hydrogenation. **B**. Two β-sheet serve as scaffold for the coordination of a palladium artificial metalloenzyme for asymmetric allylic substitution. Reproduced from Deuss et al.[8] with permission of the rightsholders (See Appendix 17 for permission of reproduction notice).

To address the challenges in the field of catalysis, the most used scaffold for the design of artificial metalloenzymes are proteins[20]. Proteins, notably enzymes, offer a wide range of binding pockets which can be used to orient the substrate and enhance the selectivity of the reaction. This can be improved or totally replaced by a synthetic or semi-synthetic active site which will host a metal-ligand complex as well as the substrate. Enzymes are also able to operate under mild and aqueous conditions, which makes them interesting candidates for the design of novel catalysts. This literature review will describe some of the most studied

proteins used to build artificial metalloenzymes, with the aim to give an idea of the current state of the field.

A representative example is the research of Arnold's group, which focuses on redesigning the function of cytochrome P450s. These are part of a well-known family of haem-dependent enzymes, involved in a wide range of oxidation reactions with dioxygen as terminal oxidant and NADPH as electron source[32]. Cytochrome P450s are present in almost every living organisms, usually in several different forms across different tissues of a same complex organism. For instance, the hydroxylation of naphthalene using a cytochrome P450 variant, $P450_{cam}$ from *Pseudomonas putida*, was proven[33]. This work was then applied to linear alkanes using another family member, P450 BM3 from *Bacillus megaterium*, with enantioselectivity, up to 55 % *ee*, and high rate of conversion, up to 400 min^{-1}[34].

Cytochrome P450s have also been used for diverse other reactions,[35] such as carbene and nitrene transfers,[36] applied to olefin cyclopropanation[37]. Hartwig's group has focused on building artificial metalloenzymes with cytochrome P450[38]. For instance, the catalysis of the intramolecular amination of a C-H bond from a sulfonyl azide by a cytochrome P450 CYP119 provided up to 98 % yield and 95 % *ee*[39].

Metal-porphyrinoids have been used with proteins other than haem-binding ones. For example, the ability of serum albumins to bind organic molecules in their hydrophobic pockets was exploited by Reetz *et al.*, who used BSA to bind Cu^{II}-phthalocyanine, a porphyrin-like derivative, to catalyse the Diels-Alder reaction between azachalone and cyclopentadiene. This scaffold yielded a high conversion rate, up to 80 % and high enantioselectivity, up to 93 % *ee*. Another study showed a multi-vanadium complex inserted within the BSA's binding pocket, to catalyse the oxidation of sulfides with excellent asymmetric catalytic properties with up to 93 % conversion and 98 % *ee*[40]. It was also reported that the insertion of a manganese(III) salophen complex within bovine serum albumin turned the protein into a superoxide dismutase with higher rates than the metal complex alone[41]. This was due to the hydrophobicity of the protein's binding pocket which promoted higher reactivity of the metal-complex than an aqueous environment.

Streptavidin, and the well-studied biotin-streptavidin complex have also been used as scaffold for the design of artificial metalloenzymes, due to the excellent affinity of streptavidin for biotin (Figure 1). A biotinylated rhodium-based catalyst for the catalytic hydrogenation of acetamidoacrylic acid was developed, with enantioselectivity up to 96 % *ee*, thanks to the chirality brought by residues' side chains and the steric hindrance given by streptavidin's binding pocket[42]. This system has also been designed for direct coordination with vanadium oxide[43] or the incorporation of manganese-salens[44] for the catalysis of sulfide oxidation.

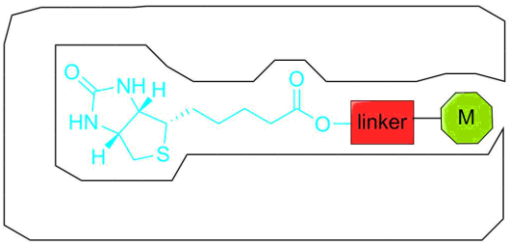

Figure 1: Artificial metalloenzymes based on streptavidin-biotin system. A linker is bound to biotin, which leads to a metal and its ligand, exploiting streptavidin binding pocket to bring selectivity to the reaction catalysed.

Another scaffold used frequently is carbonic anhydrase, which is a zinc metalloenzyme catalysing the hydration of carbon dioxide to yield bicarbonate. Substituting the zinc by a manganese led to peroxidase activity[45]. This scaffold catalysed the oxidation of *o*-dianisidine in mild conditions, as well as the asymmetric epoxidation of *p*-chlorostyrene with good enantioselectivity, 67 % *ee*. However, in both cases, the conversion and rates were low.

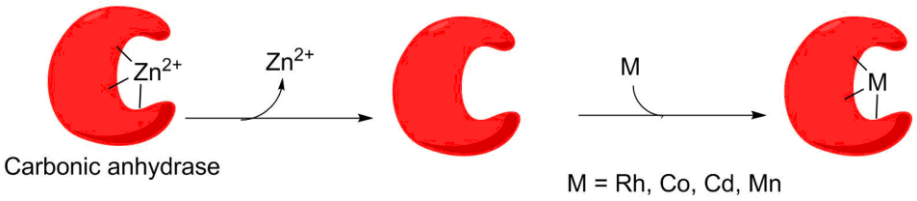

Scheme 4: Metal-substitution in carbonic anhydrase. This changes the range of reaction catalysed as well as the selectivity and reactivity of the whole scaffold, turning the carbonic anhydrase into an artificial metalloenzyme.

Mutagenesis of the key residues present in the metal binding site yielded an even lower catalytic activity, as well as poor binding of the metal, showing once more the importance of the design of the protein active site when building an artificial metalloenzyme. Ever since, much attention was given to the substitution of the natural zinc with several other metals, such as copper, cobalt, cadmium and rhodium each changing the kinetic and selectivity of the reactions catalysed (Scheme 4)[46].

Building an exhaustive list of the proteins used as scaffolds for the design of artificial metalloenzymes is beyond the scope of this literature review. Nonetheless, very interesting reviews by key leaders the field have been recently published and offer a more detailed insight into the field [47].

4.1.3 Strategies for the design of artificial metalloenzymes

Three strategies were developed for the anchoring of a transition metal centre into a biological scaffold (Figure 2). The non-covalent approaches are composed of dative anchoring and supramolecular anchoring. For both, the key parameter is a high affinity of the biological scaffold's binding site with the ligand or the metal. These approaches have an advantage over the third approach, the covalent conjugation, as protein and substrate can be simply mixed to complex them together, without the need of undergoing supplementary reactive steps as needed for covalent conjugation [8].

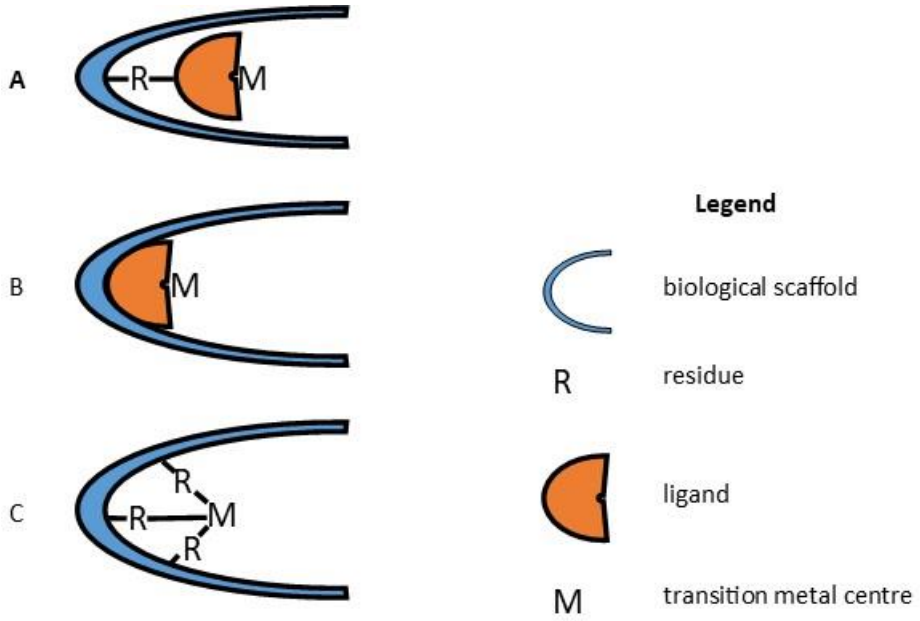

Figure 2: Graphic representation of the three strategies for anchoring a metal complex into a biological scaffold. **A**. Covalent approach, one or several residues covalently bind to the ligand which coordinates to the metal centre. **B**. Supramolecular interactions, the ligand has a high affinity for its host through hydrogen bond, electrostatic and hydrophobic interaction and is coordinated to the metal centre. **C**. Dative anchoring, the metal centre is directly coordinated with its biological host, via the residues' side chains.

4.1.3.1 Dative anchoring

Dative anchoring involves the direct coordination of the transition metal centre to its host. Taking the case of a protein scaffold as the main example, residues' side chains would directly bind the transition metal (Figure 2C). This approach stemmed from Kaiser's group's work, when the zinc centre, contained within a carboxypeptidase A was replaced by a copper(II)

centre[48]. Whilst the native protein displayed peptidase and esterase activity, the Cu(II)-modified protein was found to catalyse the oxidation of ascorbic acid. Dative anchoring was, for example, used by Kazlauskas, to insert a rhodium into carbonic anhydrase (Scheme 4)[45]. This work showed that metal substitution could drastically change an enzyme role, however, utmost care must be taken with the modification of the binding site. The rhodium-carbonic anhydrase was able to catalyse the epoxidation of activated olefins with low enantioselectivity, up to 12 %. The selectivity of the reaction was decreased by mutating key residues in the binding site[45].

This led to researchers inserting transition-metal centres within proteins which do not possess a binding site for metals. For instance, a rhodium complex was inserted within human serum albumin[49] and with papain[50] resulting in catalytic hydroformylation of styrene and 1-octene. Whilst the hydroformylation of 1-octene exhibited a yield close to none, the same reaction with styrene was performed with very high conversion, up to 98 % with the modified albumin.

4.1.3.2 Supramolecular anchoring

Supramolecular anchoring is based on the non-covalent interaction of the ligand with its biological host through hydrogen bonds as well as electrostatic and hydrophobic interactions (Figure 2B). One of the most known examples is the biotin-streptavidin complex, as described previously (Figure 1). Streptavidin possesses an extremely high affinity for biotin ($K_a = 10^{15}$ M^{-1}) and their association is considered as irreversible [8]. Wilson and Whitesides were the first to report the modification of biotin with a rhodium-diphosphine ligand and its incorporation into streptavidin for the catalysed asymmetric transfer hydrogenation of amino acid precursors with excellent enantioselectivity, up to 98 % *ee*[51]. Other examples account for the incorporation of manganese-porphyrin derivatives within human serum albumin binding pocket for the asymmetric oxidation of thioanisole[52]. Modifications of the porphyrin's substituents made it more hydrophilic which increased its affinity for its host binding pocket, resulting in an enantioselective reaction displaying up to 74 % *ee*[53]. Supramolecular anchoring gives the opportunity to optimize the binding sites by simply mutating few residues without needing a supplementary step for the anchoring of the ligand.

4.1.3.3 Covalent conjugation

Covalent conjugation is based on the covalent binding of the metal complex to the biological host (Figure 2A). When proteins are used, one or two key nucleophilic residues will bind to

the ligand coordinating with the metal through an electrophilic reaction partner. The main advantage of using covalent conjugation is that only one or two residues need to be mutated to offer an anchoring point to the ligand, decreasing the probability of harming the protein's and the binding site's structure than redesigning an entire binding pocket. Nonetheless, covalent conjugation requires an extra step to be performed in order to covalently attach the ligand to the protein, this also needs specific conditions which can be limited by the protein and the ligands resistance to temperature and pH as well as solubility in specific buffer. Adding an extra step also limits the preparation of such artificial metalloenzyme on large scales.

As an example, phosphinate-based platinum complexes were covalently conjugated with a cutinase, a serine esterase, through binding with its Ser120 residue[54]. The binding was made through an ester coupling reaction between the terminal carboxylic acid of the ligand and the hydroxyl group from Ser120. Successful binding was shown and complete inhibition of the natural activity of the cutinase was measured. The same work was then extended to other serine hydrolases, such as lipase, although this time some metal complex were replaced by fluorescent probes to measure the kinetics and efficiency of the binding of the ligand[55].

Lysine, via its terminal primary amine, has also been used as a covalent conjugation point. *Escherichia coli* tryptophan gene repressor's DNA-binding domain was modified for covalent conjugation[56]. A 1,10-phenanthroline-copper complex was bound to the protein using an iminothiolane as linker, which binds to lysine residues. This operation led to a change in the protein's role, which became an endonuclease.

Another example used lysine and cysteine to bind an iron-complex to a σ^{70} protein, a transcription initiation factor. Through nucleophilic substitution, the thiol from the cysteine and the primary amine from the lysine from σ^{70} protein managed to covalently bind the iron complex[57].

The most used covalent conjugation method to date, when proteins are used as biological scaffolds, is cysteine modification. Displaying a terminal thiol on its side chain, cysteine possesses unique abilities to covalently bind to electrophilic moieties (Scheme 5). Thiols are mostly nucleophile between pH 7 and 8.5[58], where amines are still in their ammonium form, this avoids undesired covalent conjugation with residues bearing amines on their side chains, such as lysine and arginine.

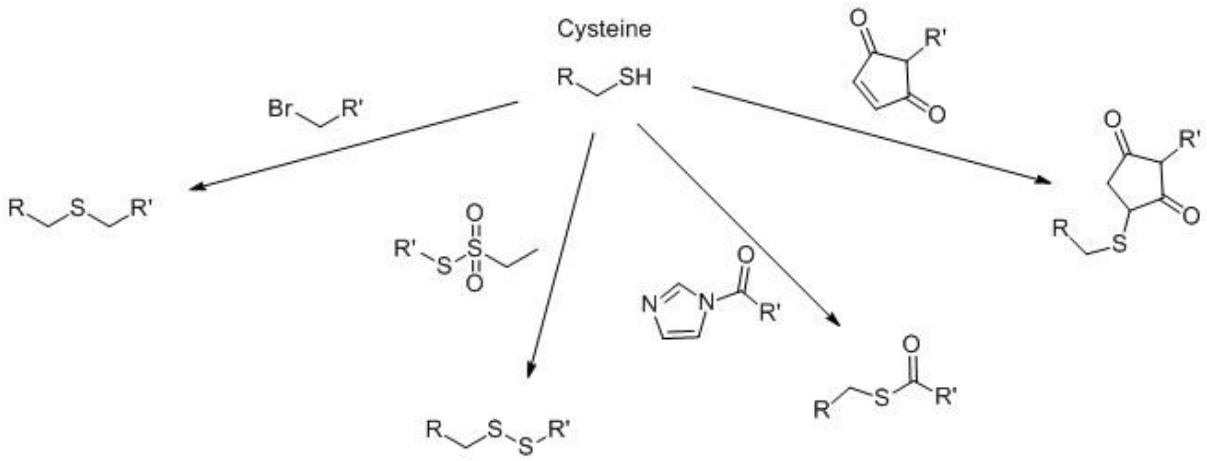

Scheme 5: The different methods of cysteine covalent modifications.

The first method is by nucleophilic substitution, when the ligand bears a halogenic compound such as bromine or iodine (Scheme 5). Using this feature, a copper-phenanthroline complex was covalently conjugated to the hydrophobic binding pocket of LmrR, a transcription factor[59]. In that purpose, a cysteine was mutated in position 89, to give M89C, in order to avoid disruption of the binding pocket structure as well as disruption of the protein's natural function. This scaffold catalysed the asymmetric hydration of α,β-unsaturated-2-acylpyridine with conversion and enantioselectivity rising up to 80 % and 84 % *ee*, respectively.

Cysteines can also bind to thiosulfonate by elimination of the sulfone and forming a disulfide bridge with the remaining sulfide. This method was used for the dual-anchoring of a manganese salen complex within apomyoglobin binding pocket through alkylation of two specifically mutated cysteines[60]. However, the downside of forming a disulfide bridges is that they can easily be reduced by reducing agents, often used in buffers, such as dithiothreitol, β-mercaptoethanol and TCEP, or undergo thiol exchange.

Nucleophilic addition of a cysteine with a carbonyldiimidazole was showed for the first time by Kamer's group[61]. At pH 8.0, thiols are highly nucleophilic, more than amines. Therefore, after reduction of the photoactive yellow protein Cys69 by DTT, the thiol bound to the carbonyl linking with a palladium-phosphine ligand. This scaffold was applied to the asymmetric allylic substitution of 1,3-diphenyl-2-propenyl acetate with benzylamine with a conversion up to 90 %. However, the enantioselectivity of the reaction was not reported. It was stated that previous attempt at covalently conjugate phosphines ligands have led to poor enantioselectivity [62].

Maleimides are Michael acceptors, which, when reacting with thiols, form a thiosuccinimide bond (Scheme 5). The first example of a cysteine-maleimide reaction was published in 1956 by Moore and Ward, where they demonstrated the cross-linking of two proteins[63]. Ever since, the method has been extensively studied and used for diverse purposes[64]. Maleimide-thiol coupling is now one of the most used techniques for chemical modifications of a protein as it occurs in very mild conditions such as physiological pH and room temperature in water. This method has been used for the covalent binding of antibody-drug conjugates[65], modification of peptide for the building of peptide-based artificial metalloenzymes[66] as well as the PEGylation of bovine serum albumin[67].

Thiosuccinimide bonds are highly stable, thanks to the succinimide ring opening upon thiol addition (Scheme 6)[68], which prevents any thiol exchange. This ring opening was accelerated when *N*-substituents had electron-withdrawing properties, making them more prone to react with water[69].

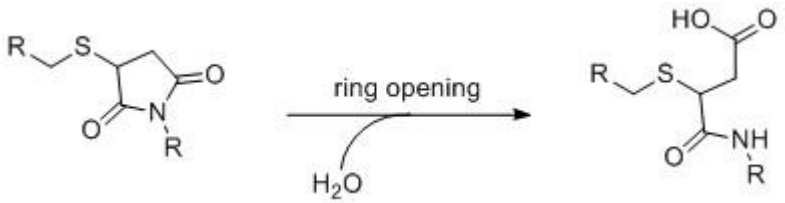

Scheme 6: Ring opening hydrolysis of thiosuccinimide once the Michael addition of cysteine's thiol on a maleimide has occurred. This process is accelerated when N-substituents are electron-withdrawing components.

Reetz's group showed the covalent conjugation of a manganese-salen complex through Michael addition of papain's cysteine on the maleimide moiety added to the metal-complex salen and reported its use on the epoxidation of olefins[70]. Maleimide-based covalent conjugation to papain was studied [71]. A rhodium-bipyridine ligand bearing a maleimide linker was successfully conjugated with papain. This led to the inhibition of papain natural activity and the scaffold was assessed for the catalytic asymmetric hydrogenation of trifluoroacetophenone. However, yields and enantioselectivity remained very low.

In the same spirit, a manganese-terpyridine complex bearing a maleimide linker was covalently conjugated with tHisF, an imidazole glycerol phosphate synthetase involved in the endogenous synthesis of histidine, and apo-nitrobindin, a haem-protein involved in nitric oxide transport[72]. As less than half of tHisF was conjugated, the researchers carried on

working with the apo-nitrobindin conjugate and subjected to the catalytic oxidation of diverse benzylic substrates with a conversion up to 99 %.

The covalent conjugation of rhodium-phosphine and ruthenium-phenanthroline complexes to a photoactive yellow protein and ALB protein, BSA's precursor, through Michael addition with a cysteine residue using a maleimide linker, were investigated by Kamer *et al.* [73]. Whilst the catalytic activity of these constructs was not reported, much attention was given to structural characterisation to prove the conjugation indeed happened in both cases. This work was further developed to optimize and standardize the covalent conjugation of metal-phosphine complexes through Michael addition of a protein's cysteine on a maleimide-linker[74]. These examples proved that maleimide is a valuable linker for the covalent conjugation of a biological host with an organometallic complex.

4.2 Apoferritin

4.2.1 Biological role and characteristics

Ferritin is a spherical-shell shaped protein displaying an important role in the long-term storage of iron ions. Without iron stored within the protein, ferritin is named apoferritin. It is expressed in all eukaryotic and prokaryotic organisms. In most of them, several copies of the gene coding for apoferritin are present across the genome to maintain a steady level of expression.

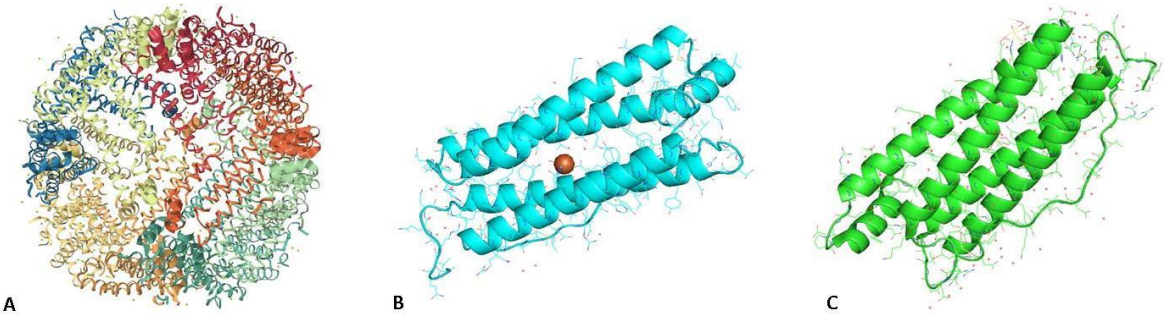

Figure 3: A. Three-dimensional structure of human H-ferritin 24 sub-units reassembled as apoferritin capsule; PDB 3AJO[2]. B. Three-dimensional structure of human H-chain with one iron atom (orange sphere) bound in the 4-helixes channel; PDB 1FHA)[7]. C. Three-dimensional structure of human L-chain; PDB 2FG4).

Apoferritin is composed of 24 sub-units forming a spherical nanocapsule of 12 nm outer diameter and an 8 nm diameter hollow core hosting up to 4000 iron atoms (Figure 3A). The protein is composed of two different sub-units, the heavy (H) and the light (L) chains (Figure 3B-C) possessing the same secondary structure distribution. The main differences between the two chains are their role and their sturdiness. Whilst heavy chains display a ferroxidase activity, involved in Ferritin's natural role of iron-storage, light chains mediate the electron transfer necessary for the ferroxidase activity of the protein[75]. In terms of sturdiness, light chains are composed of more hydrophilic residues along their channels than heavy-chains, as well as being more resistant to thermal denaturation and to pH, due to a salt bridge between two residues of a same sub-unit but different secondary structure, Lys62 and Glu107 [76]. Most of the residue of both chain types are involved in a 5 α-helixes pattern, 4 antiparallel forming a 4-fold channel and one short helix sitting at a 60 ° angle from the 4-fold channel[77]. Upon reassembly of the apoferritin nanocapsule, sub-units tend to dimerize[78]. Dimers are the first step of reassembly and are known to be very stable in solution. Along with an increase in pH, apoferritin reassemble until each sub-units interacts with five others, through interactions between their respective α-helixes, in order to form the fully reassembled nanocapsule[79].

The iron storage by apoferritin is considered as a two steps process [80]. Firstly, Fe^{II} diffuses inside the protein through either a 4-fold channel or a 3-fold channel. Whilst the 4-fold channel is mainly made of leucine, rendering it hydrophobic, the 3-fold channel is mainly composed of glutamate and aspartate residues, making it more hydrophilic than the former, leading to a faster diffusion of Fe^{II}, taking less than 3 ms[81]. It is important to note that these channels only let molecules less than a diameter of 6 Å[82] pass through, roughly the size of sucrose, which means that iron cannot diffuse through apoferritin's pores if complexed with most natural chelators.

Secondly, Fe^{II} reaches the ferroxidase site, only presents in H-chain sub-units. This site is composed of several glutamate (E27, E58, E103) and histidine (H54, H61) residues which coordinates with two iron ions, stabilized by one to three water molecules[83]. In addition to Fe^{II}, O_2 and H_2O_2 could diffuse as well and would act as oxidant within the ferroxidase site to form Fe^{III}. This is called the mineralization process and justifies apoferritin's place in the enzyme classification as an oxidoreductase [EC 1.16.3.1][84] (Scheme 7). In presence of water and dioxygen, Fe^{II} will form a hydrated diferric-oxo complex, thus releasing hydrogen peroxide in the process. The hydrolysis of such complex will lead to the formation of ferric-peroxo complex [85] which is released within the nanocage and is easily stored with little leakage due to is poor water solubility[80].

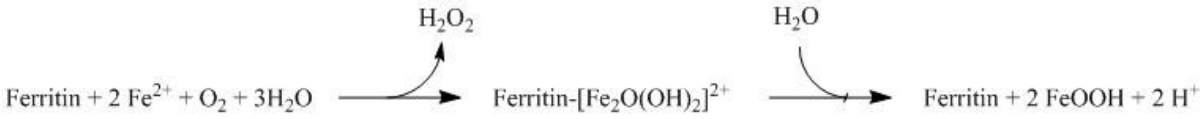

Scheme 7: Iron oxidation pathway for uptake into ferritin. First, Fe^{II} enters H-chain of Ferritin to bind glutamate and glutamine residues and then undergoes oxidation leading to its complexation into ferroxidase complex and binding to H-chain. The ferroxidase complex undergoes hydrolysis and is released into Ferritin's core as FeOOH.

The more hydrophilic residue composition of L-chains and their lack of ferroxidase site render the binding of iron slower but promote the nucleation and long-term storage of Fe^{III} through a more impermeable structure. Moreover, L-chain rich ferritins are known to be structurally more stable against chemical and heat denaturation, up to pH 8.5-9 and 85 °C making them more suitable for long-term and safe storage of iron in cells [86]. H-chain are involved in iron uptake and oxidation to promote its mineralization and, ultimately, its storage.

When iron release is needed for sustaining metabolic pathways, ferritin associates with membrane-bound ferric reductase [EC 1.16.1.7] to reduce Fe^{III} to Fe^{II} for porphyrin-complexation or exocytosis via transferrin, leaving ferritin as apoferritin, which will bind to the cell membrane for uptake of more iron[87].

One of the most interesting features of apoferritin is its pH-dependent assembling. Between pH 6 and pH 10.6, apoferritin is fully folded as a 24-mer stable nanocapsule whilst it slowly disassembles from pH 6 to pH 3, releasing sub-units[88]. Above pH 10.6 and under pH 2.8, the sub-units tend to aggregate [89]. Whilst this process has not much use for biological purpose, as the protein will be fully reassembled at physiological pH, it has been widely used to enlarge the scope of application for apoferritin, notably in the field of nanomedicine [5].

4.2.2 Targeted drug delivery and biocompatibility

One of the most known application of apoferritin is its pH-dependent reassembling which made apoferritin an attractive delivery system for various compounds (Figure 4), notably for drugs [90]. It was shown that disassembling the protein at pH 2-3 and then reassembling it at pH 7-8 in solution with a water-soluble drug would encapsulate several copies of the corresponding drugs[91].The aim for encapsulating drugs was to improve their therapeutic

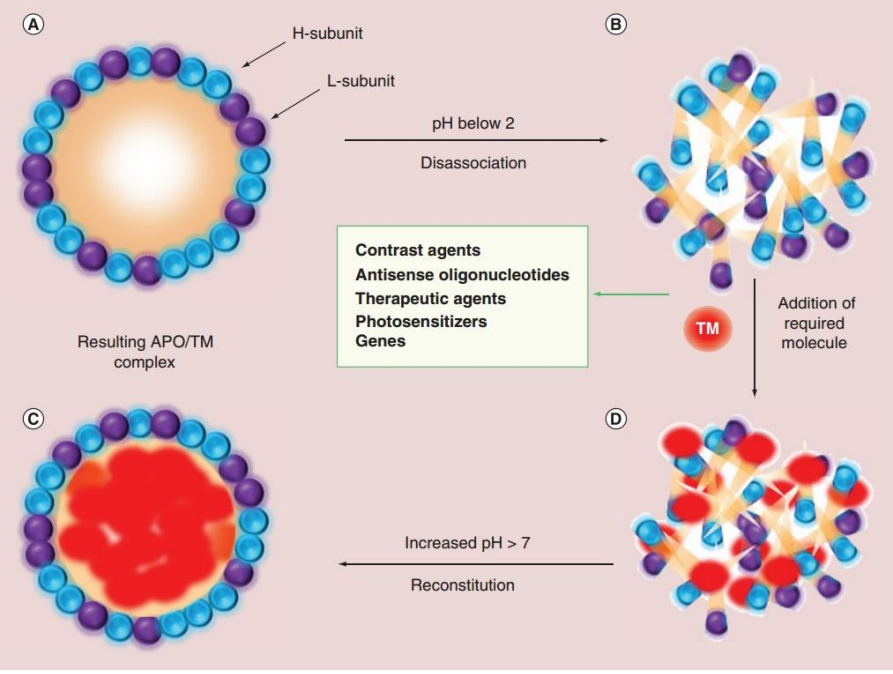

Figure 4: Model encapsulation of diverse compounds of medical interest within apoferritin hollow core through pH-dependent reconstitution. Reproduced from Heger *et al.*, 2014[5] with permission of the rightsholders (See Appendix 17 for permission of reproduction notice).

index as well as mitigating undesirable toxic effects, as the capsule would protect the drug from unwanted interactions with non-targeted tissues, but would also enhance the solubility of several drugs in the plasma. It was also shown that small hydrophobic drugs, such as Gefitinib®, could be encapsulated by diffusion through the hydrophobic channels[92]. Several other kind of drugs were encapsulated within apoferritin such as cisplatin and carboplatin, which helped reducing their non-specific toxicity[93].

Ever since, the concept of drug encapsulation was improved through biochemical and chemical modifications of apoferritin. The genetic fusion of apoferritin's coding gene with a gene coding for a 40 to 75 residues peptide, rich in proline, alanine and serine, showed reduced leakage as well as improvement of the half-life of apoferritin-doxorubicin complex's half-life in the bloodstream[94]. The same concept was developed using RGD4C peptides genetically fused to the surface of the protein to enhance its circulation half-life[95].

Most of the development has been directed towards targeting of apoferritin to specific tissues, which allows the delivery of drugs to various tissues[96], besides apoferritin natural targeting to Tfr1, Transferrin 1, the most favoured receptor involved in iron homeostasis across living organisms and displays a high affinity for ferritin[97], and Scara5, a scavenger receptor involved in the non-transferrin iron-uptake pathway which binds preferentially L-chain rich ferritin[98].

Apoferritin was covalently conjugated with antibodies for targeted delivery of doxorubicin to prostate cancer cells with high specificity of targeting as well as up to 90 % cytotoxicity on the targeted cells[99]. It was also shown that the RGD4C peptide had targeting properties to specifically bind integrins which are upregulated on tumour vasculature, leading to better tumour growth inhibition in C32 melanoma cells *in vitro*[100]. Apoferritin was also modified through a biotin-streptavidin system to conjugate with magnetic particles on its surface, leading to transport mediated by a magnetic field [101].

Whilst biocompatibility of apoferritin has been demonstrated[102], the use of horse spleen apoferritin has been criticized for its potential risk on humans, due to the difference of glycosylation which could potentially trigger an immune reaction upon release in the human system[103].

4.2.3 Application in nanotechnologies

Besides drug encapsulation, the apoferritin capsule, possessing targeting moieties, has been applied to numerous purposes. For example, it was used for the encapsulation and targeting of magnetic resonance imaging (MRI) contrast agents. Gadolinium (III), as one of them, was encapsulated into apoferritin to obtain higher relaxation of water protons within the protein cavity [104]. Apoferritin was also modified on its surface to enhance bloodstream half-life and to be targeted to tumours. Storage of gadolinium in its inner cavity allowed to achieve efficient detection without causing any serious side effect[105]. Manganese (II)-loaded apoferritin was used for the same purpose. With around 1000 manganese atoms encapsulated, apoferritin was targeted to hepatoma cells and taken up through its natural receptor Scara5 for visualization of lesions which were not always visible with gadolinium-loaded apoferritin[106]. This study was successful on different cancer cell lines as well[107].

Photodynamic therapy is another example where apoferritin was used as a delivery vector for encapsulated quantum dots. Lead-sulfur-based quantum dots were synthesized within the protein cavity[108] and such scaffold was found to induce low toxicity to cells when inactivated, whilst activation of the quantum dots lead to high cytotoxic effects on carcinoma cell lines with a cellular uptake mediated by TfR1, apoferritin natural receptor[102]. Up to 1 mg/mL of apoferritin-PbS nanoparticle concentration, it was also demonstrated that non-tumorigenic cells were not altered whilst breast cancer cell lines suffered apoptotic cell death in the same conditions, rendering this scaffold safe for medical and *in vivo* imaging applications[109].

Apoferritin has also been developed as a probe. Apoferritin nanocapsule was genetically fused to S175C GFP, rendering it fluorescent, which allowed chemical conjugation to DNA aptamer through GFP's cysteine. Such DNA-aptamers allowed the nanoparticle to bind cancer markers in phosphate buffer and diluted human serum. The DNA-GFP-apoferritin scaffold displayed enhanced sensitivity to cancer markers compared to the DNA-GFP scaffold [110]. This work was inspired by the encapsulation of iron marker hexacyanoferrate(III) and of the fluorescent marker fluorescein within apoferritin's cavity, whilst targeting was insured by a chemical modification on the protein's surface with DNA probe[111]. It was shown that the limit of detection of this scaffold was directly correlated with the quantity of marker molecules loaded inside apoferritin[112].

Besides its applications to the medical field, apoferritin has been used as an immobilization biomaterial to mimic silica beads due to the protein's capsule shape. Apoferritin has been

chemically modified to immobilize glucose oxidase at its surface, leading to a more active glucose oxidase compared to free and biotinylated glucose oxidase, mainly due to its enhanced resistance to high temperatures and extreme pH, whilst exhibiting a relatively high detection limit for glucose of 3 nM[113]. Antibodies were also attached to apoferritin's surface for immunodetection of organophosphorylated acetylcholinesterase adduct, with the aim to detect organophosphatepesticides and nerve agents. The use of apoferritin loaded with magnetic particles allowed extraction by the application of a magnetic field, once the antibody had bound to its target. This method showed great reproducibility as well as an enhanced detection limit compared to traditional methods[114].

Apoferritin was also used as nanoarchitecture for photo energy conversion. Non-water-soluble metal oxides were encapsulated within apoferritin cavity, rendering possible the dispersion of the metal oxides in solution. The electron-transfer within the cavity was performed by ferritin-mediated UV-catalysed photoreduction of Fe^{III} and release of Fe^{II}, as an artificial demineralization process[115]. Similar reduction of Cu^{II} and Cr^{VI} was achieved within the apoferritin cavity by its ferrhydrite centre low degradation of apoferritin during the process [116]. The redox reaction was used in energy conversion, by encapsulating semi-conductor nanocrystals within the protein cavity, to stabilize them. Precise band gaps measurement lead to a maximal sunlight conversion efficiency increased by *ca*. 40 % [117].

4.2.4 Bioconjugation of apoferritin and application in catalysis

One of the most interesting application of apoferritin is its use as a catalytic nanoreactor[118]. The first example of such scaffold demonstrated the encapsulation of Pd^{II} ions, by diffusion of $[PdCl_4]^{2-}$ through apoferritin's 3-fold channels, and their consecutive reduction with $NaBH_4$ *in situ* to form Pd^0 clusters without modifying the structure or the biological properties of the protein in aqueous medium. This scaffold was applied on the catalysed hydrogenation of activated olefins (Scheme 8)[4]. Without disassembling the Pd-apoferritin, only small substrates could diffuse through the protein's pores. Various compounds were assessed, molecular modelling studies predicted that positively charged compounds were diffusing faster through the negatively charged 3-fold channel of apoferritin, which was confirmed by

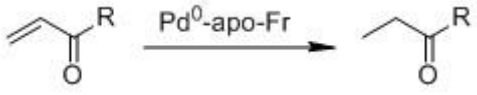

Scheme 8: Model hydrogenation reaction catalysed by zero-valent Pd cluster-containing apoferritin as demonstrated by Ueno *et al*., 2004[4].

measuring higher turnover frequencies, up to a TOF of 72 with 30 µM of Pd, when catalysing the hydrogenation of positively charged olefins. The turnover frequency was also enhanced in the Pd-apoferritin scaffold compared to Pd^0 clusters in solution.

To improve the catalytic activity of this scaffold, a bimetallic Au^0/Pd^0 alloy-loaded apoferritin was designed [119]. Binding of both metals was mediated by coordination with several residues at the inner surface of the protein cavity. Gold ions were coordinating with C48, H49, M96, H114 and C126 whilst the palladium ions were coordinating with E53, R52, E45 and H173. As opposed to the previous scaffold, here the metal ions were directly coordinated with residues rather than being encapsulated. This permitted the production of apoferritin nanoparticles pre-treated with Au^{3+}, and then treated with Pd^{2+}. The subsequent $NaBH_4$ reduction led to the formation of an alloy, whilst reducing gold ions prior to adding the palladium ions would lead to shelling the gold core with palladium. It was demonstrated that the palladium-shelled gold core-loaded apoferritin nanoparticle was more effective than any other palladium-based scaffold described previously for the hydrogenation of alkenes, with a turnover frequency increased by 2 to 4 times.

Palladium-loaded apoferritin was applied as a catalyst to other chemical reactions. Palladium nanoclusters loaded into apoferritin from hyperthermophiles *Pyrococcus furiosus* to oxidize secondary alcohols in water, using dioxygen as oxidant, were reported (Scheme 9)[9]. However, yields were quite modest, up to 67 %.

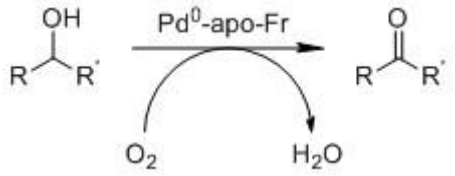

Scheme 9: Model oxidation of alcohols by zero-valent Pd cluster-containing apoferritin as demonstrated by Kanbak-Aksu *et al*., 2012[9].

Platinum and platinum-ferric apoferritin nanoparticles based on apoferritin were shown to have catalase and peroxidase activities. Monometallic platinum-based nanoparticles were made through the previously described method of encapsulating the metal ion, before reduction with $NaBH_4$ for clustering the metal. The bimetallic nanoparticles were synthesized by adding platinum to iron-containing ferritin [120]. The same study showed that such second-metal loading process could be performed with several other transition metals such as

palladium or rhodium. These protein nanoparticles were used for the oxidation of tetramethylbenzidine using hydrogen peroxide as oxidant in water. Whilst the monometallic scaffold displayed modest enzymatic constant, such as high K_M for both reactions, the bimetallic scaffold revealed to be more efficient than the naturally occurring horseradish peroxidase.

Besides the encapsulation of metal clusters, apoferritin was also used to incorporate organometallic catalysts within the protein cavity. An organometallic [Pd^{II}(allyl)Cl_2] complex was incorporated by diffusion through the 3-fold channel of apoferritin (Figure 5)[6]. Two binding domains for the Pd-complex were determined from crystallographic studies on the Pd(allyl)apoferritin complex[121]. The Pd-complex could coordinate with C48 in the cavity, and C126 in the 3-fold channel. This coordination maintained the disulfide bridges which the two cysteines were involved into.

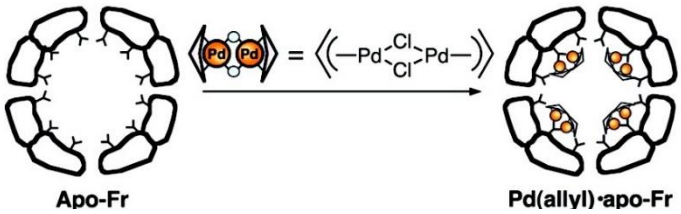

Figure 5: Coordination of Pd^{II}(allyl) complex with apoferritin's residue within the protein inner cavity. The palladium complex was either coordinated in the cavity to C48, or in the 3-fold channel to C126. Reproduced from Abe *et al.,* 2008[6] with permission of rightsholders (See Appendix 17 for permission of reproduction notice).

This biocatalyst was applied to Suzuki-Miyaura cross-coupling reaction of 4-iodoaniline with phenylboronic acid (Scheme 10). A high turnover frequency of *ca.* 3500 h^{-1} was measured. As the coordination with apoferritin's residue provided a second coordination sphere to the Pd-complex and promoted enantioselectivity as well as activity to the reaction catalysed, several apoferritin mutants were designed. The residues mutated were H49 and H114, as histidines were coordinating directly with the metal, whilst the cysteines were mutated as well. For instance, the H49A-apoferritin led to the conservation of the Pd(allyl) complex structure and an equivalent turnover frequency as with native Pd-complex apoferritin nanoparticle. However, H114A-apoferritin led to the formation of a trinuclear cluster of palladium in the 3-fold channel which led to a 75 % decrease of the turnover frequency for the same reaction, as the bulkiness of such trinuclear cluster at the entry of the 3-fold channel decreased the speed of substrate diffusion through the channel. Other mutants, such as C48A/H49A- and

C126A-apoferritin removed the coordination sites and led to an Pd(allyl) complex encapsulated within the protein cavity without coordination to the protein's residues[122]. However, without proper binding of the organometallic complex, the turnover frequency decreased by 1.8- and 4-times respectively.

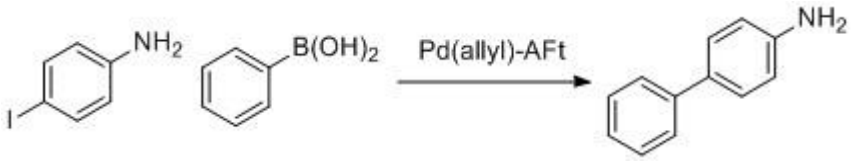

Scheme 10: Suzuki-Miyaura reaction of 4-iodoaniline with phenylboronic acid catalysed by Pd(allyl) complex coordinated inside apoferritin cavity as shown by Abe *et al.*, 2008[6].

Following these studies, the same method was applied to the incorporation of rhodium(I) norbornadiene (nbd) catalyst complexes, Rh^{I}(nbd), into the apoferritin cavity[3]. Similar crystallographic studies of the Rh^{I}(nbd)-apoferritin complex were performed to determine the coordination points of the organometallic complex to apoferritin. These studies revealed that one rhodium atom was coordinated to H114 in the 3-fold channel, whilst a second atom

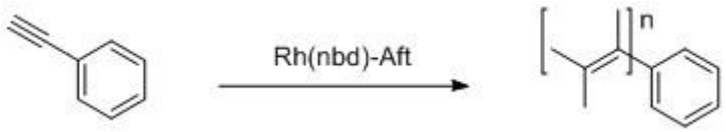

Scheme 11: Polymerization of phenylacetylene by Rh(nbd)-Aft within the protein cavity as described by Abe *et al.*, 2009[3].

was found coordinated to H49. Interestingly, a third rhodium atom was coordinated with G45 single hydrogen side chain and C48, where iron naturally accumulates. Its position was also coordinated to three water molecules, which stabilized the rhodium complex, as well as to another norbornadiene ligand, forming a cross-link rarely described in the literature[123]. The Rh^{I}(nbd)-apoferritin was then applied on the catalysis of phenylacetylene polymerization within the protein cavity (Scheme 11).

After 12 h, the polymerization stopped as the protein cavity was saturated with polyphenylacetylene of a number-average molecular weight of *ca.* 13 kDa. It was observed that the [Rh^{I}(nbd)Cl_2] free organometallic complex led to the polymerization of heavier products, with a number-average molecular weight of *ca.* 63 kDa, however, these were not water soluble. On the contrary, the apoferritin itself did not display any catalytic activity which

proved the beneficial effect of Rh(nbd) coordination within apoferritin cavity and 3-fold channel in the synthesis of water-soluble polymers.

Covalent conjugation to apoferritin has been studied as well[124]. An iron(III)-enterobacterin analogue, bearing a maleimide linker, was synthesized. The maleimide linker allowed covalent conjugation to a cysteine residue. The already present cysteine was mutated to alanine, C126A, to avoid unfavourable conjugation, whilst a cysteine was inserted by mutation A119C, at the intersection of three sub-units, allowing three cysteines to be present. Hence, three ligands were conjugated and coordinated to one Fe^{III} ion, without disrupting the protein's quaternary structure. Whilst the catalytic activity of this scaffold was not assessed, this study has pioneered the use of apoferritin for covalent conjugation of chemical catalysts[125].

4.3 Catalysts for the enantioselective oxidation of sulfides

Enantiopure sulfoxides are of significant interest because many of these compounds are used as auxiliaries for several reactions such as Diels-Alder cycloaddition as well as carbon-carbon and carbon-oxygen bond formation [126]. Enantiopure sulfoxides are of great interest in the pharmaceutical industry as well (Scheme 12). Omeprazole® **1** and its derivatives (**2-4**) are a famous family of sulfoxide-based drugs used in the treatment of gastric acidity and peptic ulcers which act by inhibiting proton efflux pumps, thus leading to the suppression of stomach acid secretion. This family of drugs is amongst the most prescribed drugs worldwide. Other examples exist, such as Modafinil® **5** and Sulindac® **6**, prescribed to treat narcolepsy and inflammation, respectively. Therefore, the synthesis of biologically active sulfoxides is a timely and relevant research area [127]. Whilst enantiopure sulfoxides are of great interest, many sulfoxidation catalysis systems often lead to overoxidation of the product and formation of sulfones. These are treated as contaminants, especially when synthesizing an active pharmaceutical ingredient, and need to be removed from the product. Thus, catalysis systems need to control the reaction to offer the best yield and enantioselectivity, without formation of sulfones.

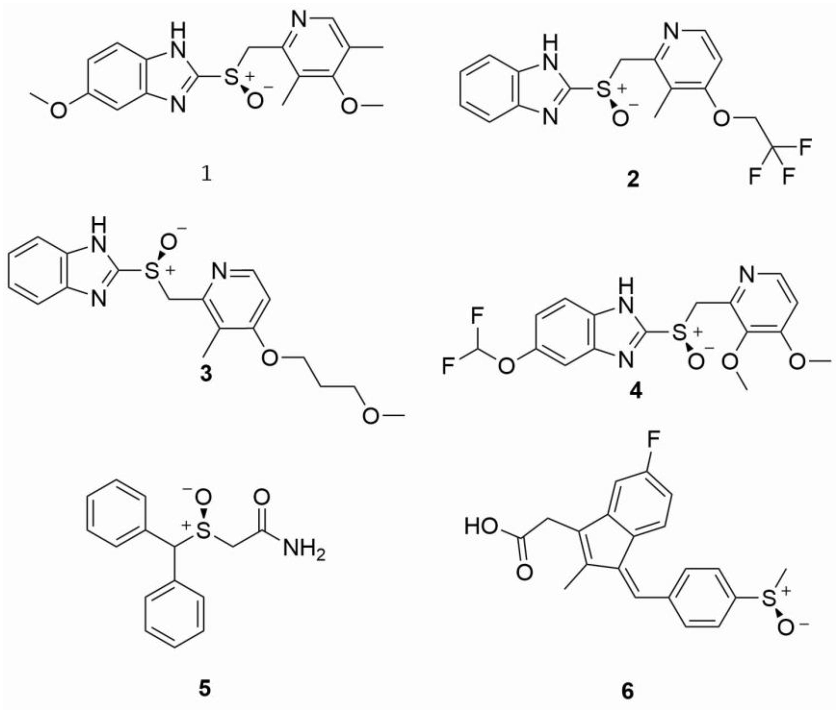

Scheme 12: Sulfoxide-based drugs. Omeprazole®-based drugs are known gastric acidity inhibitor whilst Madafinil® and Sulindac® treat narcolepsy and inflammation, respectively.

4.3.1 Transition-metal catalysts for enantioselective sulfoxidation

Sulfoxides can be obtained by two main methods: nucleophilic substitution or oxidation. The latter is the most popular due to the large scope of existing redox metal-catalysts. First, the effect of ligands on catalytic activity and selectivity will be studied.

4.3.1.1 Development of catalysts

In the development of transition-metal catalysts for enantioselective sulfoxidation, a set of several ligands has drawn most of the attention.

Binaphthols (binols) are a group of bidentate ligands widely used for oxidation, notably with a titanium centre (Scheme 13). The chirality induced during catalysis comes from the arrangement of the aryl substituents around an axis, and their restricted rotation. Titanium-binaphthol catalyst **7** was used for the oxidation of *p*-tolyl methyl sulfide with 73 % enantiomeric excess, however the yield remained moderate, around 40 % (Table 1) [128]. This asymmetric catalysis was one of the first *in vitro* sulfoxidation reported. Interestingly, whilst the presence of water deactivated this catalyst for the epoxidation of alkenes, it promoted sulfoxidation for this specific substrate. Later studies showed that a too high or too low quantity of water had an impeding effect on catalysis, hence the quantity of water had to be finely tuned[129]. Several studies using modified Ti^{IV}-binaphthol reported improved enantioselectivity. Titanium fluorinated-BINOL **8** was reported to yield 80 % *ee*[130], whilst equilenin-based Ti^{IV}-binaphthol **9** displayed an enantiomeric excess up to 92 % with a yield of 76 %[131]. Complex oxido-vanadium binaphthol nanocages were also reported for the sulfoxidation of thioanisole **10**. Such molecular cages were based on a hemicryptophane complex, added to a cyclotriveratrylene moiety and three binol complexes. A vanadium-oxide complex was added to this ligand, which led to 97 % enantiomeric excess and 93 % yield.

Ligand	Metal	Solvent	Oxidant	Substrate	Conversion (%)	ee (%)
Binol **7**	Ti^{IV}	toluene	TBHP	methyl *p-tolyl sulphide*	40	73
Fluorinated-binol **8**	Ti^{IV}	toluene	TBHP	methyl *p-tolyl sulphide*	55	80
Equilenin-based binol **9**	Ti^{IV}	toluene	TBHP	methyl *p-tolyl sulphide*	76	92
Binol cage	V^{V}	water	CHP	*thioanisole*	93	97

Table 1: Catalytic activity and selectivity of Binol ligands for the oxidation of aryl sulfides.

Such rates were obtained by the hydrophobic cage formed by the assembly of moieties, making it of a suitable size to accommodate and convert aryl sulfides substrates [132].

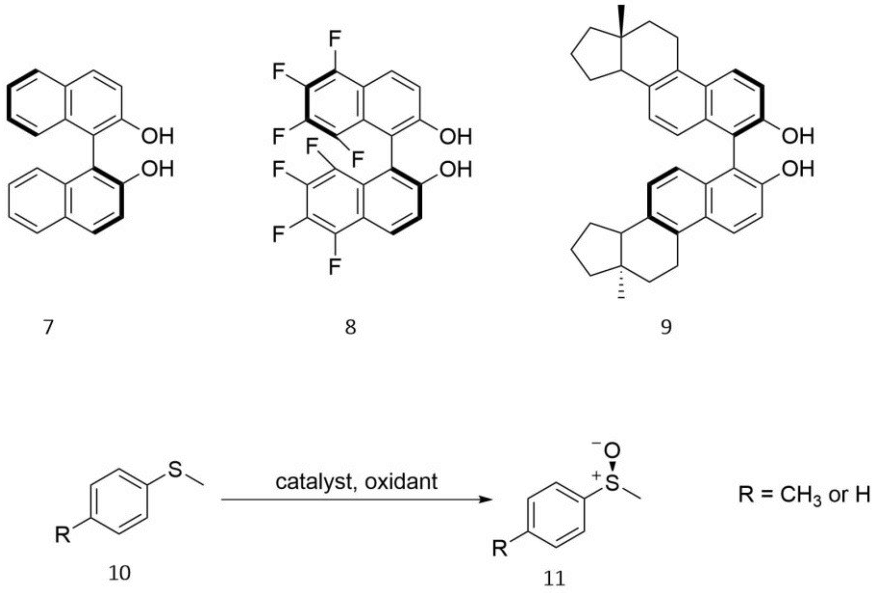

Scheme 13: Binaphthol ligands used with titanium and vanadium metal centres for the oxidation of sulfide **10**

Porphyrins, a second group of well-known ligands is notably recognized for their natural role as precursor to haem (Fe^{II}-porphyrin), contained in several redox proteins. Whilst iron-porphyrin incorporated to myoglobin is known to fix and transport oxygen throughout living organisms, iron-porphyrins incorporated into cytochrome P450s and horseradish peroxidase was shown to play an important role in redox-based metabolic pathways. When incorporated into cytochrome P450s, Fe-porphyrin was oxidized by oxygen and regenerated by reduction with NADP(H)[133]. However, in horseradish peroxidase, the Fe-porphyrin was shown to use a range of oxidant such as hydrogen peroxide and sodium chlorite, which did not need regeneration via a cofactor, this was called peroxidase shunt[134]. In both case, iron-porphyrin was shown to catalyse a wide-range of C-H, N-H and S-H oxidation. Iron-porphyrins have been used for the oxidation of sulfides as well. An interesting study on the oxidation of several sulfides demonstrated excellent yields, up to 95 % with aryl sulfides, in each case when using Fe-tetrakis(pentafluorophenyl) porphyrin **12** as catalyst (Scheme 14)[135]. However, no enantioselectivity could be obtained with these planar catalysts, as in redox biocatalysis, the three-dimensional environment of the proteins iron-porphyrins were incorporated into provided selectivity.

In the race to improve transition-metal catalysts, manganese-porphyrins were developed in the 1980s, as a replacement for iron-porphyrins, these were less susceptible to ligand degradation[136] and could be used to widen the scope of oxidations catalysed[137]. Manganese-porphyrins were shown by Groves's group to catalyse the oxidation of C-H bond

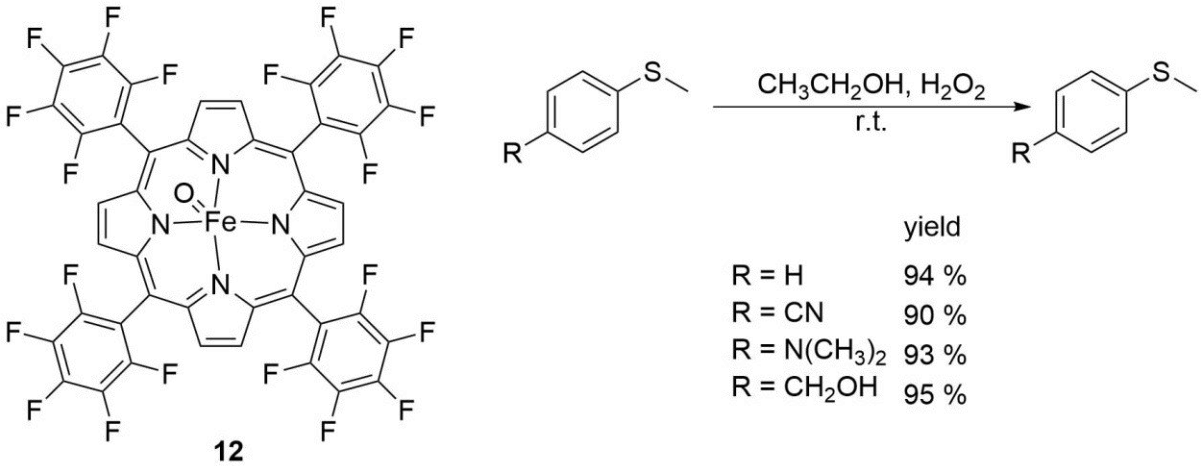

Scheme 14: Fluorinated iron-porphyrin **12**, applied on the oxidation of substituted thioanisole with hydrogen peroxide in ethanol, yields were high (up to 95 %) but the planar ligand did not bring enantioselectivity.

on a range of substituted cyclohexyls, using iodosylbenzene as oxidant in dichloromethane, with a yield up to 70 % when using cyclohexyl chloride, which was better than iron and chromium porphyrins, at the time of publishing[138]. Manganese-porphyrins were also applied on the catalysis of epoxidation of olefins, on *cis*- and *trans*-β-methylstyrene, using *meta*-chloroperoxybenzoic acid as oxidant[136]. Such reaction resulted in yields up to 99 % with 9.6 *cis*/*trans* ratio. However, these reactions were not enantioselective due to the planar structure of the ligands. These studies investigated the mechanism of action of manganese-porphyrins, here shown for epoxidation of olefins (Scheme 15). The Mn^{III} was oxidized by *m*-CPBA, yielding Mn^{V}, which subsequently transferred its oxygen onto its substrate, which regenerated the catalyst.

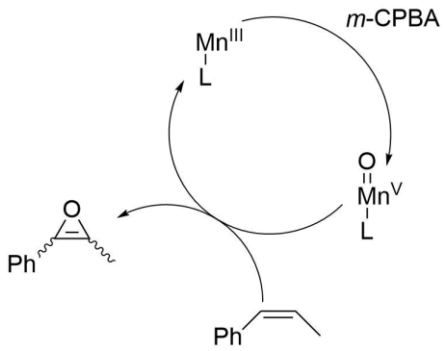

Scheme 15: Mechanism of the epoxidation of olefins by Mn^{III}-porphyrin

The enantioselective oxidation of thioanisole using hydrogen peroxide as terminal oxidant and manganese porphyrin **13** as catalyst was studied in a 3/1 ratio of methanol/phosphate buffer solution (Scheme 16). Whilst yield ranged from 61 to 95 %, attempt to vary the pH, the equivalence of oxidant and axial ligands did not improve the enantioselectivity of the reaction which reached its highest at 57 % (S) [139]. However, when applied to the asymmetric synthesis of Sulindac **6**, the yield was optimised to 100 % and the enantiomeric excess reached 82 % on a quantitative scale. Interestingly, the same ligand bearing an Fe^{III} centre was previously reported to catalyse the oxidation of a large range of sulfides with moderate to good enantioselectivity (34 – 87 % *ee*) in the same methanol/phosphate buffer solution[140].

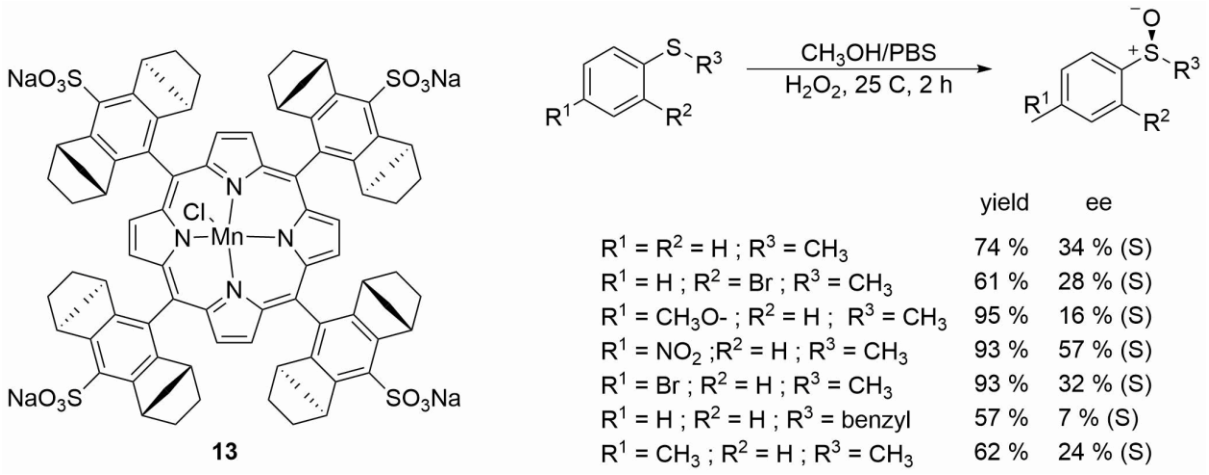

Scheme 16: Manganese-porphyrin used as catalyst for the asymmetric oxidation of phenyl sulfides.

Schiff bases are a group of bidentate, tridentate and tetradentate ligands that are prepared by condensation of a primary amine with an aldehyde or a ketone to form an imine, which will coordinate with the metal centre. Schiff bases are also used as ligands for oxidation reactions. A titanium-Schiff base derivative **14** was used for the oxidation of benzyl phenyl sulfide (Scheme 17) [141]. The conversion reached 96 %, the enantioselectivity was modest with 60 % *ee*. Schiff bases have also been widely used with vanadium as a metal centre. The first vanadium-Schiff base published, substituted either by methoxy, ethoxy and *tert*-butyl groups, was shown to catalyst sulfoxidations and reported poor enantioselectivity (14 to 40 % *ee*)[142], showing that the presence of electron-donating groups was improving the enantioselectivity. This was later improved through further investigations of the ligand's substituent effect on catalysis (Scheme 17)[143]. The ligand **15**, substituted by a nitroxy group

and a tert-butyl group on its cyclic moiety, was reported to give 70 % *ee* and 76 % *ee* for the oxidation of thioanisole and 1,3-dithiane respectively. Ligand **16**, substituted by two *tert*-butyl groups on its cyclic moiety, afforded 59 % *ee* and 85 % *ee* for the same reactions, respectively. Therefore, it was concluded the ideal ligand depended on the structure of the substrate to be oxidized[144]. More investigation on the ligand's substituents led to the conclusion that a *tert*-butyl group was necessary in R_3 position for the ligand to achieve high enantioselectivity due to this substituent's bulkiness. However, the substituent at position R_2 did not play any steric role. Nevertheless, its electronic role was deemed important, as inducing and resonance effect in the ligand tunes the activity of the transition-metal it is coordinated to. Lastly, the substituent in position R_1 did play a critical role in the steric hindrance necessary to achieve high enantioselective catalytic oxidation of sulfides with such bidentate ligands [145].

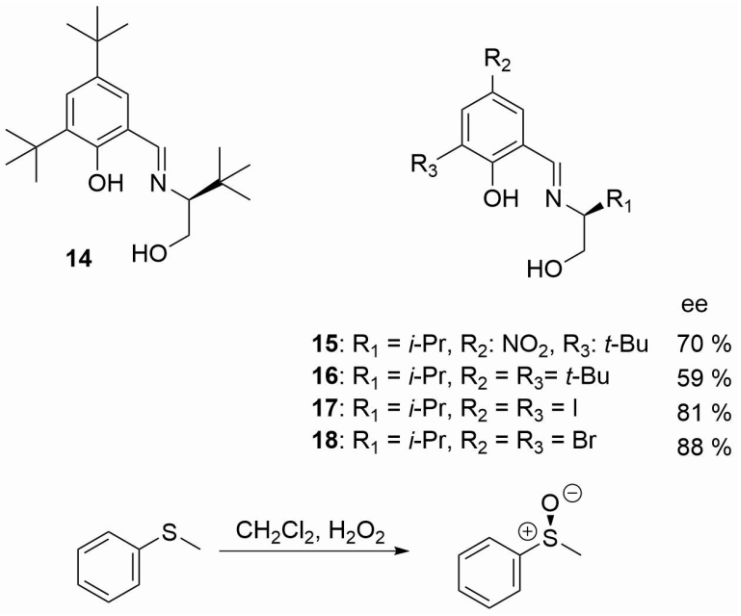

Scheme 17: Schiff base used as ligands for titanium and vanadium-based catalyst, notably for the oxidation of thioanisole using hydrogen peroxide an oxidant.

Interestingly, when R_2 and R_3 substituents were replaced by iodine (**17**) or bromine (**18**), the enantioselectivity for the oxidation of thioanisole reached 81 % *ee* and 88 % *ee*, respectively. This was supposedly due to the electronic effect of these halogen substituents rather than steric hindrance[146]. This was observed during oxidation of aryl alkyl sulfides by both titanium- and vanadium-Schiff base complexes, substituted with iodine on R_2 and R_3 positions. As expected, the yield and enantioselectivity was highly substrate-dependent, however, a maximum of 98 % *ee* was reached with 86 % yield using hydrogen peroxide as terminal oxidant and phenyl propyl sulfide as substrate in chloroform[147].

Salens are a tetradentate group of Schiff base ligands, which are prepared by the condensation of a diamine and with an aldehyde or a ketone. Salens, with a manganese metal centre, were known to catalyse the epoxidation of alkenes[148]. The yields and enantioselectivities reached with these catalysts are excellent. Moreover, an investigation on the effects of pH revealed that alkaline conditions had a positive impact on yield (87 %) and enantioselectivity (82 % *ee*), when using "Jacobsen's catalyst" **19** (Scheme 18) [148]. In this ligand, the cyclohexane-diamine moiety brought the selectivity to the reaction. This was later improved by replacing the two *o*-methyl substituents on the phenyl moiety by a *tert*-butyl, exhibiting a maximal yield of 84 % and 92 % *ee* with simple phenyl methyl alkene[149].

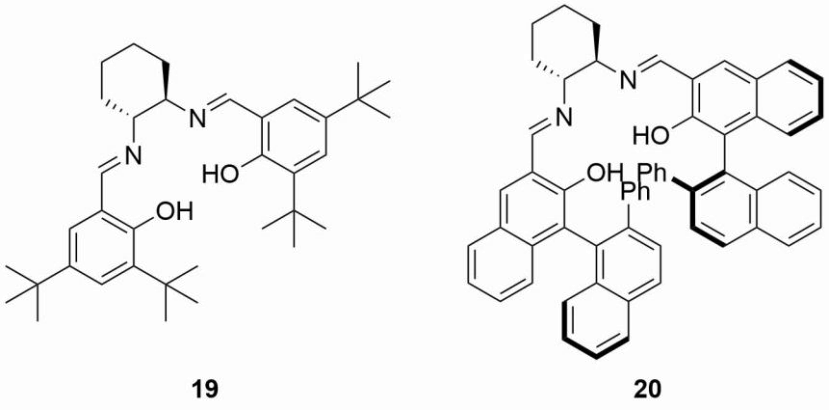

Scheme 18: Jacobsen's catalyst (**19**) and Katsuki's catalyst (**20**)

At the same time as Jacobsen's early work, another manganese-salen, based on binol derivatives, was developed by Katsuki and co-workers[150], "Katsuki's catalysts" **20** (Scheme 18). As for Jacobsen's catalyst, the selectivity was brought by the three-dimensional structure of cyclohexane-diamine moiety, but also from binol's moieties. These manganese-catalysts exhibited high enantioselectivities for conjugated alkenes with electron-rich substituents such as aryl, alkenyl and alkynyl. However, the enantioselectivity was quite modest in presence of alkyl-substituted alkenes. In each case of aryl-substituted alkene, the enantiomeric excess accounted for 96 % to 99 % [151].

This work was pursued with the development of ruthenium-salen (using the same ligand as **20**) which showed dependence of enantioselectivity with the electron-richness of the substrate substituents and displayed a maximal value of enantiomeric excess of 95 % with a 2-(propene-1-yl)naphthalene. The most interesting features of this catalyst were its

photoactivation[152] and its ability to use oxygen as a terminal oxidant[153]. However, the molar proportion of catalyst had to be as high as 5 mol %.

Jacobsen's group was the first to report an oxidation of sulfide with a manganese-salen (Scheme 19) [154], using hydrogen peroxide as terminal oxidant, given its excellent reactivity and relative low cost. In acetonitrile, the Mn-**21** catalyst led to a 47 % *ee* for the oxidation of thioanisole whilst a maximum of 68 % *ee* was obtained using *o*-bromophenyl methyl sulfide as substrate. Katsuki's group modified Jacobsen's catalyst, by adding more steric hindrance and removing both methoxy substituents on the phenyl moiety, for less electron induction effect, **22** (Scheme 19). This manganese-salen complex exhibited good enantioselectivity, up to 90 % *ee* with an *o*-nitrophenyl methyl sulfide as substrate, however the yield was lower, around 60 % [155]. As these two manganese-salen complexes were used with different oxidant, it was difficult to compare their activity, however, it was shown that the effect of electron withdrawing group on the substrate was promoting higher enantioselectivity.

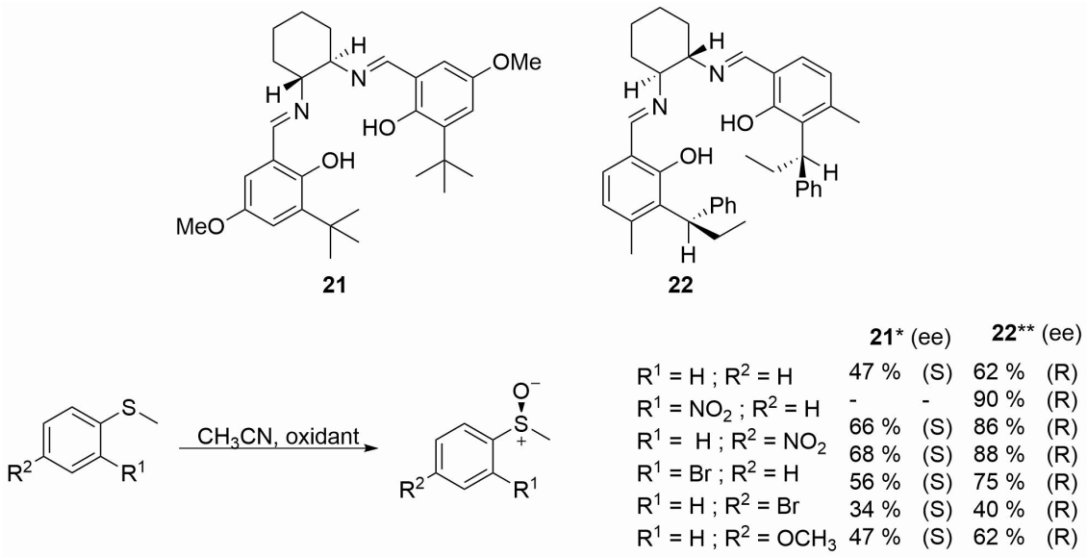

	21* (ee)		**22**** (ee)	
R^1 = H ; R^2 = H	47 %	(S)	62 %	(R)
R^1 = NO_2 ; R^2 = H	-	-	90 %	(R)
R^1 = H ; R^2 = NO_2	66 %	(S)	86 %	(R)
R^1 = Br ; R^2 = H	68 %	(S)	88 %	(R)
R^1 = H ; R^2 = Br	56 %	(S)	75 %	(R)
R^1 = H ; R^2 = OCH_3	34 %	(S)	40 %	(R)
	47 %	(S)	62 %	(R)

Scheme 19: *Jacobsen's catalyst and Katsuki's catalyst for the oxidation of thioanisole. *Hydrogen peroxide was used as oxidant. **Iodosylbenzene was used as oxidant.*

Katsuki's binol ligand (**20**) was also used with a manganese centre for the oxidation of aryl sulfides[156], with high enantioselective reactions, up to 94 % *ee*. This level of enantioselectivity was reached after a study of the effect of solvent on the rate of reaction. It was shown that the highest enantioselectivity was achieved in the presence of an axial ligand when acetonitrile was used as solvent, whilst the absence of such ligand in hexane, chlorobenzene and ethyl propionate led to a decrease of the enantiomeric excess around 70

%, a value that was slightly increased when 4-phenylpyridine *N*-oxide was added as an axial ligand, in these solvents. A titanium-salen incorporating this axial ligand afforded the oxidation of thioanisole, using hydrogen peroxide as terminal oxidant, with moderate conversion (65 %) but very high enantioselectivity (97 % *ee*)[157].

In addition to manganese, other metal centres have been incorporated in salen ligands to perform catalysed oxidation of sulfides. Katsuki's ligand (**20**) has been used with a titanium centre, and yielded high enantioselectivity (up to 93 %) and high yield (96 %), using urea•hydrogen peroxide complex as terminal oxidant and *o*-bromophenyl methyl sulfide as substrate when the reaction was carried out in methanol [158]. It was also shown that 30 % aqueous hydrogen peroxide reduced enantioselectivity of Ti-salen compared to urea•hydrogen peroxide complex as water slowly formed hydroperoxo Ti-salen with higher conformational freedom, thus leading to a less enantiopure product[159]. Vanadium-salens have received a lot of attention from researchers as well. The development of vanadium-oxide-salen with a ligand derived from Jacobsen's ligand, bearing secondary amines instead of imines without any substitution on the phenyl moieties led to a highly enantioselective oxidation of thioanisole, up to 94 % *ee* and 80 % yield [160]. The effect of solvents was investigated as well. As opposed to what was previously mentioned, acetonitrile led to low enantioselectivity (37 %) as toluene did (22 %), the catalyst had a preference for chlorinated solvents as the highest value reported above were obtained in chloroform, with dichloromethane following as a close second, due to the higher solubility of the catalyst in these solvents[160].

Other ligands could be cited, such as amino-based ligands. For instance, bipyridines are shown to incorporate a wide range of transition-metals (copper, ruthenium, platinum, etc.) and known to oxidize water[161].

4.3.1.2 Sulfoxidation in aqueous solutions

The oxidation of thioanisole in water was investigated using hydrogen peroxide as the terminal oxidant and Fe^{III}-salen complexes, one ligand being Katsuki's (**24**) and the other was Jacobsen's original ligand (**23**) (Scheme 20). Whilst the latter led to very low yield and

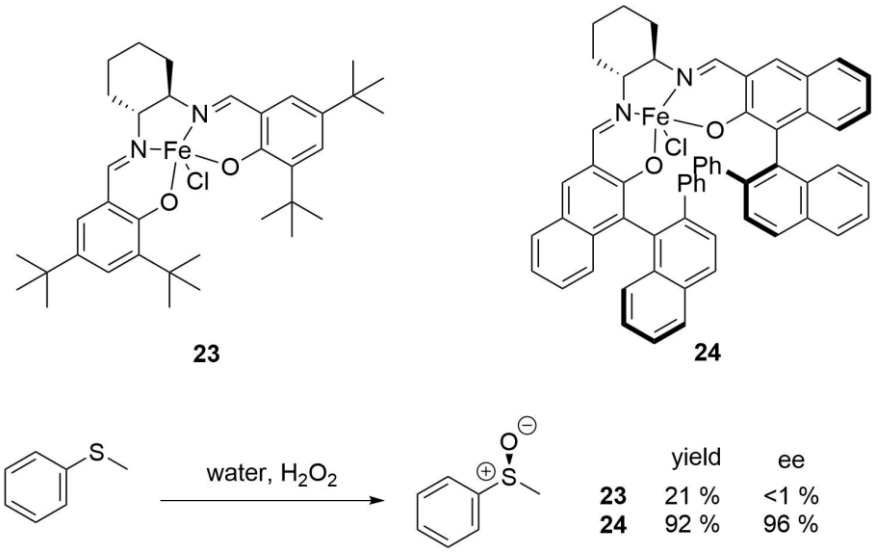

Scheme 20: Asymmetric oxidation of thioanisole in water using hydrogen peroxide and Fe^{III}-salen.

enantioselectivity (21 % yield and less than 1 % *ee*) due to poor water solubility, the former led to 92 % yield and 96 % enantioselectivity. This was an important step for the oxidation of water-soluble sulfides in mild conditions, notably the oxidation of biologically active sulfides, as the reaction was performed at 20 °C for only 3 h [162]. Jacobsen's catalyst bearing an iron ion was used for sulfoxidation in water, with optimized conditions[163]. Under reflux for 2 h and using *tert*-butyl hydroperoxide as oxidant, high yields (81 to 93 %) and high enantioselectivities (81 to 99 %) were reached on a large range of substituted phenyl sulfide, despite the poor solubility of this catalyst. Iron-porphyrins have been applied to sulfoxidation in water as well. A water-soluble iron-tetraphenylporphyrin was used to catalyse the non-selective oxidation of aryl sulfides using hydrogen peroxide as oxidant[164]. This led to high yields, up to 90 % with *p*-methoxyphenyl ethyl sulfide. Several water-soluble porphyrins, such as sulfonated porphyrins, have been reported, however, they have mainly been applied on the catalysis of olefin epoxidation[165], carbene transfer[166] and oxidation of alcohols[167]. Therefore, the oxidation of sulfides in water by transition-metal catalyst is a field in development. However, for catalysis in aqueous media, and especially in mild conditions, the attention is increasingly drawn to artificial metalloenzymes.

4.3.1.3 Effect of axial ligands

The effect of axial ligands coordinated with the transition metal incorporated in salens has been investigated. Manganese-salen (Katsuki's binol catalyst **20**) was shown to bind one molecule of water and one cyclopentane oxide, directly on the manganese[168]. This was shown to improve the enantioselectivity of sulfoxidation and epoxidation of olefins, by sterically constraining the substrate approach on the manganese, revealing that not only the

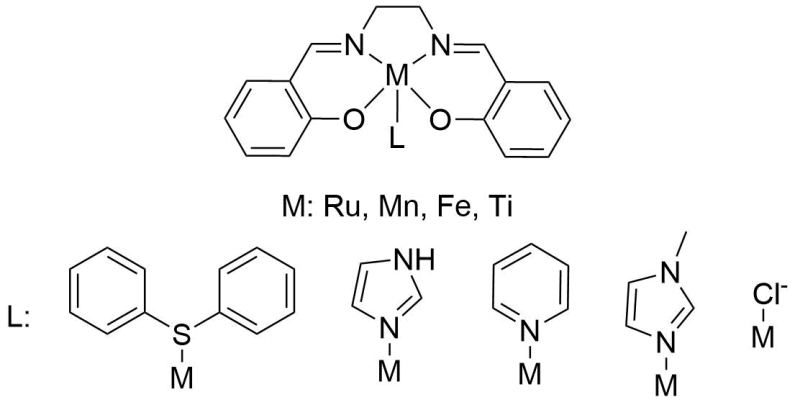

Scheme 21: Range of axial ligands coordinated with metal-salen complexes

substituents on the salen's cyclic moieties, such as *tert*-butyls, had a significant steric effect impacting the selectivity of the reaction catalysed. Asymmetric epoxidation of styrene was even performed using a planar ruthenium-salen, by adding chiral sulfoxide axial ligands, mimicking the chirality provided by the cyclohexane amine moiety from Jacobsen's catalyst (**19**) and resulting in equivalent enantioselectivity[169]. More recently, an iron-salen was used for the oxidation of thioglycolic acid, and several axial ligands were compared. The iron was originally coordinated with an apical chloride, thus the effect of imidazole, 1-methylimidazole and pyridine was assessed. These nitrogenous compounds were strong electron donating group, which resulted in the decrease of the reaction rates, also because their size induced too much steric hindrance for the substrate, which could only approach the catalyst more slowly. In comparison, chloride, as an electron withdrawing, was shown to be the best axial ligand in these conditions [170]. Therefore, axial ligands were shown to have an important effect on the rates and selectivity of reactions catalyst by metal-salens (Scheme 21). Electron withdrawing axial ligands, such as chloride, were shown to improve the transition-metal activity, but the steric hindrance brought by these axial ligands was also important in orienting the substrate during its approach of the catalyst.

4.3.1.4 Mechanism of sulfoxidation by manganese-salen and decomposition of hydrogen peroxide

These studies led to understand the mechanism of thiol oxidation by manganese-salen using hydrogen peroxide (Scheme 22A)[171]. Upon addition of hydrogen peroxide and release of a proton, the sulfide coordinates with manganese as well and interact with an oxygen, liberating a hydroxyl ion and the oxidized thiol. However, it was also shown that in excess of hydrogen peroxide over substrate, a second hydrogen peroxide molecule could coordinate with manganese (Scheme 22B), which then adopts a catalase-like activity and decompose hydrogen peroxide in water and dioxygen[171-172].

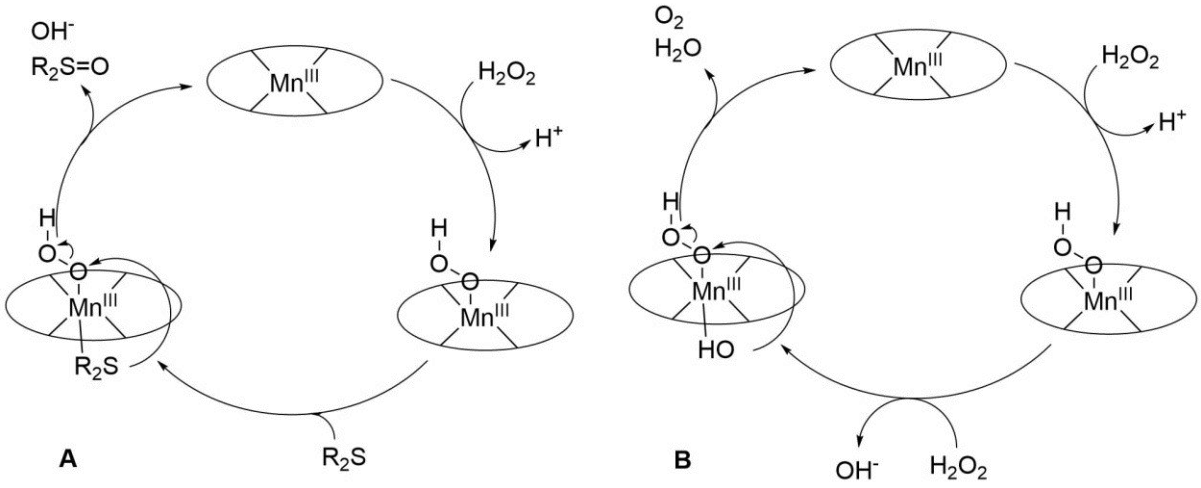

Scheme 22: A. Mechanism of sulfoxidation by hydrogen peroxide catalysed by a manganese-salen. **B**. Decomposition of hydrogen peroxide by manganese-salen, following a catalase-like activity, when hydrogen peroxide is in excess.

4.3.2 Bioconjugated salen catalysts for sulfoxidation

In addition to being extensively used as ligands for catalysis of sulfide oxidation, in organic solvents and in water, salens have also been used as the first coordination sphere in the development of artificial metalloenzyme, by supramolecular or covalent conjugation with biological scaffolds, which bring a chiral environment, this explains why many conjugated ligands are planar.

The first notable example was brought by Watanabe's group in 2003[173]. A chromium-salen (Cr-**25**) (Scheme 23) was incorporated in the catalytic site of a sperm whale apomyoglobin by supramolecular interactions, in place of an iron-protoporphyrin IX. Despite modifications of the catalytic site through mutagenesis of several residues, the enantioselectivity remained around 30 % for the oxidation of thioanisole. The same work was carried with a manganese-

salen, using the same ligand (Mn-**25**). Whilst the enantioselectivity remained at the same level, the rate of reaction was greatly improved, with a turnover of 2.7 min^{-1}[174].

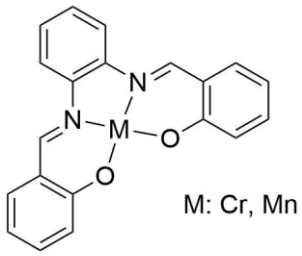

25

Scheme 23: Metal-salen ligand incorporated in the catalytic site of a sperm whale apomyoglobin

Lu's group also incorporated a manganese-salen (**26**) into the catalytic site of apomyoglobin[60]. Whilst supramolecular interaction led to poor enantioselectivity in Watanabe's studies, Lu's approach was the dual covalent anchoring strategy. By mutating two residues into cysteines (L72C and Y103C), the catalyst could covalently bond through disulfide bridges thanks to the methyl thiosulfonate moiety of the ligand (Scheme 24). This approach led to higher enantioselectivity, although average (51 % *ee*), as the mobility of the catalyst around its covalent links with the protein was greatly reduced[60].

Further studies on the same system involved attachment of the salen at a different position (T39C instead of Y103C) and led to an increased enantioselective reaction (66 % *ee*)[175]. This was due to a better placement of the catalyst as well as enhanced steric control of the substrate compared to the first study[60].

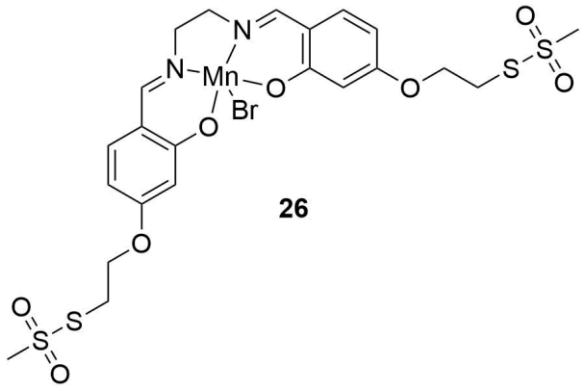

26

Scheme 24: Manganese-salen covalently conjugated to the catalytic site of apomyoglobin via its two methylsulfonate substituents.

Besides apomyoglobin-based salen insertion, salens were incorporated in serum albumin (both bovine and human) to perform the catalysed oxidation of thioanisole[176].These studies have originally started with insertion of iron- and manganese-porphyrins, leading to a good enantioselectivity of the reaction (up to 74 %)[53].

The same work was then realised by Menage's group using manganese-salen with various substituents on its phenyl moieties (Scheme 25, **27**-**30**) inserted in human serum albumin (HSA) [177]. The studied showed that easily ionisable and bulky substituents, such as in **28** and **29**, promoted affinity of the catalyst with the binding pocket, through tighter binding, and restricted movement of the catalyst. Hence, the highest enantiomeric excess of 97 % was measured on reaction catalysed by **28**-HSA, with a yield of 97 %. This was an additional proof that the protein environment brings selectivity to the reaction. Interestingly, after 5 successive additions of substrate and oxidant, the enantioselectivity was still as high as 92 %. Therefore, this scaffold had remarkable recycling properties of great interest for industrial purposes.

Menage and co-workers have also shown, by docking studies, that iron-salen could be inserted within NikA's binding pocket, a nickel binding periplasmic protein precursor, and such protein environment would bring selectivity to a reaction catalysed by the iron-salen[178]. Whilst this specific scaffold has not be applied to sulfoxidation, the incorporation of a bipyridine-based ruthenium-BPHMEN (*N*,*N*'-bis(2-pyridylmethyl)-*N*-methyl-1,2-ethanediamine), by supramolecular interactions, was shown to bring up to 100 % *ee* with 78 % conversion on the oxidation of various aryl sulfides[179]. The same ligand, coordinated with an iron ion, was inserted in human serum albumin, and gave up to 78 % *ee* for the oxidation

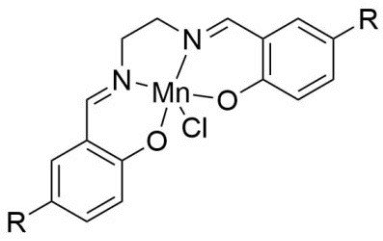

27: R = H
28: R = COOH
29: R = SO_3H
30: R = OH

Scheme 25: Manganese-salen inserted into human serum albumin binding pocket. Different substituents on the cyclic moieties improved the catalyst binding, thus the selectivity.

of thioanisole[180]. However, overoxidation of the sulfoxide product to sulfone was observed, with up to 97 % of overoxidation.

Reetz and co-workers covalently bound the manganese-salen **31** to a single cysteine residue in the active site of papain [70]. This ligand contained a maleimide linker substituent to one of the ligand's cyclic moiety (Scheme 26), which allowed covalent conjugation by Michael addition with a free thiol. Whilst the construct was applied to epoxidation of alkenes, the data were not published, but were described as around 10 % *ee*, due to the movement of the catalyst around its single bond to the protein, and having only one cyclic moiety substituted with bulky electron donor groups, *tert*-butyl [70b].

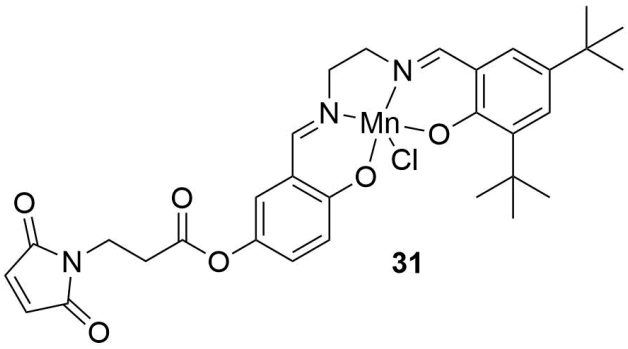

Scheme 26: Manganese-salen bearing a maleimide-linker. This catalyst was covalently conjugated to papain to catalyse the epoxidation of olefins.

Ward's group focused on the incorporation of manganese-salen into a biotin-streptavidin system. Biotin (**32**), is a molecule which has an excellent affinity for streptavidin's binding pocket. This system is therefore well known as a robust protein scaffold, which is the reason why it has been extensively used as a host system for various organometallic catalysts, such as biotinylated rhodium-based catalysts for the catalytic hydrogenation of acetamidoacrylic acid[42].

Initial studies focused on the insertion of vanadyl-oxide in place of biotin in the vicinity of streptavidin's binding pocket. The vanadyl complex was coordinated directly with the protein's residues. Rational design studies led to improvement one of the binding pocket's loop by mutation of residues, which led to better affinity for the vanadyl-oxide complex. Thus, oxidation of sulfides gave up to 93 % enantiomeric excess [43]. Further studies reported the

design of several achiral manganese-salen complexes and their insertion into recombinant streptavidin through covalent binding to biotin (Scheme 27) [44].

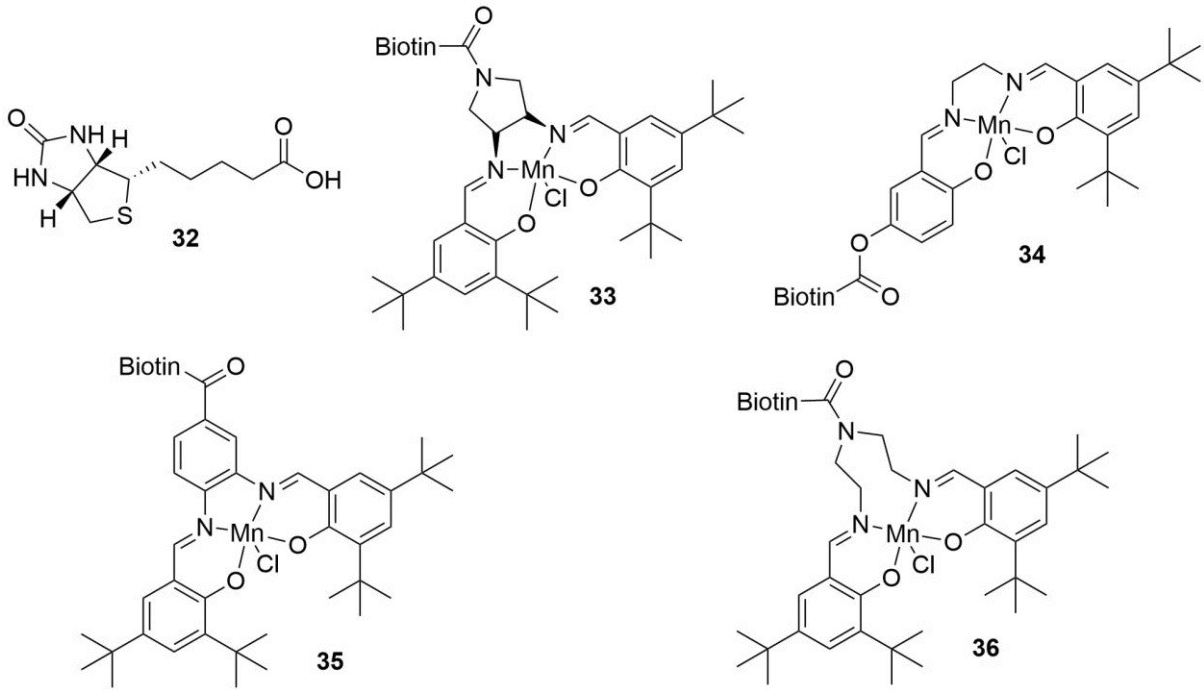

Scheme 27: Biotin (**32**) and biotin-manganese-salens (**33**-**36**) which were inserted into streptavidin binding pocket and used to catalyst the oxidation of sulfides.

Overall, the conversion and enantioselectivity of the oxidation of thioanisole in water catalysed by biotin-streptavidin manganese-salen were quite modest (Table 2). Whilst in acetonitrile, the yield rises up to 86 %, the enantiomeric excess stagnated at 36 %. These values were halved when the reaction was carried out in water. However, as previously explained, the insertion of achiral catalyst within a protein environment leads to enantioselective reaction as the selectivity is brought by the protein's binding site, here streptavidin binding pocket [44].

Amongst the several transition-metal catalysts used for the design of artificial metalloenzymes, manganese-salens have been extensively studied. Manganese-salen complexes have been incorporated into proteins both by supramolecular interactions as well as covalent conjugation, which led to enantioselective oxidation of sulfides catalysed by planar manganese-salens.

Entry	Conversion (%)	Enantioselectivity (ee %)	Solvent
33	10	-	H_2O
33-(S112G)Sav	34	11	H_2O
34	86	-	Acetonitrile
34-(S112D)Sav	44	36	H_2O/DMF (99/1)
35	30	1	H_2O/DMF (99/1)
35-(E116A)Sav	38	-	H_2O/DMF (99/1)
36	56	7	H_2O/DMF (99/1)
36-(S112D)Sav	19	-	H_2O/DMF (99/1)

Table 2: Summary of conversion and enantioselectivity of biotin-streptavidin manganese-salen complexes for oxidation of thioanisole.

4.4 Introduction summary

The field of artificial metalloenzymes has dramatically grown and drawn much attention in the past decades. The design of first coordination spheres, using organic ligands, has developed mainly by getting inspired by the work done in the field of transition-metal catalysts and by adapting these to biocatalysis, widening the scope of reactions catalysed by artificial metalloenzymes beyond what native enzyme catalysis can do. Moreover, the design of second coordination sphere has proven that a protein or a DNA strand could be totally diverted from their natural roles by few modifications to make possible the conjugation to transition-metal catalysts.

Whilst many proteins have been used as second coordination spheres for the building of artificial metalloenzymes, apoferritin has yet to prove its value in this field. So far, the most used feature of this protein is its pH-dependent assembling property, which led to its use as a vector of many different molecules, from drugs to quantum dots, with many applications, from medical to energy production. Very few examples reported the conjugation of apoferritin to transition-metals catalysts and fewer the actual evaluation of such artificial metalloenzyme on synthetic reactions.

Since their development at the beginning of the 1990s, metal-salen catalysts have proven valuable for the catalysed oxidation of sulfides and the epoxidation of alkenes. The electronic configuration of the inserted metal was proven to be easily modified through the large array of substituents salens can bear. Salens have also been growingly involved in the field of artificial metalloenzymes by being covalently conjugated to several proteins, such as streptavidin, papain, and myoglobin. These studies all led to the improvement of covalent conjugation techniques, and the possibility to perform the reactions metal-salens catalyse in water, with better rates and selectivity than with the catalyst alone, thanks to the chiral environment provided by the protein.

5. AIMS

The aim of this project was to develop an artificial metalloenzyme using apoferritin as a second coordination sphere. Apoferritin was to be covalently conjugated to a salen, acting as first coordination sphere for the selected transition-metal, manganese. The catalytic activity of this scaffold was then to be evaluated on the oxidation of a model sulfide.

6. OBJECTIVES

Four objectives were developed in order to achieve the aims of this project (Figure 6).

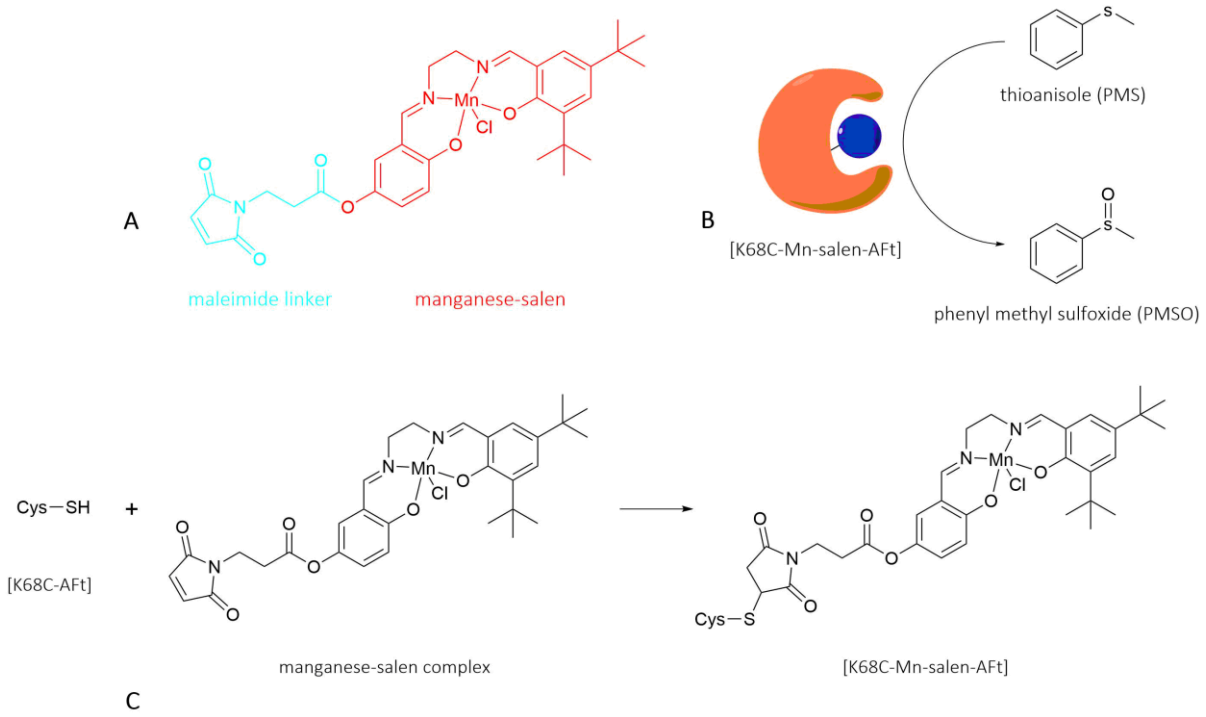

Figure 6: Summary of conversion and enantioselectivity of biotin-streptavidin manganese-salen complexes for oxidation of thioanisole

The first objective was the synthesis of a manganese-salen complex bearing a maleimide linker on one of its cyclic moiety (Figure 6A). Such a salen could undergo Michael addition with a cysteine's thiol. The second objective was the preparation of an apoferritin containing a single cysteine, K68C pointing towards the inner cavity of the protein to covalently conjugate with the catalyst inside the apoferritin nanocapsule's hollow core. Therefore, the third objective was to conjugate the recombinant protein with the maleimide-manganese-salen to form the conjugate [K68C-Mn-salen-Aft] (Figure 6C) and assemble a conjugate-based nanocapsule. The fourth objective was to assess the catalytic activity of the conjugate and the conjugate nanocapsule the selectivity brought by the protein environment on the oxidation of thioanisole, using hydrogen peroxide as oxidant, in water (Figure 6B).

7. MATERIALS AND METHODS

7.1 Materials

Commercially available reagents from Sigma-Aldrich were used without purification. All aqueous solutions were prepared using milliQ grade water. NMR spectra were acquired on a DPX300 (Bruker) spectrometer (300 MHz ^{1}H frequency, 75 MHz ^{13}C frequency). Chemical shifts are quoted in ppm and coupling constant, *J*, are quoted in Hz. Mass spectra were recorded with a microTOF 61 (Bruker) mass spectrometer using electrospray ionization (ESI). Infrared spectra were recorded using a Nicolet Avatar 320 FTR-IR spectrometer equipped with an OMNI-SamplerTM Smart Accessory for HATR (Germanium crystal, DTGS detector) over the range 4000-600 cm^{-1}. Protein purification was performed on an AKTA purifier 10 (GE Healthcare) using a HisTrap 5 mL crude column (GE Healthcare). DNA concentrations were measured with a NanoDrop 2000c spectrophotometer (Thermo Scientific) unless otherwise stated. Protein concentrations were measured on a Fluostar OPTIMA plate reader (BMG Labtech). UV spectra were acquired on a UV-2600 with a CPS-100 cell positioner (Shimadzu). HPLC analysis were carried on a 1220 Infinity LC (Agilent Technologies) using an OD column Chiralcel (Daicel Chemical Industries Ltd.). Multi-elemental analysis was undertaken by ICP-MS iCAP-Q (Thermo Fisher Scientific).

7.2 Methods

7.2.1 Chemical synthesis

Synthesis of 3-maleimidopropionic acid 37

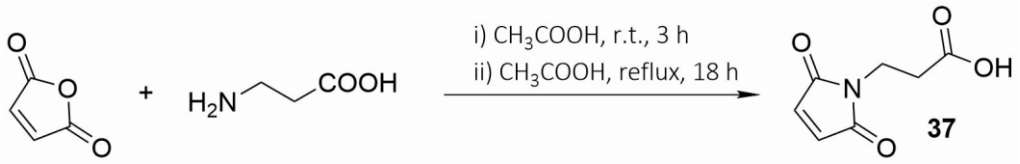

To a solution of β-alanine (1.05 g, 11.8 mmol) in acetic acid (10 mL) was added dropwise a solution of maleic anhydride (1.16 g, 11.8 mmol) in acetic acid (5 mL). The resulting solution was then stirred at room temperature for 3 h then heated to reflux for 18 h. The solvent was removed under high vacuum. Ethyl acetate (20 mL) and water (20 mL) were added then the biphasic solution was transferred to a separating funnel. The organic phase was extracted, and the aqueous phase was further extracted with ethyl acetate (2x20 mL). Organic phases

were combined and washed with brine (20 mL) then dried over Na_2SO_4. After filtration, the solvent was evaporated under pressure. The product was purified by column chromatography (SiO_2, 75 g) using dichloromethane/methanol 95/5. The product was obtained as a white solid (920 mg, 46 %). This protocol was adapted from Mantovani *et al.*[67]

^{1}H NMR (300 MHz, $CDCl_3$): δ = 6.73 (s, 2H, CH), 3.85 (t, *J* = 7.2 Hz, CH_2), 2 .72 (t, *J* = 7.2 Hz, CH_2). ^{13}C NMR (75 MHz, $CDCl_3$) 173.1, 170.7, 134.1, 33.3, 32.0. ESI-MS (in methanol): theoretical m/z [M+Na^+] = 192.0267; measured= 192.0248. mp 104 – 106 °C.

Synthesis of 3-maleimidopropionic-*N*-hydroxysuccinimide ester 38

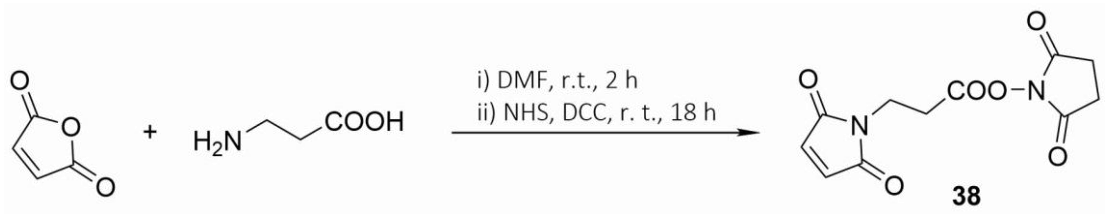

To a solution of maleic anhydride (1.0 g, 10 mmol) in DMF (10 mL) was added β-alanine (0.91 g, 10 mmol). The resulting solution was stirred at room temperature for 2 hours. The solution was then cooled down to 0 °C *N*-hydroxysuccinimide (1.44 g, 12.5 mmol) was added followed by DCC (4.12 g, 20 mmol), the temperature was kept at 0 °C for 15 min, then the ice bath was removed. After few hours of stirring, the solution became a thick white slurry, which was stirred at room temperature for total of 18 h. The slurry was filtered and the solid (dicyclohexyl urea) was washed with H_2O (15 mL) and dichloromethane (15 mL) and discarded. The filtrate was then resolubilized in ethyl acetate (20 mL). Water (50 mL) was added then the phases were separated. The aqueous layer was extracted with ethyl acetate (3 x 20 mL) and the organic phases were combined then washed with brine (2 x 20 mL). The organic solution was then washed with a saturated solution of $NaHCO_3$ (20 mL) and dried over Na_2SO_4. After filtration, the solvent was removed under vacuum. The product was purified by column chromatography (SiO_2, 30 g) using hexane/ethyl acetate 30/70 as eluent. The solvent was removed to give a white solid (1.00 g, 50 %). This protocol was adapted from Vigier-Carriere *et al.*[181]

^{1}H NMR (300 MHz, DMSO-*d*6) δ = 7.06 (s, 2 CH), 3.75 (t, *J* = 7.0 Hz, CH_2), 3.06 (t, *J* = 7.0 Hz, CH_2), 2.80 (s, 4H). ^{13}C NMR (75 MHz, DMSO-*d*6) δ = 173.0, 165.9, 135.1, 132.9, 109.3, 35.7,

35.6, 29.4, 25.8. ESI-MS (in methanol): theoretical [M+H$^+$] = 267.0612, measured = 267.0608, theoretical [M+Na$^+$] = 289.0236, measured = 289.0430. mp 156 – 158 °C.

Synthesis of 5-(propionic ester)-2-hydroxybenzaldehyde 39

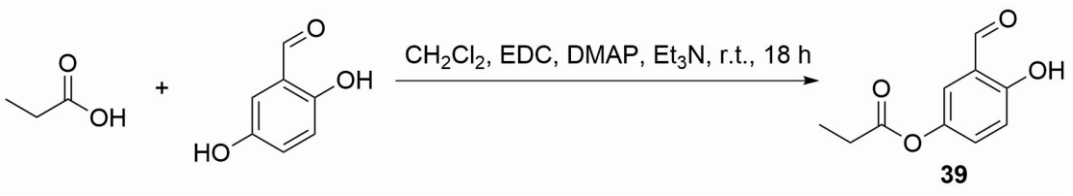

To a solution of 2,5-dihydroxybenzaldehyde (138 mg, 1 mmol), propionic acid (74 mg, 75 µL, 1mmol), dimethylaminopyridine (25 mg, 0.2 mmol) and triethylamine (162 mg, 223 µL, 1.6 mmol) in anhydrous dichloromethane (10 mL), was added dropwise a solution of 1-ethyl-3-(3-dimethylaminopropyl)carbodiimide (201 mg, 229 µL, 1.3 mmol) diluted in anhydrous dichloromethane (1 mL). The yellow solution was stirred overnight at room temperature. Dichloromethane (10 mL) was then added and the solution was then transferred onto a separating funnel. Water (20 mL) was added then the phases were separated. The aqueous phase was extracted with dichloromethane (3 x 10 mL). The organic phases were combined and washed with brine (20 mL) then dried over Na_2SO_4. After filtration, the solvent was evaporated. The product was purified by column chromatography (SiO_2, 75 g) using hexane/ethyl acetate 50/50 as eluent. The solvent was evaporated then the product was recovered as a pale-yellow oil (90 mg, 46 % yield).

^{1}H NMR (300 MHz, $CDCl_3$) δ = 10.92 (s, OH, 1H), 9.87 (s, HC=O, 1H), 7.35 (d, *J* = 2.8 Hz, CH, 1H), 7.28 (m, CH, 1H), 7.02 (d, *J* = 2.8 Hz, CH, 1H), 2.62 (q, *J* = 7.6 Hz, CH_2, 2H), 1.29 (t, *J* = 7.6 Hz, CH_3, 3H).

Synthesis of 5-(3-maleimidopropionic ester)-2-hydroxybenzaldehyde 40

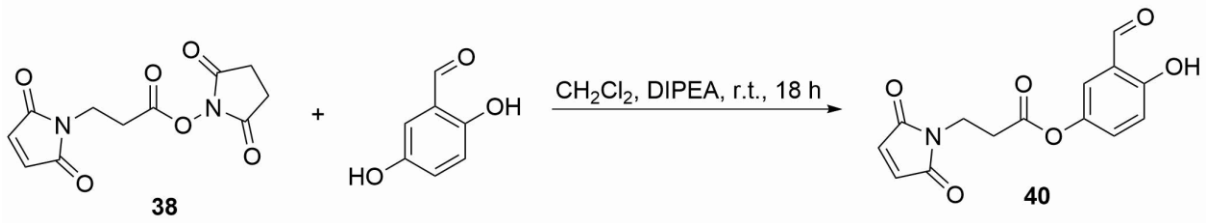

To a solution of 2,5-dihydroxybenzaldehyde (91 mg, 0.66 mmol) and 3-maleimidopropionic-*N*-hydroxysuccinimide ester **38** (176 mg, 0.66 mmol) in anhydrous dichloromethane (10 mL)

was added dropwise *N*,*N*-diisopropylethylamine (128 mg, 0.99 mmol) diluted in anhydrous dichloromethane (1 mL). The yellow solution was stirred overnight at room temperature. The solution was transferred to a separating funnel and dichloromethane (20 mL) was added. Water (30 mL) was added and the phase were separated. The aqueous phase was extracted with dichloromethane (3 x 20 mL) then the organic phases were combined and washed with a saturated solution of $NaHCO_3$ (40 mL) then with brine (40 mL). The organic phase was dried over Na_2SO_4 then filtered. The solvent was removed under vacuum. The yellow solid was purified by column chromatography (SiO_2, 50 g) with a gradient of solvent starting from pure dichloromethane increasing up to dichloromethane/methanol 99/1. The solvent was evaporated yielding a pale-yellow solid (112 mg, 59 %).

^{1}H NMR (300 MHz, $CDCl_3$) δ = 2.88 (t, *J* = 6.8 Hz, CH_2, 2H), 3.97 (t, *J* = 6.8 Hz, CH_2, 2H), 6.99 (d, *J* = 9.0 Hz, CH, 1H), 7.29 (m, CH, 1H), 7.36 (d, *J* = 2.8 Hz, CH, 1H), 9.85 (s, HCN, 1H), 10.91 (s, OH, 1H). ^{13}C NMR (75 MHz, $CDCl_3$) δ = 33.2, 33.6, 118.7, 125.3, 130.6, 134.3, 159.4, 169.4, 170.3, 195.7. ESI-MS (in methanol): theoretical [M+Na^+] = 309.1901, measured = 309.1911.

Synthesis of *N*-(2,5-dihydroxysalicydene)-*N'*-(3,5-di-*tert*-butyl-2-hydroxysalicydene) ethylenediamine 41

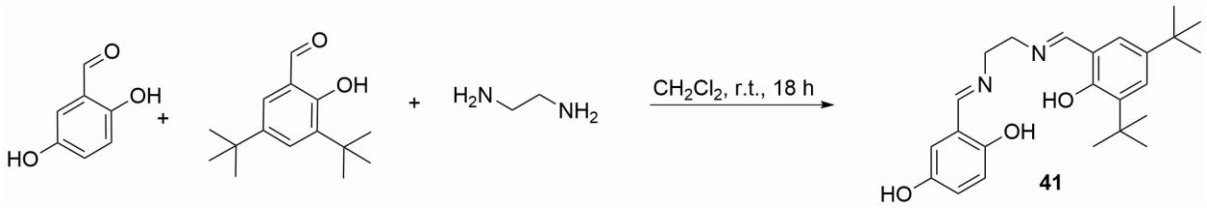

To a solution of 2,5-dihydroxybenzaldehyde (138 mg, 1 mmol) and 3,5-di-*tert*-butyl-2-hydroxybenzaldehyde (234 mg, 1 mmol) in anhydrous dichloromethane (20 mL), was added dropwise ethylenediamine (60 mg, 1 mmol) diluted in a solution of anhydrous dichloromethane (500 µL). The solution instantly became yellow. A desiccant (molecular sieves 3Å, 10 % w/v) was added to the solution. The slurry was stirred at room temperature for 18 h. The solvent was removed under vacuum whilst avoiding high temperature. The product was purified by column chromatography (SiO_2, 20 g). The first side-product *N*,*N'*-(3,5-di-*tert*-butyl-2-hydroxysalicydene)ethylenediamine **42** was eluted with hexane/diethyl ether 80/20, then the product was eluted using hexane/diethyl ether 50/50. This had to occur rapidly to avoid degradation of the desired product on silica. The product was recovered as a

yellow-orange solid (66 mg, 51 %) containing 7 % of starting materials due to degradation during purification. This protocol was adapted from Reetz *et al.*[70b]

^{1}H NMR (300 MHz, d_6-DMSO) δ = 1.26 (s, CH_3, 9H), 1.36 (s, CH_3, 9H), 3.90 (s, CH_2, 4H), 6.67 (d, *J* = 8.5 Hz, CH, 1H), 6.75 (d, *J* = 2.9 Hz, CH, 1H), 6.78 (m, CH, 1H), 7.24 (d, *J* = 2.5 Hz, CH, 1H), 7.30 (d, *J* = 2.5 Hz, CH, 1H), 8.47 (s, HC=N, 1H), 8.58 (s, HC=N, 1H), 8.96 (s, OH, 1H), 12.48 (s, OH, 1H), 13.97 (s, OH, 1H). ^{13}C NMR (75 MHz, d_6-DMSO) δ = 31.7, 33.1, 33.7, 34.3, 35.0, 118.1, 118.9, 126.1, 126.8, 136.1, 140.0, 158.7, 166.6, 168.7. ESI-MS (in methanol): theoretical [M+H$^+$] = 397.2488, measured = 397.2486, 398.2520; theoretical [M+Na$^+$] = 419.2305, measured = 419.2311. mp 228-230 °C.

Synthesis of *N,N'*-(3,5-di-*tert*-butyl-2-hydroxysalicydene)ethylenediamine 42

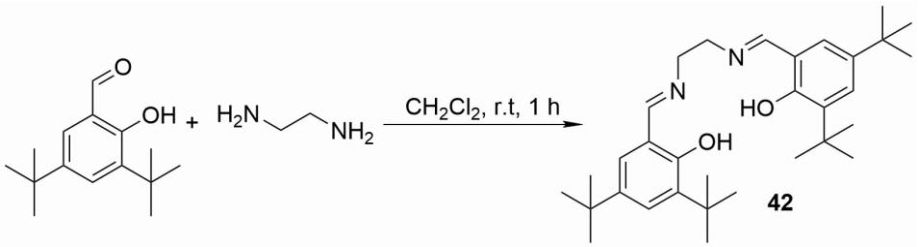

To a solution of 3,5-di-tert-*butyl*-2-hydroxybenzaldehyde (1.87 g, 8 mmol) in dichloromethane (20 mL) was added dropwise ethylenediamine (0.24 g, 267 µL, 4 mmol). The solution instantly became yellow and was left stirring for 1 h. The solvent was then evaporated without further purification, yielding a yellow solid (1.95 g, 97 %). This protocol was adapted from Kasumov *et al.*[182]

^{1}H NMR (300 MHz, $CDCl_3$) δ = 1.31 (s, CH_3, 9H), 1.46 (s, CH_3, 9H), 3.95 (s, CH_2, 4H), 7.09 (d, *J* = 2.4 Hz, CH, 2H), 7.39 (d, *J* = 2.4 Hz, CH, 2H), 8.42 (s, HC=N, 2H), 13.66 (s, OH, 2H). ^{13}C NMR (75 MHz, $CDCl_3$) δ =29.4, 31.5, 34.1, 35.0, 42.6, 59.6, 62.9, 117.8, 125.9, 127.0, 136.5, 140.0, 158.0, 167.6. ESI-MS (in methanol): theoretical [M+H$^+$] = 493.3455, measured = 493.3794, 494.3829, 495.3854; theoretical [M+Na$^+$] = 515.3654, measured = 515.3615, 516.3646. λ_{max} (CH_3CN)/nm 269 (ε/dm^3 mol^{-1} cm^{-1} 9844), 328 (8311). mp 180-182 °C

Synthesis of *N,N'*-(3,5-di-*tert*-butyl-2-hydroxysalicydene)ethylenediamine manganese chloride 43

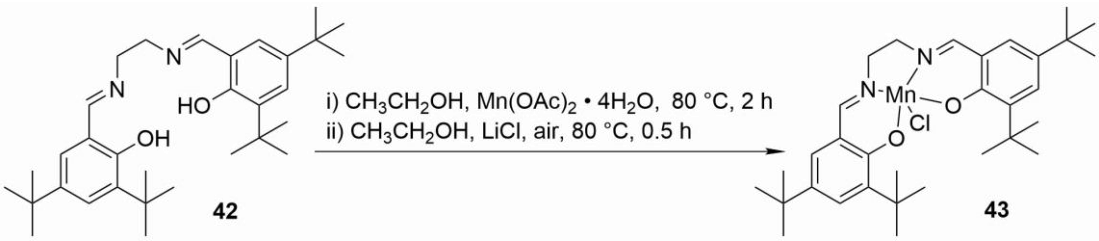

In a solution of hot ethanol (10 mL) were added *N*,*N'*-(3,5-di-*tert*-butyl-2-hydroxysalicydene) ethylenediamine **42** (100 mg, 0.2 mmol) and manganese(II) acetate tetrahydrate (107 mg, 0.4 mmol). The solution instantly became brown and was stirred under reflux for 2 hours. LiCl (25 mg, 0.6 mmol) was then added. The solution was stirred under reflux for a further 0.5 hour under air. The reaction was cooled down to 0°C then cold water (5 mL) was added dropwise. The ethanol was removed under vacuum to allow the product to precipitate. The product was then filtered, washed with cold water (5 mL) and dried yielding a brown solid (111 mg, 96 %). The protocol was adapted from Zhang and Jacobsen[148].

ESI-MS (in methanol): theoretical [M+H$^+$] = 545.2934, measured = 545.2930. ICP-MS analysis, ratio Mn/ligand = 93 %. λ_{max} (CH_3CN)/nm 259 (ε/dm^3 mol^{-1} cm^{-1} 31022), 418 (5067).

Synthesis of *N*,*N'*-(2,5-dihydroxysalicydene)ethylenediamine 44

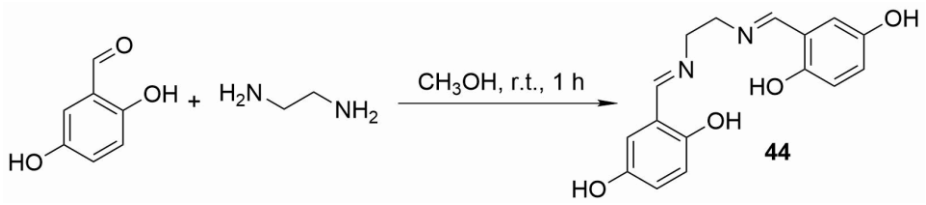

To a solution of 2,5-dihydroxybenzaldehyde (2.76 g, 20 mmol) in methanol (20 mL) was added dropwise ethylenediamine (0.60 g, 0.667 mL, 10 mmol). The solution instantly became orange and was stirred at room temperature for 1 h. The orange slurry was then filtered and washed with ethanol (20 mL) without further purification. The product was then dried under vacuum and obtained as an orange solid (2.91 g, 97 %).

^{1}H NMR (300 MHz, *d*$_6$-DMSO) δ = 12.50 (s, 2H, OH), 8.97 (s, 2H, OH) 8.48 (s, 2H, CH), 6.80-6.70 (m, 6 H), 3.88 (s, 2H, CH_2). ^{13}C NMR (400 MHz, *d*$_6$-DMSO) δ = 167.0, 153.4, 149.7, 120.3, 118.9, 117.3, 116.9, 59.5. ESI-MS (in methanol): theoretical [M+H$^+$] = 301.1183, measured = 301.1184; theoretical [M+Na$^+$] = 323.1002, measured = 323.1005. λ_{max} (CH_3CN)/nm 285

(ε/dm^3 mol^{-1} cm^{-1} 15600), 351.5 (10067). mp 244-246 °C. This product was synthesized as described by Frost *et al.*[183]

Synthesis of *N*,*N'*-(2,5-dihydroxysalicydene)ethylenediamine manganese chloride 45

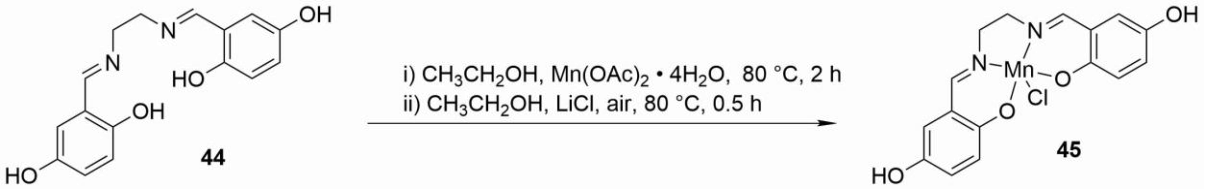

In a solution of hot ethanol (10 mL) were added *N*,*N'*-(2,5-dihydroxysalicydene) ethylenediamine **44** (100 mg, 0.33 mmol) and manganese(II) acetate tetrahydrate (177 mg, 0.66 mmol). The solution instantly became brown and was stirred under reflux for 2 hours. LiCl (42 mg, 0.99 mmol) was added and the solution was then stirred under reflux for a further 0.5 hour. The solution was cooled down to 0°C then cold water (5 mL) was added dropwise allowing the precipitation of the product. The product was then filtered and washed with water yielding a brown solid (75 mg, 59 % yield).

ESI-MS (in methanol): theoretical [M+H$^+$] = 353.0329, measured = 353.0322. ICP-MS analysis, Mn/ligand = 92 %. λ_{max} (CH_3CN)/nm 257 (ε/dm^3 mol^{-1} cm^{-1} 17244), 449 (2689). This protocol was adapted from Zhang and Jacobsen.[148]

Synthesis of *N*-(5-(3-maleimidopropionic ester)-2-hydroxysalicydene)-*N'*-(3,5-di-*tert*-butyl-2-hydroxysalicydene)ethylenediamine 46

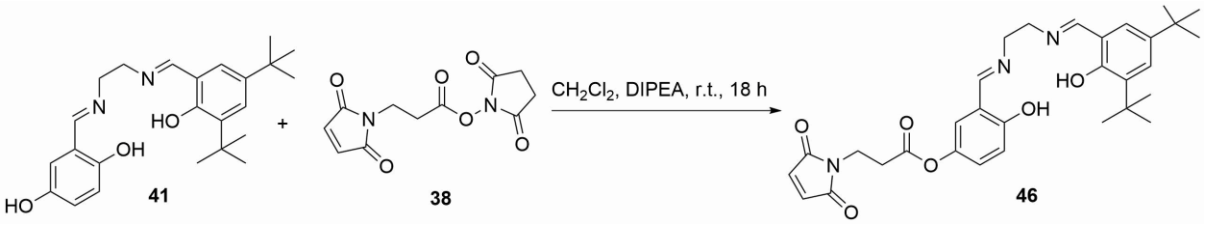

To a solution of *N*-(2,5-dihydroxysalicydene)-*N'*-(3,5-di-*tert*-butyl-2-hydroxysalicydene) ethylenediamine **41** (30 mg, 0.08 mmol) and 3-maleimidopropionic-*N*-hydroxysuccinimide ester **38** (43 mg, 0.16 mmol) in anhydrous dichloromethane (9 mL) was added a solution of DIPEA (25 mg, 35 µL, 0.2 mmol) diluted in anhydrous dichloromethane (1 mL). The reaction was left stirring at room temperature for 18 h then dichloromethane (10 mL) was added and the solution was transferred to a separating funnel. Water (20 mL) was added then the phases

were separated. The aqueous phase was further extracted with dichloromethane (3 x 10 mL) then the organic phases were combined. The organic solution was washed with brine (20 mL) then dried over Na_2SO_4. After filtration, the solvent was evaporated under vacuum and the product was purified by column chromatography (SiO_2, 30 g) using hexane/ethyl acetate 80/20 yielding a pale-yellow solid (22 mg, 51 %).

^{1}H NMR (300 MHz, *d*$_6$-DMSO) δ = 1.26 (s, 9H, CH_3), 1.36 (s, 9H, CH_3), 2.82 (t, *J* = 6.9 Hz, 2H, CH_3), 3.77 (t, *J* = 6.9 Hz, 2H, CH_2), 3.92 (s, 4h, CH_2), 6.88 (d, *J* = 8.9 Hz, 1H, CH_2), 7.05 (s, 2H, CH=CH), 7.08 (dd, *J* = 2.9, 8.9 Hz, 1H, CH), 7.21 (d, *J* = 2.9 Hz, 1H, CH), 7.25 (d, *J* = 2.4 Hz, 1H, CH), 7.30 (d, *J* = 2.4 Hz, 1H, CH), 8.58 (d, *J* = 5.5 Hz, 2H, HC=N), 13.26 (s, 1H, OH), 13.95 (s, 1H, OH). ^{13}C NMR (75 MHz, *d*$_6$-DMSO) δ = 31.7, 33.1, 33.7, 34.3, 35.0, 118.1, 118.9, 126.1, 126.8, 136.1, 140.0, 158.7, 166.6, 168.7. ESI-MS (in methanol): theoretical [M+H$^+$] = 548.2758 measured = 548.2772; theoretical [M+Na$^+$] = 570.2584, measured = 570.2575. λ_{max} (CH_3CN)/nm 258 (ε/dm^3 mol^{-1} cm^{-1} 7756), 325 (2778). mp 212-214 °C.

Synthesis of *N*-(5-(3-maleimidopropionic ester)-2-hydroxysalicydene)-*N'*-(3,5-di-*tert*-butyl-2-hydroxysalicydene)ethylenediamine manganese chloride 31

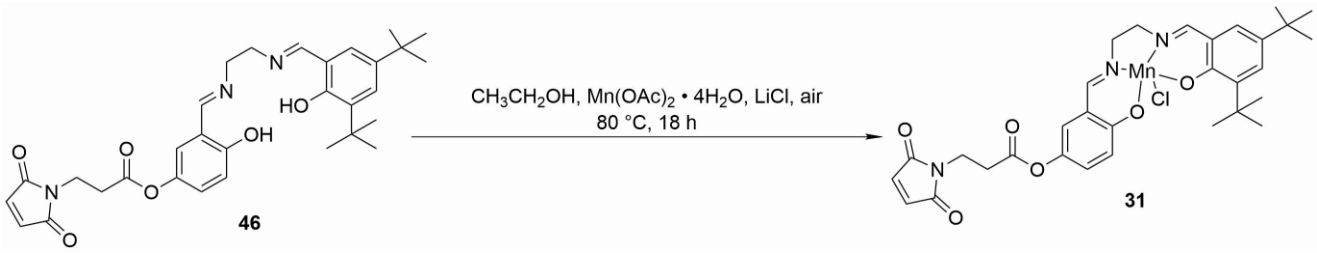

The product was synthesized as described by Reetz *et al.*[70b]. To a solution of *N*-(5-(3-maleimidopropionicester)-2-hydroxysalicydene)-*N'*-(3,5-di-*tert*-butyl-2-hydroxysalicydene) ethylenediamine **46** (20 mg, 0.037 mmol) and manganese acetate tetrahydrate (18 mg, 0.074 mmol) in methanol (4 mL) was added a solution of LiCl (1.6 mg, 0.037 mmol) diluted in methanol (1 mL). The reaction was left stirring at room temperature for 18 h. The solvent was then evaporated under vacuum and the brown slurry was solubilised in dichloromethane (10 mL) and transferred on a separating funnel. The organic phase was washed with brine (5 mL) and the phases were separated. The aqueous phase was further extracted with dichloromethane (5 mL). The organic phases were combined, and the solvent was evaporated under vacuum, yielding a brown solid (21 mg, 90 %). ESI-MS (in methanol): theoretical [M+H$^+$]

= 600.1906 measured = 600.1903. ICP-MS analysis, ratio Mn/ligand = 96 %. λ_{max} (CH_3CN)/nm 285 (ε/dm^3 mol^{-1} cm^{-1} 10178), 318 (8911), 418 (3622).

7.2.2 Protein expression and purification

The plasmid containing the mouse recombinant heavy chain K68C apoferritin (K68C-Aft) was obtained from Prof. Neil R. Thomas[184]. The gene was inserted into pJexpress414 vector, which provided IPTG-inducible transcription, ampicillin resistant and an N-terminal His-tag on the protein. *Escherichia coli* BL21 (DE3) competent cells were transformed with the plasmid, by following the manufacturer's protocol for heat shock transformation (42 °C for 40 s for 50 µL of competent cells with 50 ng DNA). Once transformed, the cells were grown in 200 µL SOC growth medium at 37 °C for 1 h at 250 rpm.

The transformed cells were plated on an autoclaved solid medium, composed of LB-agar and carbenicillin (50 µg/mL), in a Petri dish, and grown overnight at 37 °C. Afterwards, the plates were stored at 4°C for a maximum of one week.

To extract and purify the recombinant apoferritin gene, one colony of the transformed cell was transferred into a liquid media LB-carbenicillin (10 mL, 50 µg/mL carbenicillin) and grown overnight at 37 °C at 250 rpm. The cells were pelleted at 14000 x g at 4 °C and the supernatant was discarded. The DNA was extracted using GenElute Plasmid MiniPrep® kit (Sigma-Aldrich), following manufacturer instructions. Purified DNA concentrations were assessed by Nanodrop analysis, giving a 50.4 ng/µL, a 260/280 absorbance ratio of 1.92 and a 260/230 absorbance ratio of 2.05, indicating acceptable purity for sequencing. The DNA solution was stored at -20 °C.

K68C-Aft was expressed from freshly transformed cells, plated on solid medium. A single colony was inoculated in LB-carbenicillin medium (100 mL, containing 50 µg/mL carbenicillin) and incubated overnight at 37°C at 250 rpm. From this preculture, a suitable volume was transferred to LB-carbenicillin medium (1 L, containing 50 µg/mL carbenicillin) to obtain a starting OD_{600} of 0.1. The culture was incubated at 37°C and 250 rpm shaking until the OD_{600} reached 0.8. Protein expression was induced with 0.5 mM IPTG, followed by incubation overnight at 30°C at 180 rpm shaking. The cells were then pelleted by centrifugation at 5000 x *g* (4°C, 10 min), the supernatant was discarded, the cell pellets were resuspended with 5 mL IMAC binding buffer (20 mM Tris, 300 mM NaCl, 10 mM imidazole, pH 8.0.) and stored at -80°C.

The thawed pellets were disrupted by passing 5 times at 25000 psi through a cell disruptor. The cell debris were removed by centrifugation at 15000 x *g* (4°C, 20 mins) to yield the cell soluble fraction. From the soluble fraction, K68C-Aft was purified using a HisTrap FF® crude 5 mL column (GE Healthcare), using a gradient with elution buffer (20 mM Tris, 300 mM NaCl, 2 M imidazole, 1 mM DTT, pH 8.0) The purified K68C-AFt was dialysed at 4 °C overnight in dialysis buffer 1 (20 mM Tris, 1 mM EDTA, pH 10.3) then 4 hours in dialysis buffer 2 (20 mM Tris, pH 10.3). Recombinant apoferritin was characterised by MALDI-TOF, after mixing with an equal volume of saturated sinapic acid solution (acetonitrile:0.1 % TFA 1:1). The yield of protein expression was up to 35 mg protein per litre of cell culture. The same process was applied to the expression and purification of the mouse heavy chain wild-type apoferritin (WT-Aft), resulting in an equivalent yield.

7.2.3 Quantitative determination of protein concentration

Protein concentration was determined using Lowry assay with DC Assay Reagent Kit (BioRad). A volume of protein in aqueous medium (5 µL) was poured into a 96-wells plate. The DC Assay Reagent A was added (20 µL) and mixed, then DC Assay Reagent B was added (175 µL) and mixed. A protein concentration standard curve, spanning from 0 to 2 mg/mL of BSA was prepared in the same way during each set of measurement. Each sample was measured in triplicates, at a wavelength of 750 nm on a spectrophotometer.

7.2.3 Reduction and quantitative determination of free thiols in K68C-Aft

The buffer K68C-Aft was placed in after purification was exchanged, by overnight dialysis at 4 °C, for a urea-tris buffer (20 mM Tris, 50 mM NaCl, 8 M urea, pH 7). 50 molar equivalents of a reducing agent, TCEP, was added to the protein solution. The sample was incubated at 37 °C for 3 h. Then, an equivalent volume of cold acetone (stored at -20 °C) was added to the protein solution and was incubated at -20 °C for 30 min. The protein was centrifuged for 20 min at 16900 x *g* at 4 °C, yielding a protein pellet. The pellet was washed with cold acetone twice, then resuspended in the urea-tris buffer. This washing cycle was repeated one more time. The protein solution was stored under nitrogen up to a week at - 20°C. The proportion of free thiols was measured by Ellman assay[185], yielding an average of 73 % of free thiols.

The Ellman assay was performed by adding 18 µL of protein, in a concentration superior to 10 µM, with 4 µL of a DTNB solution (4 mg/mL in Ellman buffer) and 178 µL of Ellman buffer (100

mM sodium phosphate, 1 mM EDTA, pH 8.0). The solution was briefly mixed and incubated at room temperature for 15 min. The absorbance was measured at 412 nm. The proportion of free thiols was determined by using the following equation:

$$[free\ SH] = \frac{\left(A_{sample} - A_{control}\right) \times 10^9}{14150 \times 90}$$

Where A_{sample} represents the absorbance value at 412 nm of the protein sample, $A_{control}$ represents the absorbance value of the protein buffer at 412 nm (as a blank), 10^9 and 90 represent the dilution factors as well as change of unit between molar and micromolar, and 14150 is the molar extinction coefficient of TNB^-.

7.2.4 Conjugation of apoferritin with manganese-salen complex by Michael addition

After cysteine reduction, K68C-Aft was treated with 10x molar excess of manganese-salen complex (from a 100 mM stock in acetonitrile), with a final concentration of acetonitrile of 2 %. The suspension was mixed and incubated for 3 h at 37 °C. The solution was then centrifuged to remove excess manganese-salen **31**. Then, the buffer was exchanged on a PD-10 desalting column, equilibrated with 150 mM NaCl at pH 3. The conjugate [K68C-Mn-salen-Aft] was analysed as such, or mixed with the wild-type mouse heavy-chain apoferritin WT-AFt in a ratio of conjugate:wild-type sub-units of 1:23 or 2:22. The conjugate was analysed by SDS-PAGE, showing a band around 25 kDa. MALDI-TOF (same method as for K68C-Aft) allowed more accurate measurement: Theoretical mass: 24971 Da, measured mass: 24651 Da. ICP-MS analysis showed up to 92 % of [Mn]/[protein] ratio. Lowry assay[186] showed a protein recovery of up to 87 % with up to 87 % conjugation efficiency, as determined by Ellman assay.

7.2.5 Sulfoxidation catalysed by manganese-salen complexes

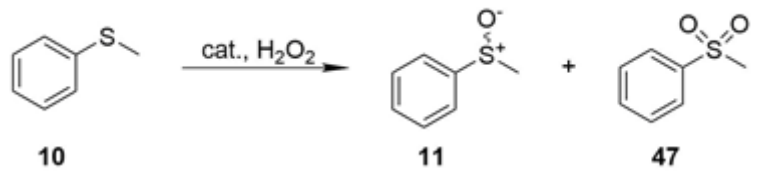

10 **11** **47**

To a solution of thioanisole (10 mM) and manganese-salen (0.1 mM, 1 mol %), in water or acetonitrile, was added hydrogen peroxide (10 mM, 1 equivalent). The reaction mixture was stirred for 5 h at 20 °C. Reactions in acetonitrile were dried with a gentle nitrogen flow, to

remove the solvent. Reactions in water were extracted three times with diethyl ether. The product solution in diethyl ether was then dried with $MgSO_4$ and filtered. The solvent was then dried with a gentle nitrogen flow. The product was dissolved in ethyl the catalyst was removed on a silica pad, using ethyl acetate as mobile phase. The solvent was evaporated with a gentle nitrogen flow, then the product was dissolved in deuterated chloroform for ^1H NMR analysis, as it is a reliable method for relative quantification of products.

Thioanisole (PMS): ^1H NMR (300 MHz, $CDCl_3$) δ = 2.42 (s, 3H), 7.11 – 7.16 (m, 5H). Phenyl methyl sulfoxide (PMSO): ^1H NMR (300 MHz, $CDCl_3$) δ = 2.73 (s, 3H), 7.48-7.53 (m, 3H), 7.63-7.68 (m, 2H). Phenyl methyl sulfone ($PMSO_2$): ^1H NMR (300 MHz, $CDCl_3$) δ = 3.04 (s, 3H), 7.54-7.66 (m, 3H), 7.92 (d, *J* = 7.5 Hz, 2H).

7.2.6 Sulfoxidation catalysed by apoferritin conjugate

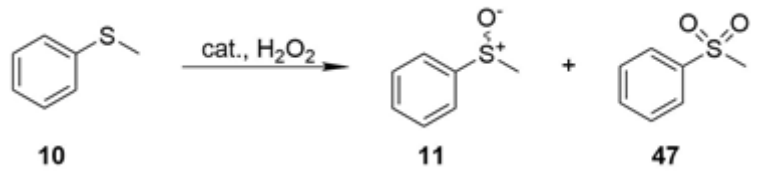

To a solution of thioanisole (2.5 mM) in 50 mM sodium phosphate (at pH 3 to 11) and apoferritin conjugate (0.05 mM, 2 mol %), was added hydrogen peroxide (2.5 mM, 1 equivalent). The reaction mixture was stirred for 20 h at 20 °C. The product was then extracted three times with diethyl ether then dried with $MgSO_4$ and filtered. The solvent was evaporated with a gentle nitrogen flow, then the product was dissolved in hexane/isopropanol 90/10 for HPLC analysis on an OD-H chiral column, using hexane/isopropanol 90/10 as mobile phase, with a flow of 0.5 mL/min and absorbance reading set at 254 nm. In these conditions, thioanisole (PMS) retention time was t = 8.4 min. For phenyl methyl sulfoxide's (PMSO) enantiomers, retention times were t_R 23.6 min, t_S = 26.1 min. For phenyl methyl sulfone ($PMSO_2$), the retention time was t = 28.7 min (See Appendix 3).

8. RESULTS

8.1 Synthesis of a maleimide-tagged salen

Covalent attachment of a manganese-salen to the free thiol of the Aft K68C could be performed using different bioconjugation strategies [44, 60]. Bioconjugation with a maleimide anchor was selected because this linker reacts efficiently and specifically with thiols at pH 7 through a straightforward procedure[187], and provides a stable covalent bond between the protein and the ligand[69]. Moreover, Reetz *et al.* reported a similar strategy to covalently attach a manganese-salen to the free thiol in the papain active site [70b]. A non-symmetrical salen ligand **46** was designed bearing a maleimide linker on one of the aromatic imine units, whilst the other imine was functionalised with two *tert*-butyl groups. These are known to give manganese-salen complexes with good activities as shown by Jacobsen's work [149, 154].

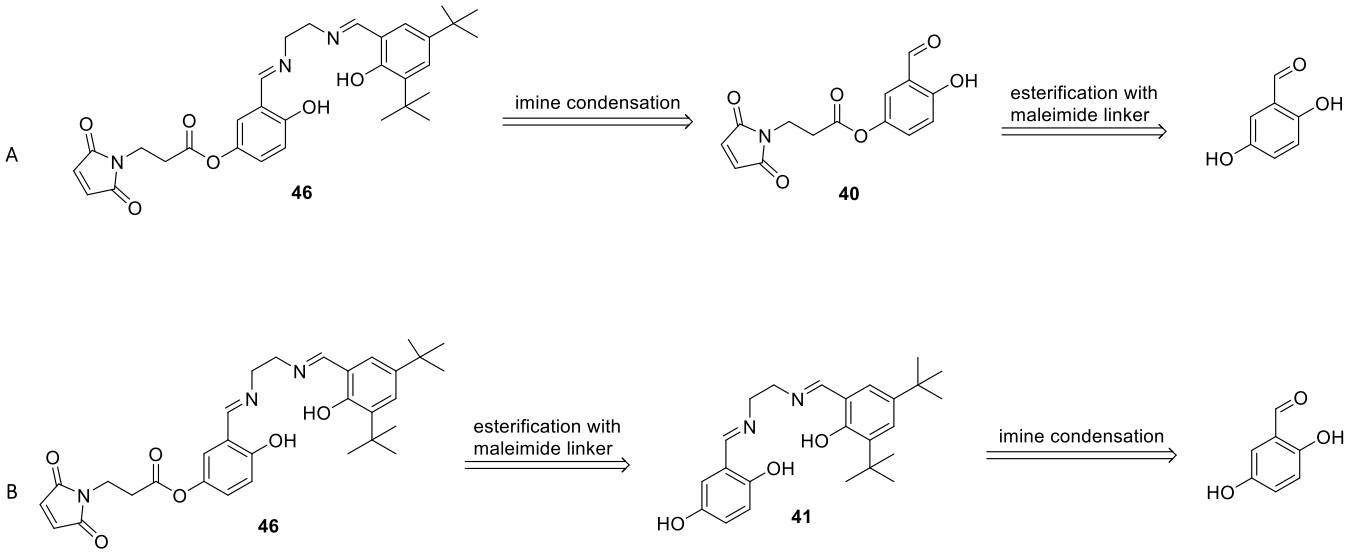

Scheme 28: Retrosynthesis analysis of the two synthetic routes to prepare a maleimide-bearing salen. Whilst in synthetic route **A**, the esterification with maleimide linker was performed first, then the salen was prepared by imine condensation, in synthetic route **B**, the salen was prepared first by imine condensation and only then, the maleimide linker was added by esterification.

Two synthetic routes were designed for the synthesis of a salen ligand tagged with maleimide linker **46** (Scheme 28). In both routes, the maleimide linker was to be introduced by esterification between maleimide propionic acid and a phenol group. In synthetic route (**A**), the aim was to perform the esterification with the benzaldehyde precursor prior to the synthesis of the non-symmetrical salen **46** by imine condensation, following what was developed by Pordea *et al.* in the design of a biotinylated-salen[44]. Synthetic route (**B**)

consisted in synthesizing the salen ligand **41** first before coupling it with the maleimide propionic acid linker by esterification. Both synthetic routes were explored in parallel but given previous difficulties in synthesizing and purifying the non-symmetrical salen, synthetic route **A** was prioritized.

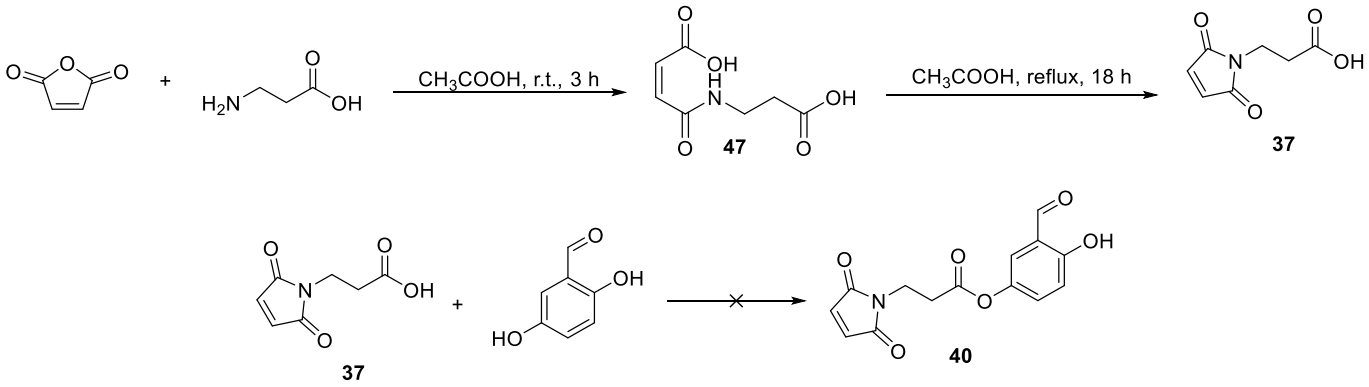

Scheme 29: Reaction synthesis for maleimide linker **37** and attempted synthesis of benzaldehyde ester **40** by ester coupling.

Initially, the synthesis of maleimide-tagged aldehyde **40** was attempted by direct esterification with 3-maleimidopropionic acid **37** (Scheme 29). Firstly, maleimide propionic acid **37** was synthesized. Interestingly, this compound was always obtained as a mixture with a non-identified contaminant (2 %, estimated by NMR) which was not reported in the literature. Following longer reaction times and several attempts of purification with various methods (aqueous work-up, acid-base work-up, precipitation in diethyl ether, column chromatography) the contaminant was still observed in the same proportion. Therefore, the compound was used as such without further purification.

Nevertheless, the synthesis of **40** by ester coupling of 2,5-dihydroxybenzaldehyde with maleimide linker **37** was unsuccessful (Scheme 29), despite several attempts using different coupling reagents (DCC, DIC, EDC), catalysts (DMAP, HOBt) and bases (Et_3N, DIPEA).

Given the difficulties to perform the ester coupling with the maleimide propionic acid **37**, a model reaction was performed to assess the reactivity of the 2,5-dihydroxybenzaldehyde towards ester coupling (Scheme 30). An ester coupling with propionic acid was performed. Compound **39** was synthesized with moderate yield (46 %) without optimisation of the reaction and NMR analysis showed the ester coupling occurred on the phenol hydroxyl group, at position 5 of the 2,5-dihydroxybenzaldehyde. This was confirmed as the ^1H NMR shift for the OH in position 2 was observed at 10.60 ppm whilst the shift for the OH in position 5 was

observed at 4.70 ppm, and only the latter shift was not observed in the final product. Therefore, it was hypothesized that the reactivity of the carboxylic acid function of the maleimide linker **37** was responsible for the lack of ester formation.

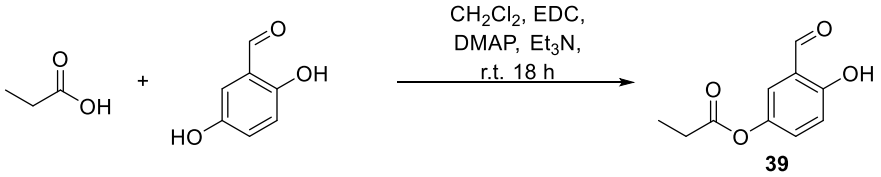

Scheme 30: Model reaction for the ester coupling of 2,5-dihydroxybenzaldehyde with propionic acid.

It was then decided to synthesize the maleimide propionic acid *N*-hydroxysuccinimide ester **38** (Scheme 31). Despite adding one more step in the synthesis, this compound has the advantage to bear an activated ester, and therefore does not need a coupling reagent to couple with a hydroxyl group. Compound **38** was synthesized in reasonable yield (50 %), compared to the literature [67].

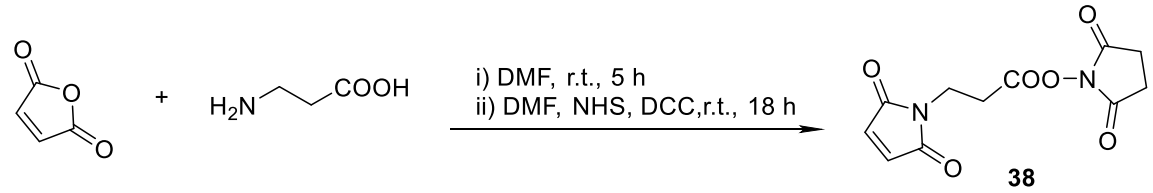

Scheme 31: Reaction scheme for the synthesis of 3-maleimidopropionic *N*-hydroxysuccinimide ester linker **38**. This maleimide linker is activated by the presence of the *N*-hydroxysuccinimide, thus ester coupling with this compound will not require the addition of a coupling reagent.

As the esterification with *N*-hydroxysuccinimide uses dicyclohexylcarbodiimide (DCC) as coupling reagent, in a 4:1 ratio of coupling reagent:starting materials, a large amount of dicyclohexyl urea was formed. Whilst the separation of the formed urea was done by aqueous wash in many published methods [67], extensive aqueous wash of compound **38** resulted in loss of product and incomplete wash of the urea. Therefore, the product was purified by column chromatography.

Ester **40** was then synthesized *via* coupling of 2,5-dihydroxybenzaldehyde with the activated maleimide-ester **38** (Scheme 32). The ester **40** was obtained in reasonable yield (59 %) after purification by column chromatography. However, it is worth noting that this product was obtained with only 82 % purity (as determined by ^{1}H NMR), containing 2,5-dihydroxybenzaldehyde as contaminant, as both compound were difficult to elute separately. The product was used as such in subsequent reactions.

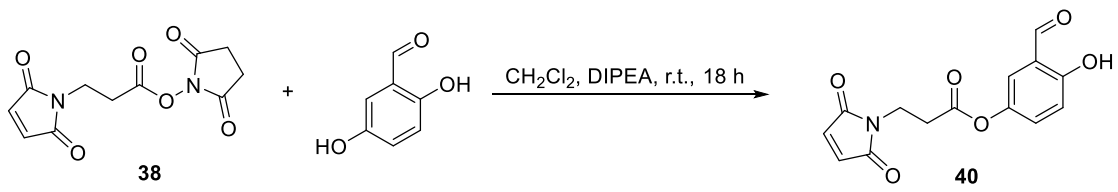

Scheme 32: Synthesis of ester **40** by coupling of maleimide linker **38** and 2,5-dihydroxybenzaldehyde

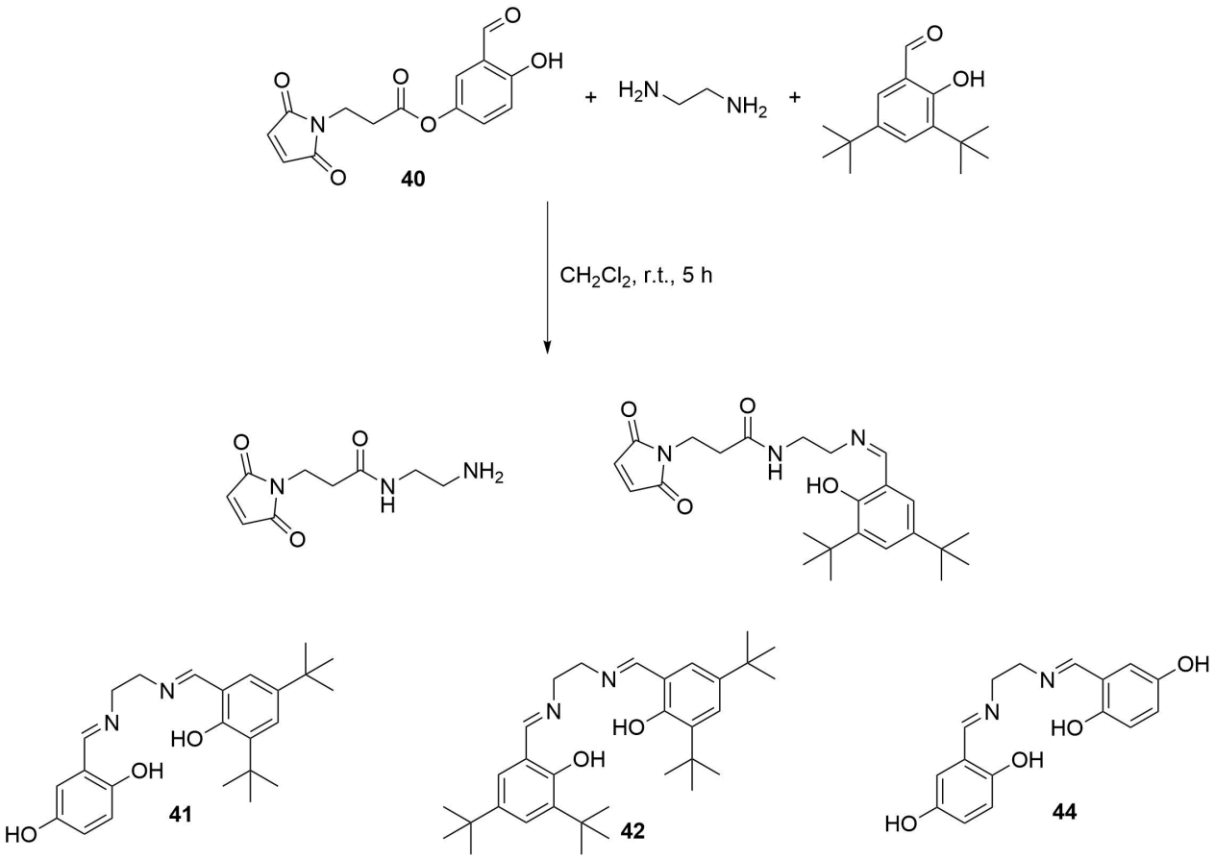

Scheme 33: Possible side-products for maleimide-tagged salen formed during the attempted synthesis of salen **41**.

The maleimide-bearing aldehyde **40** was used to synthesize salen **41**, using a procedure adapted from Reetz *et al.*[70b]. In the presence of ethylenediamine (1 equiv.), 3,5-di-*tert*-butyl-2-hydroxybenzaldehyde (1 equiv.) and a desiccant (silica gel or molecular sieves 3 Å, 10 % w/v), a non-symmetrical salen was formed. However, NMR analysis, of the crude fraction and of after separation by column chromatography, showed no presence of the maleimide linker but rather the formation of salen **44**. It was hypothesized that ethylenediamine acted as a nucleophile to attack the maleimide propionic acid esters (either aldehyde **40** or the supposedly formed salen **41**), thus yielding salen **41** (4 % yield) as a by-product, along with

the other two symmetrical salens **42** and **44** (Scheme 33). Given this issue, it was decided to perform the esterification after the synthesis of the salen, thus following synthetic route (**B**).

Therefore, 2,5-dihydroxybenzaldehyde, ethylenediamine (1 equiv.) 3,5-di-*tert*-butyl-2-hydroxybenzaldehyde (1 equiv.) and a desiccant (silica gel or molecular sieves 3 Å, 10 % w/v) were mixed and salen **41** was synthesized in a 51 % yield, along salens **42** and **44** as side-products. As reported in the literature [70b], salen **41** was sensitive to high temperature and to acidic environment, therefore the purification had to be performed very rapidly to avoid further degradation of the product. Given this issue, purification by column chromatography was optimised to first elute **42** promptly, then **41**. This was achieved by reducing the amount of silica used and using a gradient of hexane/diethyl ether as eluents. Deactivation of the silica by flowing 1 % (v/v) Et_3N in hexane through the column prior to purification of the compound was assessed, however, this yielded in the co-elution of both **42** and **41**. Performing a second separation by column chromatography led to further contamination with by-products caused by the degradation of product **41**, yielding a mix of the desired product with two of its starting materials, 2,5-dihydroxybenzaldehyde and 3,5-di-*tert*-butyl-2-hydroxybenzaldehyde.

Maleimide-tagged salen **46** was synthesized by coupling the activated maleimide ester **38** and the non-symmetrical salen **41**. As stated before, the advantage of an ester coupling reaction with such activated ester was that no coupling reagent was needed, only a base. This reaction was performed with DIPEA as a base. DIPEA has the advantage over triethylamine that its two diisopropyl chains give enough steric hindrance to decrease its nucleophilicity, reducing the probability of side-reactions to occur. After an aqueous wash allowed the separation of the base, the product was purified by column chromatography. As the salen **41** was sensitive to temperature and acidic conditions, the maleimide-tagged salen **46** was cautiously purified as well, by reducing the amount of silica used and performing the procedure rapidly. The product was obtained with 51 % yield.

8.2 Preparation of manganese salen complexes

Salen **42** and **44** were synthesized by condensation of ethylenediamine and the corresponding benzaldehyde, respectively 3,5-di-*tert*-butyl-2-hydroxybenzaldehyde and 2,5-dihydroxybenzaldehyde, to be used as model catalysts. The manganese complexes **43** and **44** (Scheme 34) were prepared according Zhang and Jacobsen procedure[148] which involved a two-step reaction.

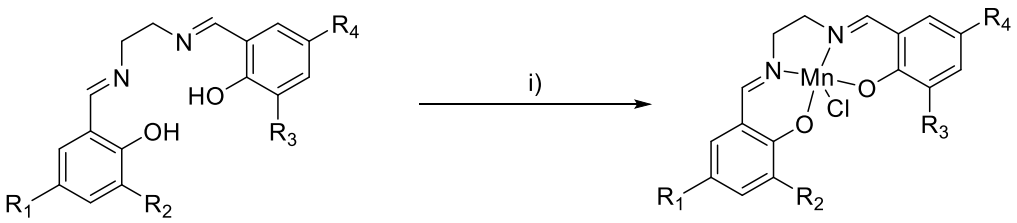

41: R_1 = maleimide linker ; R_2 = H ; R_3 = R_4 = *tert*-butyl
42: R_1 = R_2 = R_3 = R_4 *tert*-butyl
44: R_1 = R_4 = OH; R_2 = R_3 = H

31: R_1 = maleimide linker ; R_2 = H ; R_3 = R_4 = *tert*-butyl
43: R_1 = R_2 = R_3 = R_4 *tert*-butyl
45: R_1 = R_4 = OH; R_2 = R_3 = H

Scheme 34: Manganese salen complexes prepared from salen **41**, **42** and **44**.
i) CH_3CH_2OH, $Mn(OAc_2) \bullet 4H_2O$, LiCl.

First the salen was reacted with manganese acetate tetrahydrate at reflux in ethanol, then lithium chloride was added, and reflux was continued under vigorous stirring to allow oxidation of manganese(II) to manganese(III) by the air contained in the flask. Manganese-salen **43** was obtained with 96 % yield, whilst **45** was obtained with 97 % yield. Due to the moderate water solubility of product **45**, filtration using cold methanol instead of water yielded a better recovery rate. Mass spectrometry and IR spectroscopy analysis confirmed the incorporation of the metal. ICP-MS analysis were performed in order to determine the degree of manganese incorporation into the ligand. For manganese-salen **43** and **45**, the proportion of manganese ion per unit of ligand ranged from 92 to 96 %. It was observed that without vigorous stirring, the proportion of manganese per unit of ligand would dramatically decrease, down to 22 % for **45**. This is caused by the lack of oxidation of the manganese by air, thus rendering impossible the coordination with its chloride axial ligand, which stabilize the metal [170].

The maleimide-bearing manganese-salen **31** was prepared as well. However, as maleimide-bearing salen **46** was sensitive to high temperatures, stirring under reflux was not possible. Thus, the reaction was performed at room temperature for 18 h, in the same conditions of

reagent equivalence, which led to 90 % yield. The manganese content of **31** was analysed by ICP-MS, the ratio [Mn]/[ligand] was of 96 %, indicating almost full incorporation of manganese into the ligand.

The incorporation of manganese into salen ligands was also identified by UV-Vis spectroscopy (Figure 7). For each manganese-salen, **31** ; **43** ; **45**, the absorbance profile between 250 and 850 nm is different from the original salens. In each case, the maximum peak at around 350 nm for each salen is not present in the absorbance profile of manganese-salens. Whilst the maximum peak at around 255 nm is conserved in both manganese-salen **43** and **45**, in manganese-maleimide-salen **31**, the maximum peak is red-shifted to 285 nm. Moreover, a maximum followed by a decreasing slope is observed in each manganese-salen at around 450 nm, indicating the incorporation of manganese.

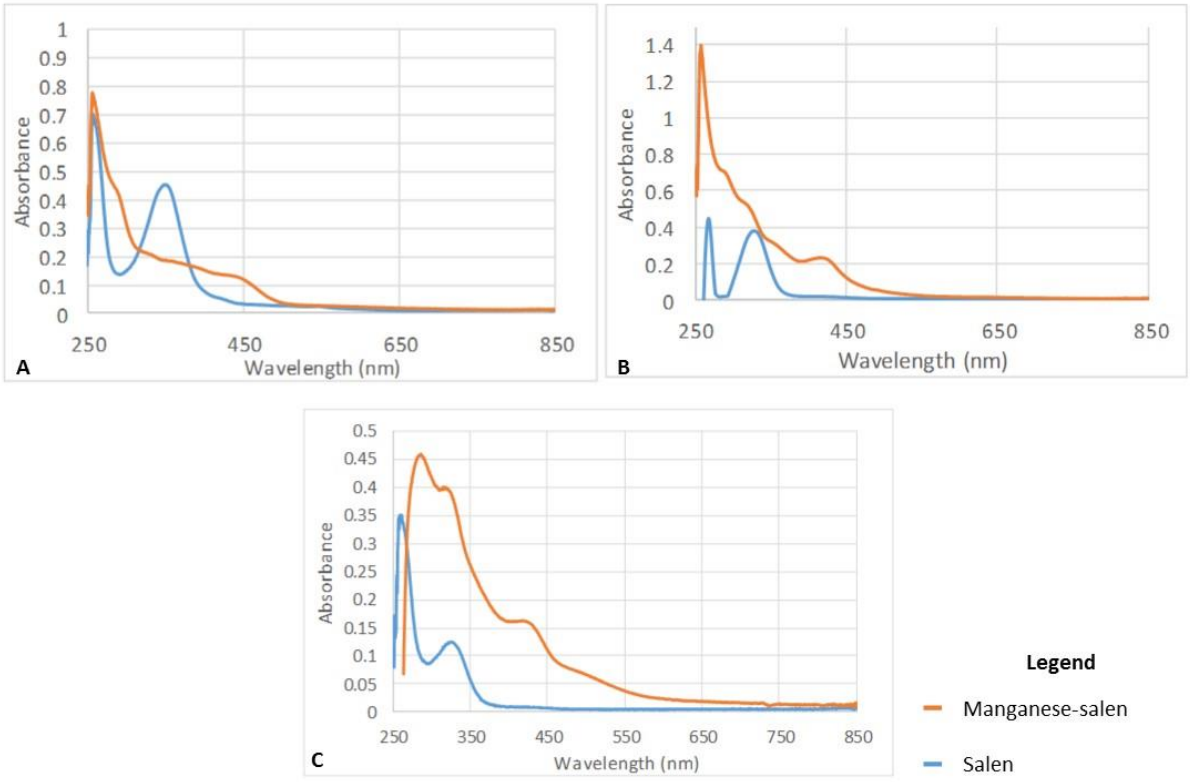

Figure 7: Absorbance spectra of manganese-salens and corresponding salens in acetonitrile superimposed. **A**. Absorbance spectra of salen **44** and manganese-salen **45**. **B**. Absorbance spectra of salen **42** and manganese-salen **43**. **C**. Absorbance spectra of maleimide-salen **46** and corresponding manganese-salen **31**.

A range of manganese-salen was synthesized, each bearing different substituents on their cyclic moieties which tune the electronical properties of manganese, which should impact their catalytic activity. Manganese-salen **31** was synthesized with a maleimide-linker as one

of its substituents to allow covalent conjugation through Michael addition with a cysteine-bearing apoferritin.

8.3 Preparation of a recombinant mouse apoferritin mutant K68C

8.3.1 Expression and purification

An apoferritin mutant bearing a unique reactive cysteine side-chain was available from Prof. Neil Thomas laboratory[184]. A heavy chain homomeric apoferritin was selected as heavy chain sub-units channels are more hydrophobic than light chains'. This was interesting for the uptake of hydrophobic or non-water-miscible substrate such as thioanisole. The crystal structure of mice heavy-chain homomeric apoferritin was available, released shortly after the start of this project, which also directed the choice of this variant (PDB: 3WNW). An interesting characteristic of this variant is also that it did not bear any cysteine, rendering the building of this mutant easier. One cysteine needed to be inserted. As the chemical catalyst needed to be inserted inside the protein's cavity, this cysteine's side-chain had to point towards the inside of apoferritin's hollow core. Position 68 was chosen as the lysine 68 was

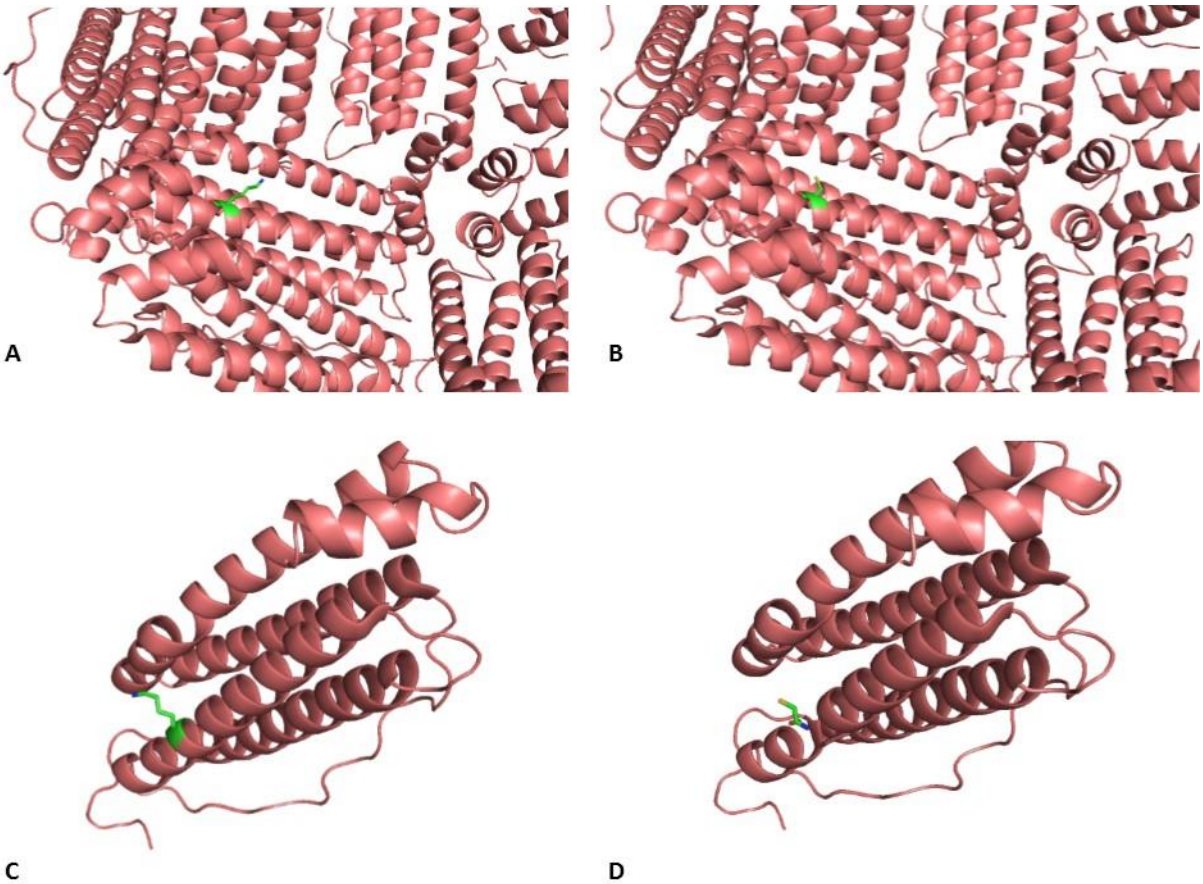

Figure 8: 3D structure of mouse heavy-chain apoferritin (PDB: 3WNW). **A**. Structure of native variant. In green, lysine 68's side chain is shown to point towards the inside of the protein's cavity. **B**. Structure of K68C mutant. In green, K68 cysteine's side-chain is shown to point towards the inside of the protein's cavity as well. **C**. Structure of a native variant sub-unit. In green, lysine 68. **D**. Structure of K68C mutant sub-unit. In green K68 cysteine.

not involved in any inter-sub-unit bond and its side chain was pointing towards the protein's cavity (Figure 8). The K68C-AFt variant was shown to have the same properties. K68C was pointing towards the protein's cavity as well and simulations with PyMol did not detect any incoherence in residues positions[188]. The gene sequence inserted into the expression vector was confirmed by sequencing (100 % match, see Appendix 1).

K68C-AFt was then expressed and purified by immobilized metal affinity chromatography (IMAC) using Ni^{2+}. DTT (1 mM) was added to the elution buffer to insure K68C-Aft free thiol would not form disulfide bond between two sub-units which led to precipitation of the protein in the conditions of IMAC purification. The quantity of protein recovered was measured by Lowry assay. K68C-Aft was recovered (70 mg), yielding 35 mg of protein recovered per litre of cell culture.

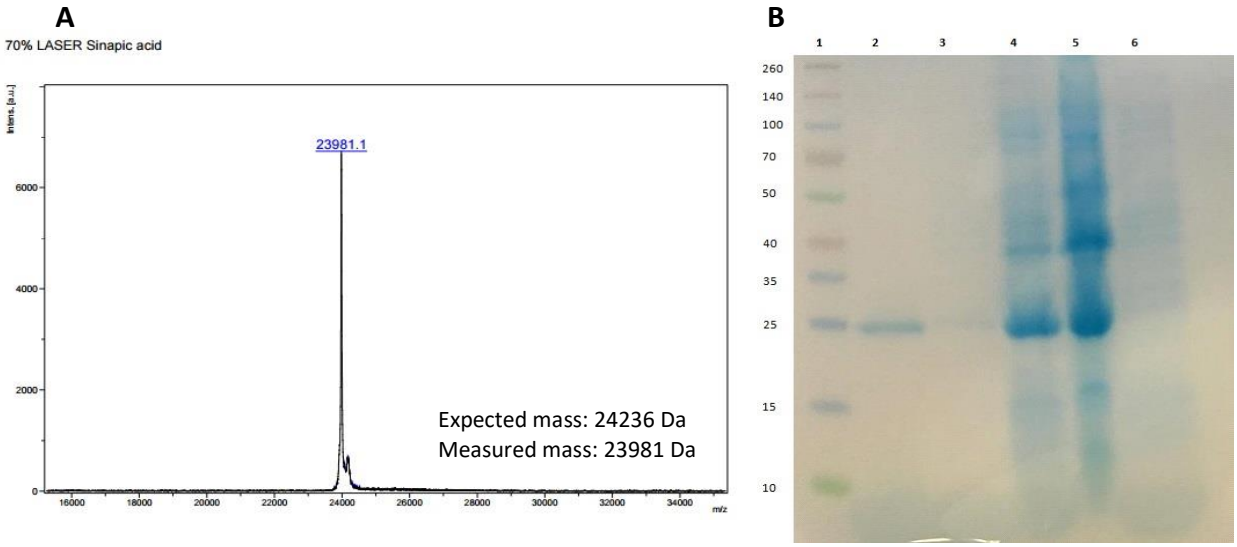

Figure 9: Characterization of mouse recombinant K68C apoferritin. A. MALDI-TOF spectrum, theoretical mass is 24.2 kDa while measured mass was 23.9 kDa. B. SDS-PAGE of purified fractions of apoferritin. 1. Protein ladder; 2. Purified apoferritin; 3. Flowthrough; 4. Soluble fraction from cell extract before purification; 5. Insoluble fraction from cell extract before purification. 6. Non-induced cells.

Purity of the protein was assessed by MALDI-TOF and SDS-PAGE. MALDI-TOF spectrum (Figure 9A) showed a single peak of high intensity at 23981 Da, lower than the theoretical mass of 24236 Da, by 255 Da. This difference was explained by the depletion of the first methionine (149 Da), a post-translational modification occurring in *Escherichia Coli*[189], and by the instrument error margin, which depends on instrument calibration. SDS-PAGE (Figure 9B) showed only one band slightly under 25 kDa, which was consistent with expected position, suggesting a purity over 90 %. It was noticed that a significant amount of protein was present

in the insoluble fraction of cell lysate (Figure 9B, lane 5). Increasing the number of cell disruption cycles, or alternative use of sonication did not increase yields. It was therefore hypothesized that this fraction of protein in the insoluble fraction of cells was due to precipitation of the protein when expressed in high concentrations.

ICP-MS analysis of the recombinant protein revealed that 0.455 µM of iron was present in the protein sample, for a protein concentration of 0.9 µM, giving an iron/protein concentration ratio of 0.51 (Table 3), after expression and purification. In order to prepare the apo form, the protein was dialysed against 20 mM Tris and 1 mM EDTA at pH 10.3 overnight at 4 °C. Then a dialysis in the same buffer without EDTA at room temperature for 2 h was used to remove the chelator. After this treatment, the concentration of iron in the protein sample was measured at 0.014 µM, for the same protein concentration as stated before, yielding a ratio of iron/protein concentrations of 0.02. In its apo form, K68C-Aft was ready to undergo chemical modifications. This chelation process was incorporated in the purification process of K68C-Aft and was always performed.

	Protein concentration (µM)	Fe concentration (µM)	Ratio [Fe]/[K68C-AFt]
K68C-AFt (without EDTA treatment)	0.90	0.455	0.51
K68C-AFt (after EDTA treatment)	0.90	0.014	0.02

Table 3: Iron content of purified K68C-Aft without or after treatment with EDTA, as measured by ICP-MS

8.3.1 Accessibility of K68C-AFt cysteine

To alkylate K68C-Aft thiol using a maleimide-bearing salen, a pH between 7 and 8.5 was necessary for efficient Michael addition[58]. Given that at this pH K68C-Aft is fully assembled[88], the size of manganese-salen complexes suggested they would not be able to enter the protein cavity by diffusion through apoferritin's pores, which diameter was measured at 6 Å[82]. Reversible denaturation of K68C-Aft using urea was used to render the thiol accessible for modification. To do so, urea (8 M) was added to the buffer used for conjugation.

To assess the concentration of free thiol available for conjugation, the Ellman assay was used. This assay relies on reaction of 5,5'-dithiobis-(2-nitrobenzoic acid) (DTNB), also known as Ellman's reagent, with a free thiol, to release TNB^-, which can be tracked by measuring

absorbance at 412 nm (Scheme 35). The known extinction coefficient of TNB^- was used to calculate the amount of reactive thiol functions available in the single cysteine mutant, K68C-Aft, as a proportion to the total amount of protein.

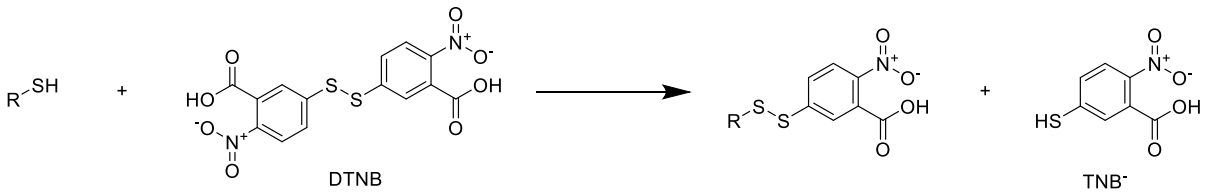

Scheme 35: Mechanism of TNB^- release during Ellman assay. DTNB oxidizes free thiols to form a disulfur bond whilst releasing a stoichiometric quantity of TNB^-, which is followed by a rise in absorbance at 412 nm.

Initial assay of free cysteines in K68C-AFt after reaction with DTNB (240 equivalent) showed that the proportion of free cysteines was very variable depending when the measurement was taken. Two separate sets of triplicate measurements of the purified protein showed 49 % and 80 % of free cysteines respectively, whilst a third set of measurement, taken after 24 h, showed 27 % of free cysteines. It was hypothesized that the amount of reduced thiol during sample preparation was variable, due to cysteine oxidation in the presence of air. However, a stable and reproducible amount of free thiols was needed to conjugate K68C-Aft with a manganese-salen.

Therefore, two reducing agents were selected, to reduce the thiols prior to Ellman assay: dithiothreitol (DTT) and *tris*(2-carboxyethyl)phosphine (TCEP) (Scheme 36). DTT is widely used for reduction of disulfide bonds in proteins and especially in sample preparation for gel electrophoresis under denaturing conditions. However, it was shown that DTT acts relatively slowly compared to phosphine-based reductant, such as TCEP, and is mostly efficient when in very high excess. Moreover, incomplete removal of DTT is likely to lead to subsequent reaction with the Ellman reagent, and with the maleimide function. On the other hand, when a ratio TCEP:maleimide higher than 1:1 was used, it was shown that TCEP could react with maleimides and prevent up to 50 % of maleimides in solution from being reactive with thiols[190].

Reduction of K68C-Aft was assessed in the presence of varying amounts of TCEP or DTT. To avoid reaction of the reducing agent with Ellman reagent or with maleimide, during subsequent bioconjugation, removal of the reducing agent was performed by precipitation of the protein and washing of the pellet, followed by re-solubilisation in Tris-urea buffer (20 mM Tris, 50 mM NaCl, 8 M urea, pH 7). When precipitation was performed with 70 % ammonium

sulfate, a high amount of protein was lost after re-solubilisation. However, when cold acetone was used, no significant loss of protein occurred. Excess reducing agents was washed twice with cold acetone after the precipitation step. Ellman assay was used to assess the amount of thiols available for bioconjugation (Table 4).

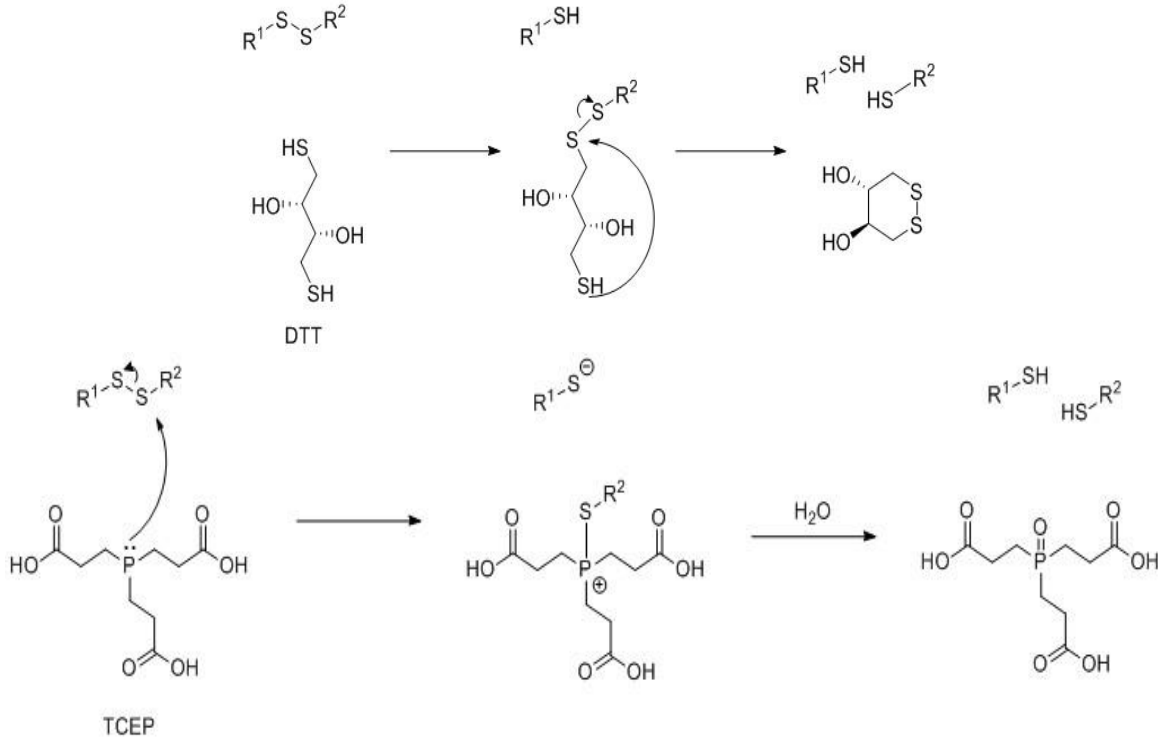

Scheme 36: Mechanism of thiols reduction by DTT (top) and TCEP (bottom)

When reduction was performed at 4 °C for 4 h, the proportion of free thiols did not exceed 34 %, despite using up to 100 equivalents excess of DTT or TCEP. The reduction was more successful when the temperature of the reaction was increased. Using 50 equivalents of DTT at 25 °C for 2 h, the amount of free thiols available for reaction with the Ellman reagent increased to 92 %, whilst using 50 equivalents of TCEP at 37 °C for 2 h yielded 73 % free thiols. However, the proportion of TNB^- released was above the quantity of thiols in solution when using 50 to 200 molar equivalents of DTT and after washing the DTT with cold acetone twice. Up to 5 washing cycles were necessary to fully remove the excess DTT. The same observation was made when using more than 200 equivalents of TCEP. When 10 equivalents of TCEP of

DTT was used, the amount of free thiol available for reaction with the Ellman reagent was decreased compared to using 50 equivalents.

Reducing agent	Molar equivalent	Temperature	Proportion of free thiols (%)
TCEP	10	4 °C	27
	10	20 °C	68
	50	4 °C	33
	50	20 °C	73
	200	20 °C	>100*
DTT	10	4 °C	24
	10	20 °C	38
	50	4 °C	29
	50	20 °C	92
	200	20 °C	>100*
-	-	20 °C	27

Table 4: Proportion of free thiols measured by Ellman assay at 412 nm, after reduction with DTT or TCEP. *A value above 100 % indicates that the entirety of reducing agents has not been washed by cold acetone after two washing cycles and reacts with DTNB. When using >50 molar equivalent of DTT, more than two washings were necessary to remove the excess, lowering the amount of protein recovered.

In conclusion, reduction with 50 molar equivalents of TCEP at 37 °C for 2 h became the method of choice to efficiently reduce K68C-Aft cysteine before conjugation.

As mentioned previously, cysteines are oxidized in the presence of air, forming disulfur bonds. After developing a method for the controlled reduction of apoferritin's cysteine prior to conjugation with a manganese salen catalyst, it became clear that leaving a reduced protein sample in contact with air would oxidize its cysteines back to their original state, annulling the effect of the reduction step. In order to measure the extent of this phenomenon, two samples were reduced with 50x TCEP for 2 h at 37 °C, using the method described above. One sample was incubated in air and on ice for 1 h, whilst the other was flushed with nitrogen, then sealed. Both samples were stored at 4°C for 6 h, then the proportion of free thiols was measured. The original sample showed 75 % free thiols immediately after reduction. The sample incubated in air saw its proportion of free thiols declining to 29 % after incubation, whilst the proportion of free thiols in the sample incubated under nitrogen displayed a steady amount of free thiols of 72 %. After this experiment, K68C-Aft were always flushed with nitrogen after reduction and throughout the conjugation process.

In conclusion, prior to conjugation with a maleimide-bearing complex, K68C-Aft was reduced by 50 equivalents of TCEP for 2 h at 37 °C in a Urea-Tris buffer. After reduction, the protein was precipitated with cold acetone and the pellet washed twice with cold acetone in order to remove excess TCEP, the cycle was repeated twice. The pellet was then resuspended in the Urea-Tris buffer before nitrogen was flushed into the sample to avoid oxidation of cysteines. The proportion of free thiols measured before reduction and after removal of excess reductant using absorbance-based Ellman assay.

8.4 Conjugation

8.4.1 Effect of organic solvents on the protein

The maleimide-bearing manganese salen complex **31** designed for bioconjugation with K68C-Aft was not soluble in water and therefore covalent attachment had to be performed in a buffer-organic solvent homogeneous mixture. Two solvents were used: acetonitrile and dimethyl sulfoxide.

The effects of organic solvents on proteins are multiple and well demonstrated[191]. The major consequence is the precipitation of the protein. In order to assess the effect of these organic solvents on K68C-AFt, different volume ratios of acetonitrile or dimethyl sulfoxide were added to a buffer containing 2 mg/mL of protein. Samples were incubated at 4 °C for 16 h in Urea-Tris buffer. After incubation, the sample were centrifuged, and the concentration of soluble protein was measured to assess protein recovery (Figure 10).

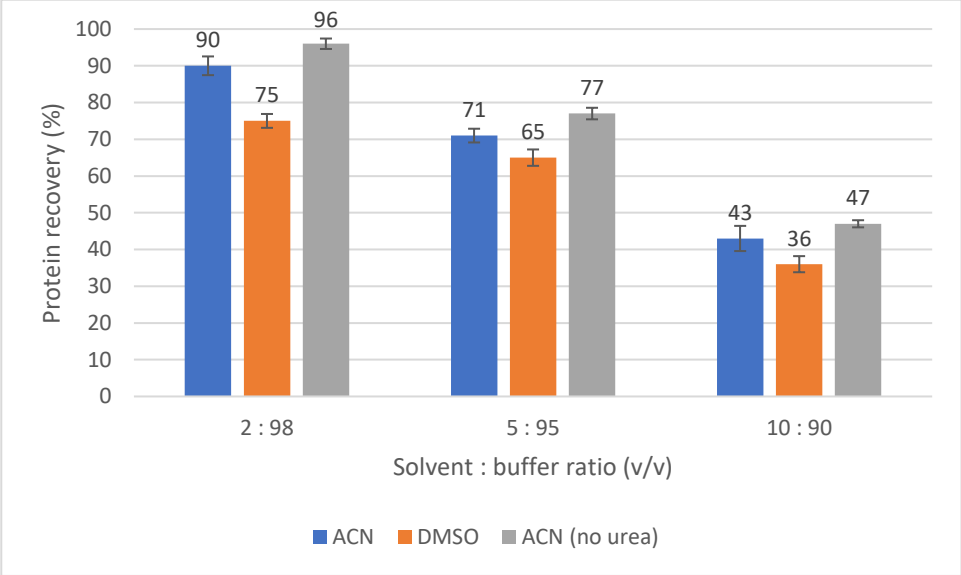

Figure 10: Protein recovery after incubation with varying amounts of organic solvents, DMSO and acetonitrile, for 16 h at 4 °C. Protein concentrations were measured by Lowry assay at 750 nm.

It was observed that the presence of both organic solvents induced protein loss. Nevertheless, the protein recovery in presence of acetonitrile was significantly higher than using DMSO. When 2 % (v/v) organic solvent was used, the protein recovery was 90 % and 75 % for acetonitrile and dimethyl sulfoxide respectively. Thus, acetonitrile was preferred as co-

solvent for covalent conjugation. The protein recovery dropped in presence of more than 5 % (v/v) organic solvent, therefore the maximum amount of cosolvent used was 2 %.

The same experiment was performed in a buffer devoid of urea, which kept the protein folded and assembled. In that case, the protein recovery was higher than in presence of the same solvent, acetonitrile, and urea-containing buffer. These results proved that, once assembled, apoferritin nanocapsules are more resistant to organic solvents effects, which could make them more difficult to modify chemically.

8.4.2 Development of conjugation conditions

After reduction under the conditions stated above, K68C-AFt apoferritin was to be conjugated via Michael addition of its free cysteine with the maleimide-bearing manganese salen complex (Scheme 37).

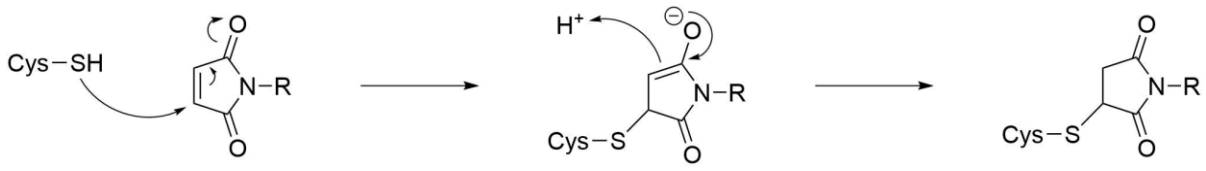

Scheme 37: Mechanism of the Michael addition of K68C-Aft cysteine with a maleimide linker, at pH 7 – 8.5. R = catalyst moiety.

First attempts were performed at 4 °C for 16 h (Figure 11). The amount of catalyst added varied between 5x and 200x molar equivalent in 5 % (v/v) acetonitrile in urea-Tris buffer. After incubation, the samples were dialysed against a Tris buffer (20 mM Tris, 50 mM NaCl, pH 7) to remove urea and excess Mn-salen, so that the conjugate could refold and reassemble as a nanocapsule.

When 5x molar equivalent of manganese-salen complex were used for bioconjugation, the protein recovery was only 60 %. This number lowered to 43 % at 10x molar equivalent and dropped to 0 % at higher molar equivalent of catalyst. Moreover, MALDI-TOF analysis revealed only recombinant protein was present in these samples and no conjugate could be observed. This conclusion was confirmed by Ellman assay results, which showed that the proportion of free thiols relative to the protein concentration did not diminish significantly after the incubation manganese-salen.

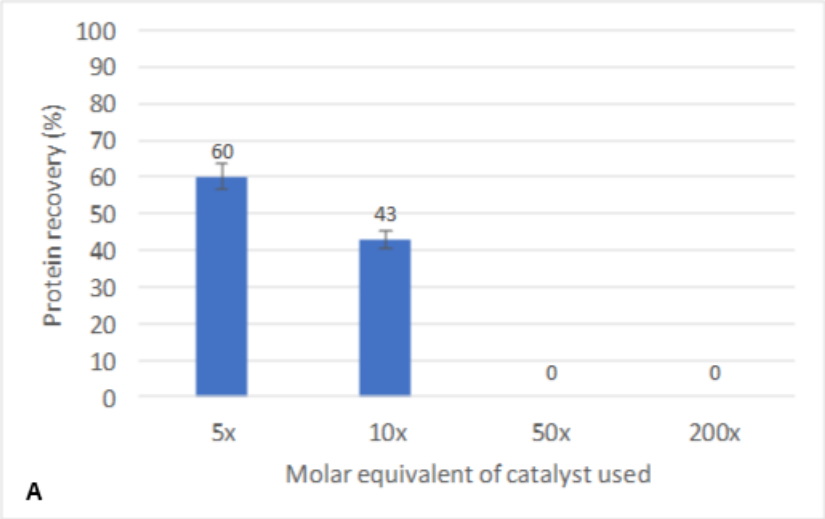

A

	Proportion of free thiols (%)
After reduction	75
5x	64
10x	62

B

Figure 11: Preliminary results of bioconjugation of K68C-Aft with various molar equivalence of manganese-salen for 16 h at 4 °C. **A**. Protein recovery after incubation measured by ratio [protein recovered concentration]/[initial protein concentration], measured by Lowry assay at 750 nm. **B**. Proportion of free thiols measured by Ellman assay at 412 nm.

These preliminary experiments suggested that the higher molar equivalent of catalyst used, the lower the amount of protein was recovered. The use of low molar equivalent resulted in little precipitation, but no cysteine modification. Therefore, it was decided to vary the physical parameters of the reaction, temperature, and time. According to the literature, cysteine alkylation by Michael addition reached completion at 37 °C within few hours[58]. Therefore, it was decided to perform this reaction at 37 °C and assess the completion of conjugation through measuring the proportion of free thiols over 3 h and 6 h by Ellman assay (Table 5). Upon incubation with 10x molar equivalent catalyst for 3 h and 6 h, the amount of free thiols dropped to from 81 % to 25 % and 33 %, respectively with a protein recovery of 53 %. When 50x molar equivalent of catalyst was used, the amount of free thiols measured after 3 h and 6 h was of 0 % and 25 %, respectively. However, as shown previously, when using 50x molar equivalent of catalyst, the protein tended to precipitate, and these amounts of free thiols may not be significant as no protein could be recovered.

These results suggested that the reaction occurred between the free cysteine in K68C-Aft and the maleimide function of the manganese-salen complex. However, the conjugate could not be observed by MALDI-TOF analysis due to the presence of urea in high concentration which prevented ionisation of the conjugate, despite desalting using commercially available mini-columns (ZipTip®). After dialysis against a Tris buffer (20 mM Tris, 50 mM NaCl, pH 7), in order to remove the urea and reform the conjugated nanocapsule, the conjugate precipitated, and no protein was recovered.

	Time of reaction (h)	Proportion of free thiols (%)
After reduction	-	81
10x	3	25
	6	33
50x	3	0
	6	25

Table 5: Proportion of free thiols measured by Ellman assay at 412 nm, after incubation of K68C-Aft with various molar equivalent of manganese-salen complex for 3 to 6 h at 37 °C.

The procedure described above involved the use of 10 to 50 molar equivalents of manganese-salen complex to protein, which corresponded to a concentration of 800 µM and 4 mM of manganese-salen complex, respectively, in the reaction mixture containing 5 % (v/v) acetonitrile. Under these conditions, the organic complex was not entirely soluble, resulting in precipitation and formation of a heterogeneous mixture. The conjugation process was therefore repeated, and the removal of the manganese-salen in suspension was achieved by centrifugation, prior to dialysis of the remaining excess catalyst against Tris buffer (20 mM Tris, 50 mM NaCl, pH 7).

During the conjugation, the maleimide-tagged manganese-salen (800 µM) was incubated with K68C-Aft (80 µM) at 37 °C for 3 h. To assess the bioconjugation, a maleimide-tagged fluorescent compound, Alexa-Fluor 594 C_5-maleimide (ThermoFischer®). The amount of free thiols was determined on the heterogeneous samples right after bioconjugation, which could be a source of inaccuracy for the Ellman assay and showed a decrease of free thiols from 77 % in the reduced K68C-Aft to 23 %, 15 % and 19%, after conjugation with manganese-salen, maleimide-salen ligand and Alexa-Fluor dye, respectively (Table 6). After removal of excess ligands by centrifugation, dialysis was performed to remove urea.

Protein precipitation was observed during dialysis and protein recovery was very low (< 7 %) in all samples. However, concentration of the sample by precipitation with 70 % ammonium sulfate allowed to observe the conjugate by MALDI-TOF analysis, despite a very low intensity of the peak measured at 24655 Da (Figure 12). As previous measurement of K68C-Aft by MALDI-TOF recorded a mass of 23981 Da, the expected mass of the conjugate was 24616 Da, given instrument error margin, this molecular weight was consistent with what was expected.

	Proportion of free thiols
After reduction	77
Mn-salen	23
Salen ligand	15
Alexa Fluor	19

Table 6: Proportion of free thiols measured by Ellman assay at 412 nm, after incubation of K68C-Aft with 10x molar equivalent of manganese-salen complex, maleimide-salen ligand or Alexa Fluor 594 C_5-maleimide for 3 h at 37 °C.

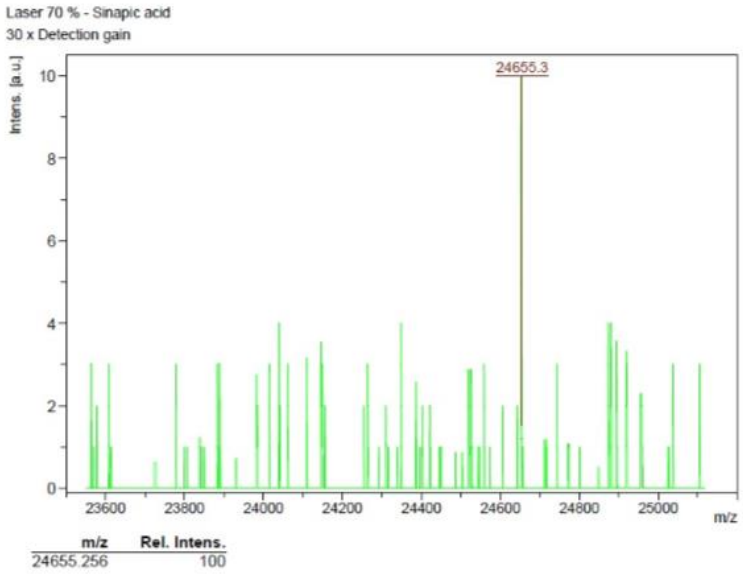

Figure 12: MALDI-TOF analysis of conjugate in a saturated solution of sinapic acid in acetone:0.1 % TFA 1:1 buffer, 70 % laser intensity and 30x detection gain.

Results obtained so far allowed the hypothesis that the conjugate of K68C-Aft with manganese-salen precipitated, either from poor water solubility or because of protein damage during conjugation reaction. To investigate this phenomenon, mouse heavy-chain apoferritin wild-type (WT-Aft) was expressed and purified, following aforementioned

procedure, and underwent the same process as K68C-Aft during reduction and bioconjugation. The protein recovery for WT-Aft was measured after reduction process, reduction, and incubation for 3 h at 37 °C, as well as reduction and incubation with various molar equivalent of the manganese-salen complex (Figure 13). Upon reduction and incubation for 3 h at 37 °C, the amount of protein remained unchanged. However, after the same process occurred in presence of the manganese-salen complex, the amount of protein recovered decreased proportionally to the molar equivalent of manganese-salen added. The addition of 10x molar equivalent of manganese-salen yielded a proportion of protein recovered of 73 %, up to 92 % when only 2.5x molar equivalent was added. These results established a direct deleterious effect of the manganese-salen on the protein. It was hypothesized that this phenomenon was due to the oxidative properties of the manganese-salen, which could harm the protein, as well as the natural ability of apoferritin to chelate transition-metals and oxidize them, which could render the protein insoluble upon aggregation in its inner cavity as soon as the urea was removed by dialysis. To reduce this effect on the K68C-Aft during conjugation, it was decided to only use 2.5x molar equivalents of manganese-salen complex during conjugation.

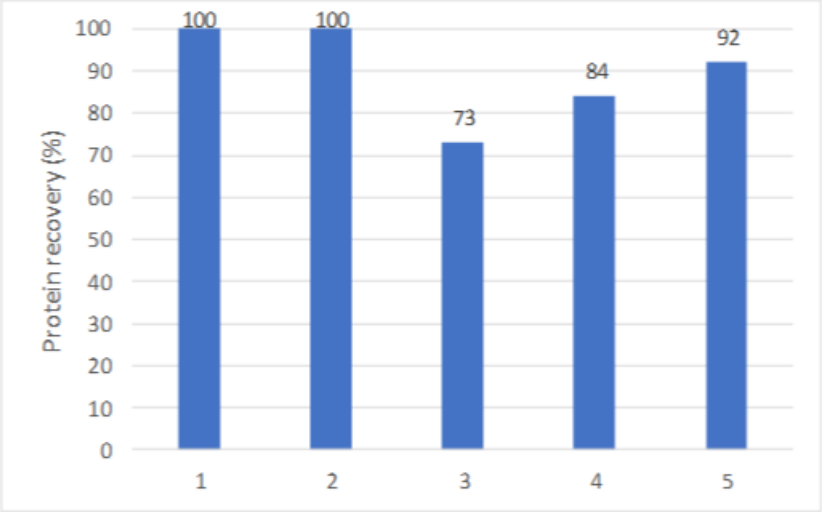

Figure 13: Protein recovery of WT AFT (**A**) (1), after reduction and 3 h at 27 °C (2), with 10x molar equivalent manganese-salen complex (3), 5x molar equivalent (4) or 2.5x molar equivalent (5). Protein concentration was measured by Lowry assay at 750 nm.

Whilst these experiments allowed to increase the amount of protein recovered, the main issue of the conjugate of K68C-Aft with manganese-salen complex solubility in buffer was not solved. Protein recovery and proportion of free thiols was measured before and after dialysis against either water or Tris buffer (Figure 14). For the sample dialysed against water, 90 % of

the protein was recovered from reduction with 85 % of free thiols. After conjugation and catalyst removal by centrifugation, the amount of protein recovered was 69 %, relative to starting concentration, with only 10 % free thiols. However, after dialysis, whilst the amount of free thiols was not significantly different, the proportion of protein recovered dropped to 11 %. The same pattern was observed after dialysis against Tris buffer. The protein recovery dropped from 70 % to 15 %. In both case, the conjugate was shown to form whilst 2.5 molar equivalent of manganese-salen complex was added, indicating this amount of catalyst was sufficient for conjugation with K68C-Aft. However, dialysing with water or Tris did not change the fate of the conjugate, which precipitated during dialysis, upon removal of urea. These results showed that the main source of protein precipitation after conjugation was the lack of water solubility of the conjugate itself. It was hypothesized that the addition of such non-

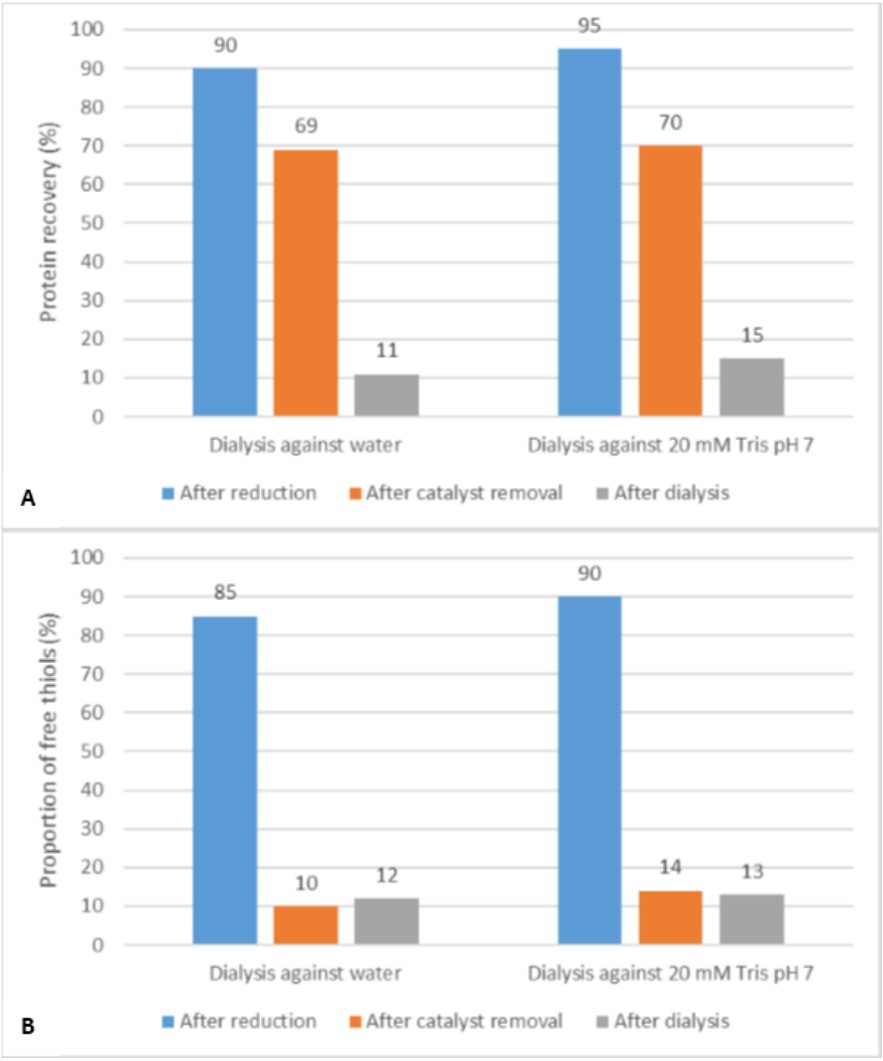

Figure 14: Protein recovery (**A**) and proportion of free thiols (**B**) measured respectively by Lowry assay at 750 nm and Ellman assay at 412 nm, at the different stage of the reduction-conjugation process of K68C-Aft with manganese-salen complex, comparing the effect of dialysis against either water or 20 mM Tris pH 7.

water soluble organic molecule to the inner cavity of apoferritin dramatically decreased the solubility of the protein around pH 7, where apoferritin is reassembled in a nanocapsule. The reassembling of the 24 sub-units could also be problematic as the inner cavity, of a diameter of 8 nm, was not sufficiently large to host 24 copies of the manganese-salen complex. This could also have occurred, not only because of urea removal, but also after removal of the co-solvent, acetonitrile, during dialysis, which rendered the organic solution of manganese-salen complex miscible with the Urea-Tris buffer used for conjugation.

To overcome this issue, one of the most important unique features of apoferritin was exploited, its ability to form a quaternary structure, assemble and disassemble, in a pH-dependent manner.

At pH 3, the apoferritin nanocapsule is disassembled. The pH-dependent solubility of the conjugate was assessed. The conjugate's buffer was changed right after conjugation, from Urea-Tris buffer, containing residual manganese-salen complex, to a salt solution (150 mM NaCl) at pH 3 via desalting column buffer exchange, allowing to wash the residual manganese-salen. Despite the dilution of the protein consecutive to the size exclusion chromatography column, the conjugate was soluble and stable under these conditions, and protein recovery was improved, up to 87 %, which rendered characterization possible.

The absorbance spectrum of the conjugate was acquired (Figure 15A). Its absorption profile is characteristic of both its components. The conjugate displays an absorbance peak at around 269 nm, characteristic of K68C-Aft, however, it forms a plateau due to the absorption of the manganese-salen complex at these wavelengths.

Moreover, from 300 nm to 550 nm, the absorption of K68C-Aft is close to none, whilst the manganese-salen complex displays two absorbance maxima, around 330 nm and 420 nm, which are visible in the conjugate's absorption spectrum. Combining both of its component profile, the conjugate has been formed. This was confirmed by MALDI-TOF analysis (Figure 15B). A value of 24651 Da was measured, close to the expected value of 24616 Da and consistent with the first measure of 24655 on a low concentrated sample. Whilst the absorbance profile measured could have been a combination of both component in solution

rather than covalent conjugation, MALDI-TOF analysis allowed to conclude on a covalent conjugation of K68C-Aft with the manganese-salen complex.

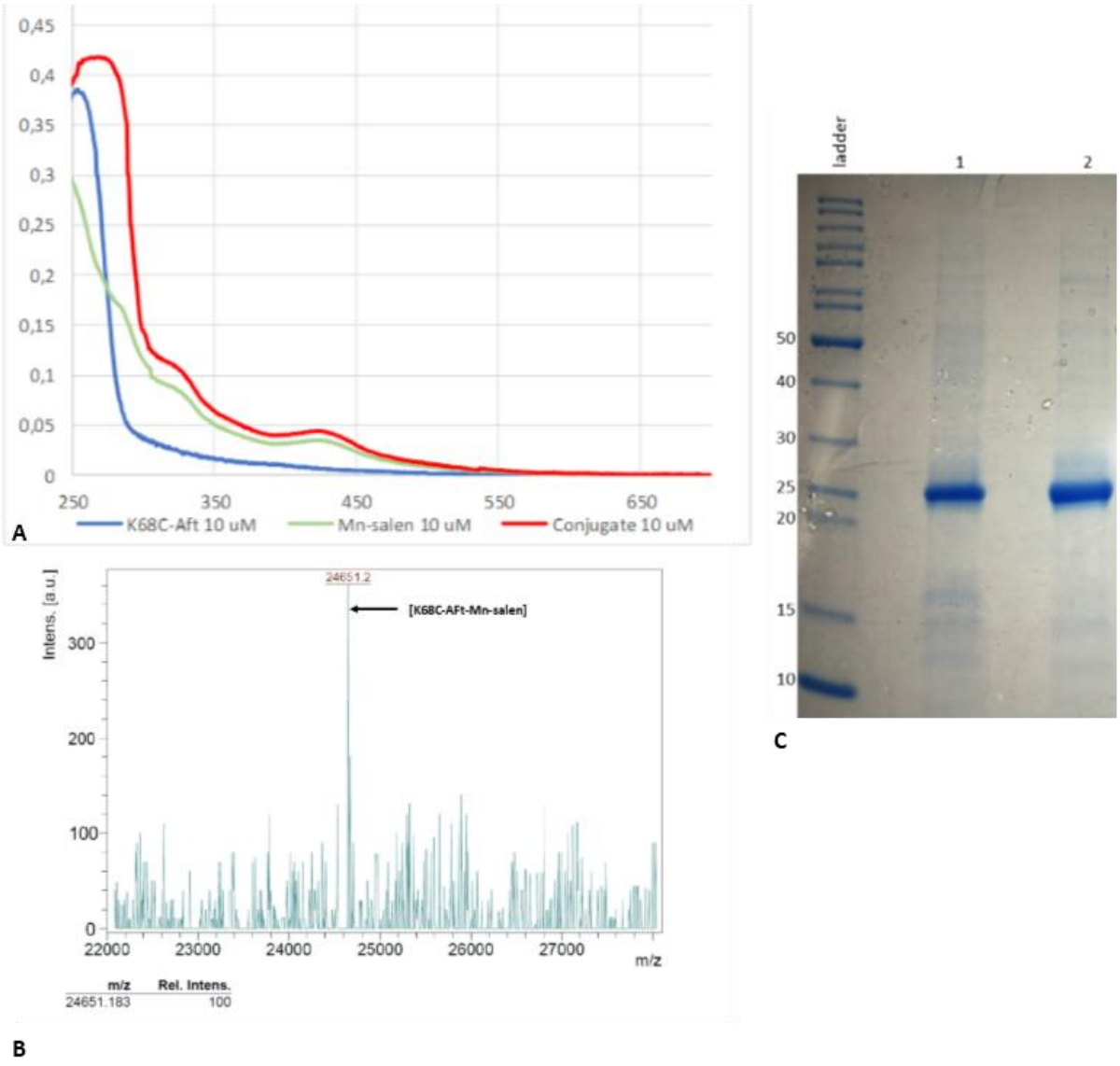

Figure 15: Characterization of the conjugate. **A**. Absorbance spectra of the conjugate (10 µM, 150 mM NaCl, pH 3), as well as K68C-Aft (10 µM, 150 mM NaCl, pH 3) and manganese-salen complex (10 µM, acetonitrile). **B**. MALDI-TOF analysis of the conjugate in a saturated solution of sinapic acid in acetonitrile:0.1 % TFA 1:1 buffer. **C**. Gel electrophoresis of K68C-Aft (lane 1) and the conjugate (lane 2) in denaturing condition (0.1 % w/v SDS)

The conjugate was also analysed by gel electrophoresis in denaturing condition (Figure 15C, SDS-PAGE, incubation at 95 °C for 10 min, 0.1 % w/v SDS and 1 mM β-mercaptoethanol in the loading and running buffers). Gel conditions were varied in order to observe a difference of size between the conjugate and K68C-Aft, knowing that the difference was 635 Da. When the polyacrylamide concentration was changed to 18 % or 20% w/w, which give a better resolution for small protein sizes (5-50 kDa and 4-40 kDa, respectively), the migration of the conjugate was similar to K68C-Aft and no difference of size was observed. Finally, a gradient

gel was used (Figure 15C, Mini-Protean Any kD®, Bio Rad, concentration of polyacrylamide not disclosed by manufacturer), the conditions of running were 180 V for 42 min. However, no size difference was observed between K68C-Aft and its conjugate with the manganese-salen complex. These results showed that SDS-PAGE was not accurate enough as a technique to discriminate the conjugate from the protein with such small size difference.

	Protein concentration (µM)	Mn concentration (µM)	Ratio [Mn]/[Protein]
K68C-AFT	80	2.08	0.03
Conjugate [K68C-Aft-Mn-salen]	80	73.6	0.92

Table 7: ICP-MS analysis for the manganese content of K68C-Aft and the conjugate in 150 mM NaCl, pH 3 mixed with an appropriate volume of 1 % HNO_3 (metal-free) for digestion of the sample.

Elemental analysis of the conjugate by ICP-MS was also performed (Table 7) for K68C-Aft and the conjugate, both placed in the same buffer allowing solubility of the conjugate (150 Mm NaCl, pH 3), to minimize interference from residual metals. This analysis showed that K68C-Aft (80 uM) contained 2.08 µM of manganese, making a [Mn]/[protein] ratio of 3 %. This showed that despite incubation with EDTA after purification, a residual level of manganese was detected in the protein sample. In the conjugation sample, 73.6 µM of manganese was measured, thus the [Mn]/[protein] ratio was 92 %. Therefore, the manganese-complex was inserted into K68C-Aft to form the conjugate and the yield of conjugation was 92 % in the aforementioned conditions. This also showed that a molar equivalence of 2.5 of manganese-salen complex was sufficient to covalently conjugate with K68C-Aft with high yield within 3 h at 37 °C.

Circular dichroism analysis was also performed in order to measure the folding and thermostability of the conjugate (Figure 16). These measurements, for both K68C-Aft and the conjugate (15 µM), were recorded at 25 °C in a sodium phosphate buffer (50 mM) at pH 3, to insure solubility of the conjugate and record the ellipticity of a single sub-unit. K68C-Aft displayed a maximum peak at around 195 nm and two minimum peaks at 210 nm and 225 nm. This profile of molar ellipticity is typical of α-helix proteins, which is consistent with the fact that apoferritin's secondary structures are only composed of α-helixes. The conjugate, however, displayed the same profile of maximum and minimum peaks, however, the molar ellipticity in each case was halved and closer to 0. This indicated the conjugate was less folded than K68C-Aft. It was hypothesized that the covalent conjugation of a bulky transition-metal

complex could disturb the proper refolding of the protein, and that some residues could coordinate with the ligand by hydrogen bonds or directly with the metal.

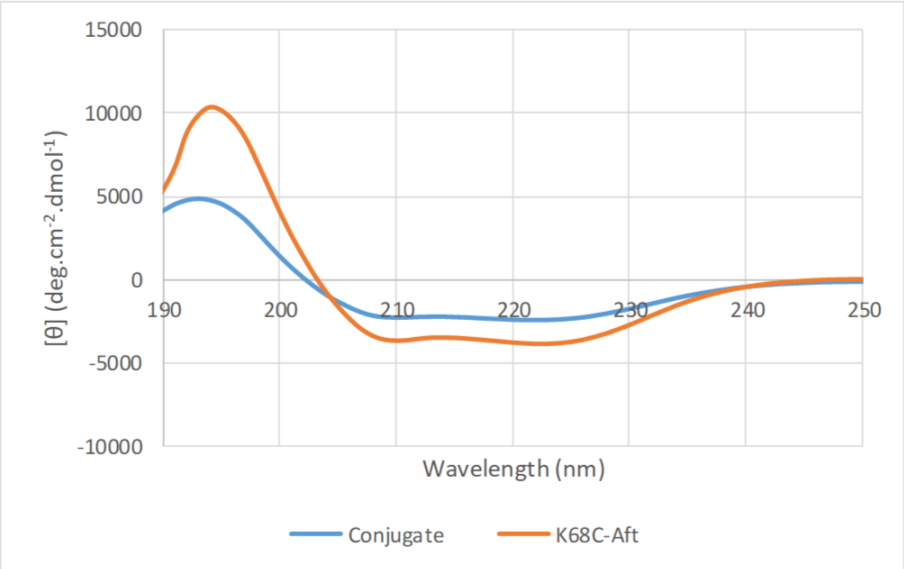

Figure 16: Molar ellipticity, as measured by circular dichroism analysis, of both K68C-Aft and the conjugate at 25 °C in a sodium phosphate buffer (50 mM, pH 3).

The thermostability of K68C-Aft and the conjugate were also determined by circular dichroism analysis. These were exposed to increasing temperature from 5 to 72 °C, whilst the ellipticity for these proteins were recorded (See Appendix for circular dichroism spectrums). It is observed that the ellipticity of the conjugate converges to 0 at lower temperatures than K68C-Aft's ellipticity, Whilst for K68C-Aft, a significant change in folding could be observed from 66 °C, the conjugate started to really unfold at 51 °C. This phenomenon was better observed on thermal unfolding curves (Figure 17) where ellipticity is measured in function of temperature at 222 nm, as a typical peak for α-helix-rich proteins. A sharp increase of ellipticity was observed from 60 °C for K68C-Aft, showing rapid unfolding of the protein and loss of structure. The conjugate ellipticity at 222 nm started much higher than for K68C-Aft showing less folding of the protein, even at low temperatures. The conjugate's ellipticity increased rapidly from 50 °C and above, thus indicating lower thermostability than the non-conjugated protein.

As stated before, it was hypothesized that the conjugation of K68C-Aft with a bulky transition-metal complex could disturb its proper refolding and disrupt certain residue interactions in favour of residues' coordination with the ligand or metal. A lower folding state of the protein

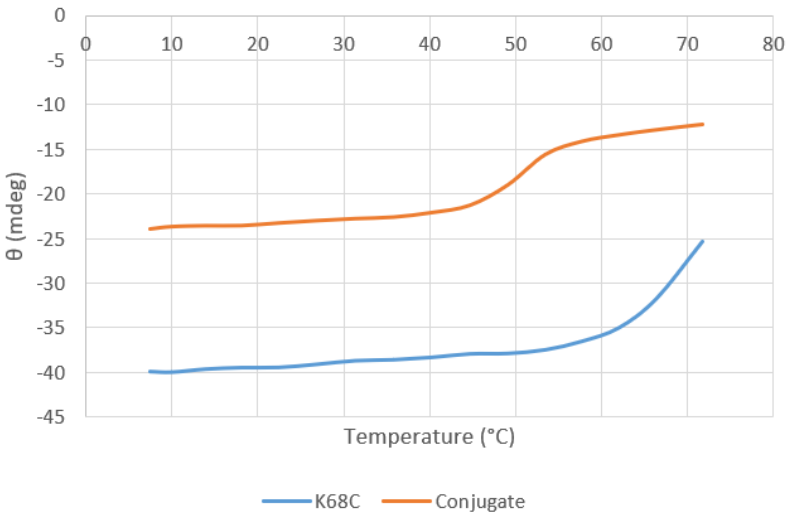

Figure 17: Molar ellipticity, as measured by circular dichroism analysis, of both the conjugate and K68C-Aft at 222 nm, in a sodium phosphate buffer (50 mM, pH 3), exposed to increasing temperature from 5 to 75 °C.

had a direct impact on its thermostability. However, being stable up to 50 °C, the conjugate could still be used in a large range of temperatures, notable mammalian physiological temperatures, for catalysis. In conclusion, K68C-Aft was conjugated with the manganese-salen complex, after reduction with TCEP, by incubation of the protein and 2.5x molar equivalent of the catalyst together for 3 h at 37 °C in a Urea-Tris buffer (20 mM Tris, 50 mM NaCl, 8 M urea, pH 7).

Once the incubation finished, the mixture was brought on a desalting chromatography column to remove the excess manganese-salen and exchange the buffer to 150 mM NaCl, pH 3, which allowed the solubility of the conjugate. UV-Vis and MALDI-TOF analysis proved that the covalent conjugation occurred, forming the K68C-Aft-Mn-Salen conjugate. ICP-MS analysis showed that the yield of conjugation was as high as 92 %.

However, the conjugate nanocapsule could not be reassembled as an increase in the pH caused precipitation of the protein.

8.4.3 Assembling of an apoferritin-conjugate nanocapsule

As the conjugation occurred at C68 pointing towards the inside of K68C-Aft's hollow core, attempted reassembly of the quaternary structure of apoferritin, by raising the pH to 8, led to precipitation of the conjugate as the 8 nm diameter hollow core was not large enough for each of the 24 sub-units to carry a catalyst, which size was estimated to 2-2.5 nm.

In order to reassemble the apoferritin-conjugate nanocapsule, the conjugate was mixed with WT-Aft in a conjugate:WT ratio of 1:23 and 2:22. Both were mixed together in the Urea-Tris buffer and were dialysed against a Tris buffer (20 mM, pH 8). This buffer exchange was realised by dialysis at 4 °C overnight to avoid brutal change of conditions, which would lead to the precipitation of the conjugate. The addition of WT-Aft had to occur either before or after the conjugation process. Adding WT-AFt to K68C-Aft before the conjugation process led to a total protein recovery of 73 %, close to the amount of protein recovered when using K68C-Aft only. This was explained by the direct deleterious effect of the manganese-salen complex had on the protein, as demonstrated above. Nevertheless, adding WT-Aft after the conjugation process and before dialysing the conjugate, led to a 100 % protein recovery after dialysis, relative to the total protein concentration of conjugate, measured after conjugation. In conclusion, adding the wild-type protein to the conjugate, notably after the conjugation occurred, dramatically increased the solubility of the conjugate, the assembling of the nanocapsule would protect the catalyst from the buffer and would prevent the conjugate from precipitating. These results showed the deleterious effect of manganese-salen on proteins. Therefore, the second method was preferred. However, given the short difference in size between the two components of the hybrid Conjugate:WT-AFt nanocapsule and the ratio used, no difference of size could be observed on SDS-PAGE.

8.5 Catalysed oxidation of thioanisole

Amongst the applications of manganese-salen complexes in catalysis, the epoxidation of activated alkenes is the most famous and first application found for these catalysts [70b, 149]. However, sulfoxidation has been shown very early in the development of salens, and manganese-salens have already been used in the context of artificial metalloenzymes to catalyse the oxidation of phenyl sulfides in water [44, 60]. Thus, the catalytic activity of the prepared manganese-salen complex and of the conjugate [K68C-Mn-salen-Aft] was measured on the oxidation of thioanisole.

8.5.1 Catalytic activity of the manganese-salen complexes

The manganese-salen complexes synthesized, **31** ; **43** ; **45**, were evaluated for the sulfoxidation of thioanisole (Scheme 38).

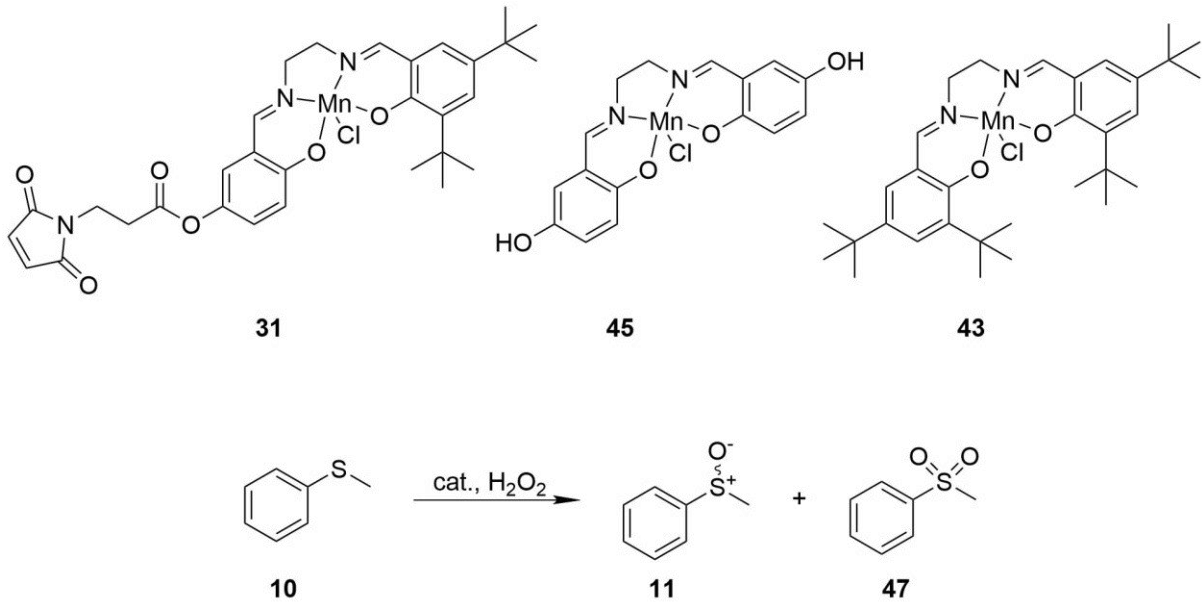

Scheme 38: Range of manganese-salen complexes prepared and catalysed sulfoxidation of thioanisole. The expected products are the enantiomers of phenyl methyl sulfoxide (PMSO), and phenyl methyl sulfone ($PMSO_2$).

Several oxidants which have been reported to perform oxidation catalysed by manganese-salen complexes were available, however, hydrogen peroxide was chosen as a primary oxidant because of its water solubility and its relatively good compatibility with manganese-salen complexes[139].

Catalyst	[Catalyst]	Conversion (%)	PMSO (%)	$PMSO_2$ (%)	Comment
-	-	38 ± 3	38	0	No catalyst
31	1 mol %	0	0	0	No oxidant
31	1 mol %	88 ± 2	74	14	
43	1 mol %	58 ± 1	58	0	
45	1 mol %	62 ± 2	50	12	

Table 8: Catalytic activity of manganese-salen complexes for the oxidation of thioanisole in acetonitrile with 10 mM thioanisole, 1 equivalent of H_2O_2, for 5 h at 20 °C.

The catalytic activity of manganese-salen complexes was first assessed in acetonitrile (Table 8), a solvent where they were all fully soluble. The reactions took place for 5 h at 20 °C in presence of 10 mM thioanisole, 1 equivalent of hydrogen peroxide and 1 mol % of manganese-salen complex. The product was extracted several times with diethyl ether, the solvent was evaporated then the product was analysed by NMR. The conversion of the Mn-salen **31** was of 88 %, including 74 % PMSO (phenyl methyl sulfoxide). Overoxidation of the product occurred, leading to the formation of $PMSO_2$ (phenyl methyl sulfone) in a proportion of 14 %. For the **43** and **45**, the conversion was of 58 % and 62 %, respectively, including 12 % of formed $PMSO_2$ for the latter. Without hydrogen peroxide, no conversion occurred, showing that the manganese-salen complexes could not use the oxygen contained in the organic solvent as oxidant.

Temperature	Catalyst	[Catalyst]	Conversion (%)	PMSO (%)	$PMSO_2$ (%)	Comment
20 °C	-	-	61 ± 2	61	0	No catalyst
	31	2 mol %	0	0	0	No oxidant
	31	2 mol %	87 ± 3	84	3	
	43	2 mol %	85 ± 2	85	0	
	45	2 mol %	88 ± 5	32	2	
4 °C	-	-	61 ± 1	61	0	No catalyst
	31	2 mol %	0	0	0	No oxidant
	31	2 mol %	67 ± 1	67	0	
	43	2 mol %	70 ± 4	70	0	
	45	2 mol %	74 ± 3	72	2	

Table 9: Catalytic activity of manganese-salen complexes for the oxidation of thioanisole in water:acetonitrile 99:1 with 10 mM thioanisole, 1 equivalent of H_2O_2, for 5 h at various temperatures.

The catalytic activity of these manganese-salen complexes were also assessed in water, in preparation of the conjugate [K68C-Mn-salen-Aft]'s own tests. Due to the low solubility of the manganese-salen complexes in water, 1 % of acetonitrile was added as co-solvent, along addition of the catalyst. Two temperatures were assessed, 4 and 20 °C and the concentration

of catalysts used was of 2 mol % (Table 9). After stirring the reaction for 5 h, the product was extracted with diethyl ether then analysed by NMR. When the reaction occurred at 20 °C, the background reaction yielded 61 % of PMSO, whilst all manganese-salen complexes ranged from 85 to 88 %, with no statistically significant difference. At 4 °C, the yields of reactions catalysed by manganese-salen complexes were reduced of an average of 19 %, ranging from 67 to 74 %, again without significant difference except between Mn-salen and Mn-OH-salen. However, despite a low water solubility, the catalytic activity of manganese-salen complexes was high and satisfying to carry on with the activity of [K68C-Mn-salen-Aft].

8.5.2 Catalytic activity of the conjugate

The catalytic activity of the conjugate [K68C-Mn-salen-Aft] was assessed for the oxidation of thioanisole (Table 10). The reaction was performed at 20 °C for 20 h without stirring of the solution to not harm the conjugate, at various pH in a 50 mM sodium phosphate buffer. This range of pH mimicked the different step of assembling of the apoferritin nanocapsule. At pH 3, the nanocapsule was not assembled, whilst at pH 5, it was only partially. The nanocapsule was fully reassembled above pH 8.

At pH 3, the conversion was of 42 % and an enantioselectivity of 8 % *ee* was observed by chiral HPLC (Table 10, see Appendix 16 for HPLC trace). The yield was thus moderate, and the selectivity of the conjugate was low. When raising the pH, the conjugate immediately precipitated yielding almost no conversion. As mentioned before, the conjugate was stabilised at higher pH and was involved apoferritin-nanocapsules by mixing the conjugated sub-unit with WT-Aft sub-units, in varying ratios, from 23:1 to 20:4 of WT:Conjugate. Increasing the number of copies of the conjugated sub-unit per nanocapsule increased the conversion, from 35 to 51 %, at pH 3. The same phenomenon was observed at pH 5. However, at pH 8 and above, the proteins precipitated when using a WT:Conjugate nanocapsule with a ratio equal or superior to 21:3, yielding no product. It was also observed that some precipitation occurred with WT:Conjugate 22:2 at pH 11, although not sufficient to prevent the reaction from occurring.

The enantioselectivity of the conjugate was observed mainly at a ratio of 23:1, as it was the only nanocapsule fully soluble, regardless of pH. Between pH 3 and 5, 10-11 % *ee* for the enantiomer (*R*) of phenyl methyl sulfoxide, was measured, but increased significantly at pH 8

and above, up to 17 % at pH 11. This allowed us to presume of a direct link between the selectivity of the catalyst and the pH, thus with the apoferritin nanocapsule's state of

	pH							
	3		5		8		11	
	Conv (%)	ee (%)	Conv (%)	ee (%)	Conv (%)	ee (%)	Conv (%)	ee (%)
31	38	-	45	-	53	-	42	-
Conjugate	42	8	1	-	0	-	0	-
WT:Conj 23:1	35	10	37	11	41	15	29	17
WT:Conj 22:2	41	9	52	12	57	12	31	5
WT:Conj 21:3	47	11	64	11	0	-	0	-
WT:conj 20:4	51	10	69	13	0	-	0	-
Background reaction	11	-	17	-	19	-	23	-
Conjugate†	40	-						
WT:conj 23:1†	32	-						

† 2.5 mM substrate, 2 mol % catalyst, 1 equiv H_2O_2, 20 h at 20 °C, in urea

Table 10: Catalytic activity of the conjugate [K68C-Mn-salen-Aft] and conjugate-based-nanocapsule of various Conjugate:WT ratio, for the oxidation of thioanisole with 2.5 mM thioanisole, 1 equivalent of H_2O_2, 2 mol % catalyst for 20 h at 20 °C. Rates were measured by chiral HPLC. Catalysis with the conjugate favoured the synthesis of the (*R*) enantiomer of PMSO.

assembly. The inner cavity of the apoferritin nanocapsule provided a narrow environment which stabilized the conjugated manganese-salen complex and chirality, as proven by the lack of selectivity when the reaction was carried in presence of urea (8 M). However, the selectivity remained low. The inner cavity was narrow enough to control the uptake of substrates but not enough to restrict their movement and provide chirality. Moreover, with only one point of covalent anchoring, through the bond between K68C and the maleimide-linker of the manganese-salen complex, the catalyst was allowed to move freely around the axis of these bonds, which was shown to decrease the selectivity of the same catalyst conjugate with papain, and applied for the epoxidation of olefins[70a]. Therefore, the enantioselectivity was provided by the chirality of side chains from residues situated closely to the catalyst anchoring point.

8.5.3 Summary of catalysis work

In conclusion, the catalytic activity of the maleimide-bearing manganese-salen complex was assessed, yielding a conversion of up to 87 % in water (5 h), similar to all the manganese-salen complexes synthesized. The conjugate [K68C-Mn-salen-Aft] displayed 42 % of conversion, but

only when solubilised at pH 3. At higher pH, the presence of WT sub-units in ratio WT:Conjugate of 23:1 allowed solubilisation of the conjugate and conversion up to 57 % and enantioselectivity of up to 17 % *ee*, favouring the synthesis of the (*R*) enantiomer of PMSO. Whilst the nanocapsule's state of assembly was presumably had an effect, the selectivity remained low as the inner cavity of apoferritin nanocapsule was too large to provide enough steric hindrance, the selectivity relying mainly on residues. Anyway, the conjugate was proven to catalyse the oxidation of thioanisole in aqueous buffer using hydrogen peroxide, earning the title of artificial metalloenzyme.

9. CONCLUSIONS AND PERSPECTIVES

This project examined the development of an artificial metalloenzyme, based on an apoferritin scaffold which brings a second coordination sphere to a covalently conjugated manganese-salen, and the evaluation of its catalytic activity on the oxidation of thioanisole.

In this purpose, a manganese-salen catalyst was synthesized, bearing a maleimide linker substituted to one of its cyclic moiety, allowing covalent conjugation with a free thiol by Michael addition. Along with this, two manganese-salen bearing different substituents were synthesized as well, as model catalysts.

In order to allow this covalent conjugation to occur, a mouse recombinant heavy-chain K68C apoferritin (K68C-Aft) was expressed and purified. The single mutated cysteine 68 was pointing toward the inner cavity of the protein and would allow the conjugation of the catalyst. The pH-dependent properties of apoferritin to disassemble and reassemble into a nanocapsule of 24 sub-units were exploited to create an artificial metalloenzymes. This was achieved by rendering the cysteine accessible to the catalyst, a urea-tris (20 mM Tris, 50 mM NaCl, 8 M urea, pH 7) was used to unfold the protein, and the cysteine's thiol was reduced with 50 molar equivalents of (tris(2-carboxyethyl)phosphine TCEP. The conjugation occurred in the same buffer, as at pH 7-8.5 thiols are sufficiently nucleophile to achieve Michael addition, and covalently conjugate the manganese-salen catalyst. The conjugate [K68C-Mn-salen-Aft] was prepared and stabilised by placing it in a salt solution at pH 3, keeping the conjugate apoferritin to be disassembled. Attempts to reassemble the conjugate apoferritin nanocapsule resulted in precipitation of the protein as the conjugate folding and stability in solution was lower than K68C-Aft and the size of the conjugated manganese-salen rendered reassembling impossible due to the small size of the nanocapsule's inner cavity, 8 nm. The nanocapsule containing conjugate apoferritin sub-units was reformed, upon increase of the pH up to 11, by adding a mouse wild-type heavy-chain apoferritin (WT-Aft) in a ratio of WT:Conjugate ranging from 23:1 to 22:2, as higher ratio ended in partial or complete precipitation of the conjugate in solution.

The catalytic activity of [K68C-Mn-salen-Aft], the artificial metalloenzyme prepared, was measured for the oxidation of thioanisole in water, using hydrogen peroxide as oxidant. Firstly, the manganese-salen complexes synthesized were used for catalysis. In acetonitrile,

the conversion was high, up to 88 %, consistent with what was demonstrated in the literature [150, 154]. In water, with 1 % of acetonitrile as co-solvent, the conversion was moderate to high, up to 74 %. The co-solvent was balancing the relatively low water solubility manganese-salen catalysts synthesized.

Catalytic reactions with the conjugate were then carried. The conjugate [K68C-Mn-salen-Aft] was used at pH 3, as higher pH resulted in precipitation, and the conversion was moderate, 42 %. Using WT:Conjugate nanocapsules, in different ratios of sub-units, yielded moderate conversion, up to 69 % at pH 5 and 57 % at pH 8. Nevertheless, background reactions were observed and led to up to 23 % of conversion, which was very high when compared to the bioconjugate catalytic activity.

The catalytic activity was directly dependent on the pH. At higher pH, where the nanocapsule is fully reassembled, a lower conversion was observed. This was due to the uptake of the substrate through protein's pores and a lower activity of the manganese-salen catalyst.

However, the selectivity of the conjugate and conjugate nanocapsule for the reaction was improved upon reassembling of the nanocapsule, from 8 to 17 % *ee*, which remained low. Single-point anchoring of the manganese-salen complex allowed movement of the catalyst in the nanocapsule's inner cavity, which was too large to exert enough steric hindrance to provide a chiral environment which would allow higher enantioselectivity. This environment was mainly provided by the chiral residues' side chains from apoferritin, located around the manganese-salen complex.

In conclusion, the apoferritin-based artificial metalloenzyme was prepared and its catalytic activity for the oxidation of thioanisole with hydrogen peroxide in water was assessed. Nevertheless, much can be done to optimize the conjugate. Further work could explore the coordination of residues' side chains with the catalyst through molecular modelling and insert point mutations to stabilize the conjugated catalyst. More modelling of the inner cavity of apoferritin could lead to a dual-anchoring system where the catalyst would bear two maleimide-linker moieties and anchored via two mutated cysteine. This system has been shown to improve the rate and selectivity of the reaction catalysed by an artificial metalloenzyme [60].

As the pores allowing diffusion of molecules through apoferritin to enter its inner cavity let only molecules as large as sucrose in, some further work could be to synthesize a range of substituted phenyl sulfide of different sizes, to study the size discrimination of this. For instance, long molecules with a diameter as large as sucrose (6 Å) could be of interest to mimic the activation of a drug, such as Omeprazole®'s derivatives. Catalysing the oxidation of various phenyl sulfides would also allow to study the mechanism of the reaction.

In future perspectives, the versatility of the scaffold should be explored. The apoferritin could be modified to fit and stabilize most of the transition-metal catalysts developed so far, as long as they would bear a maleimide linker. This would allow the conjugation with other known ligands, such as porphyrins and haems, but also to change the transition-metal used. This would allow the catalysis of several reactions of interest, and extend the range of applications as nanoreactor for apoferritin, which is limited to the catalysis of a Suzuki-Miyaura coupling reaction and the polymerization of phenylacetylene [3, 119].

The main application to this artificial metalloenzyme relies on the anchoring of targeting moieties, peptides or antibodies, as reported in the literature [5], onto the outer shell of the apoferritin nanocapsule, via chemical modification. This would allow the targeting of the artificial metalloenzyme to specific cell lines, thus tissues. This ability could be of use for the activation of prodrugs *in situ*, to improve the drug bioavailability and reduce nonspecific activation.

10. APPENDICES

Content

Appendix 1: Mouse heavy-chain recombinant K68C apoferritin sequence

```
1     MHHHHHHGLNDIFEAQKIEWHELVPRGSMTTASPSQVRQNYHQDAEAAINRQINLELYAS
61    YVYLSMSAYFDRDDVALKNFAKYFLHQSHEEREHAECLMKLQNQRGGRIFLQDIKKPDRD
121   DWESGLNAMEAALHLEKSVNQSLLELHKLATDKNDPHLSDFIETYYLSEQVKSIKELGDH
181   VTNLRKMGAPEAGMAEYLFDKHTLGHGDES
```

In red: His-tag (with first methionine). In orange: K68C

Number of amino acids: 210

Theoretical molecular weight: 24236.1 Da

Theoretical pI: 5.74

Appendix 2: pJ414express vector map

Appendix 3: Oxidation of thioanisole calibration curves for HPLC analysis

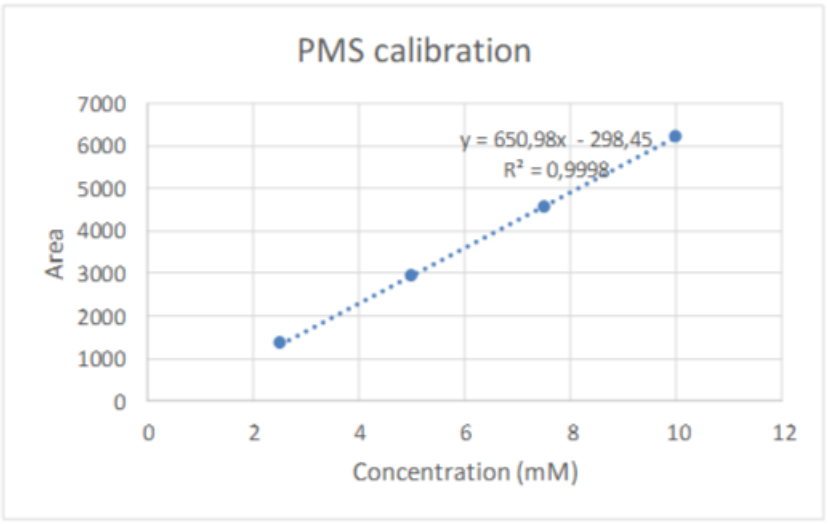

PMS						
[] (mM)	Time	Area	Height	Width	Area%	Symmetry
10	8,43	6232,8	3436,1	0,214	99,891	0,77
7,5	8,427	4565,5	3184,2	0,1922	99,905	0,78
5	8,451	2928,9	2455	0,1758	99,865	0,783
2,5	8,45	1353,5	1277,5	0,1714	100	0,785

Appendix 3A: Calibration of phenyl methyl sulfide (PMS) on HPLC OD column.

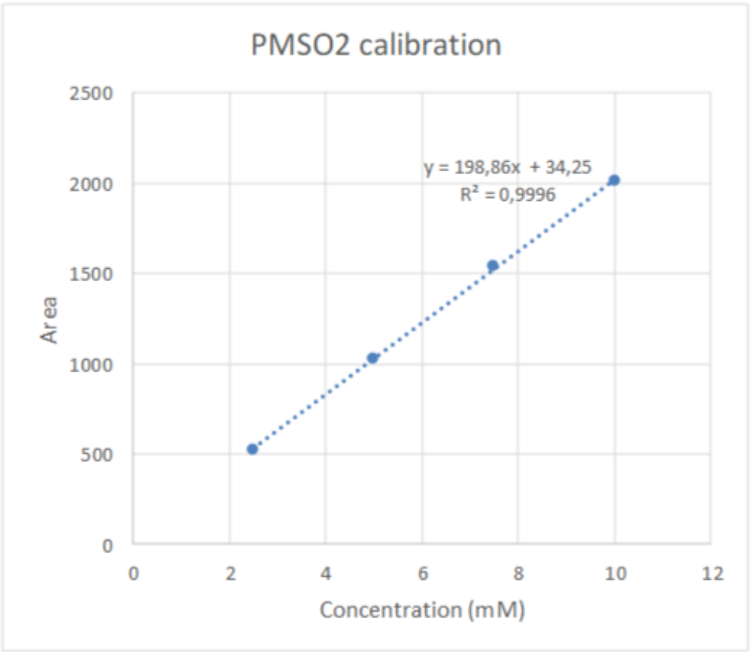

PMSO2						
[] (mM)	Time	Area	Height	Width	Area%	Symmetry
10	28,576	2010,7	47,5	0,6483	84,191	0,558
7,5	28,761	1542,3	37	0,6433	84,02	0,59
5	28,78	1032	25,5	0,6298	83,886	0,631
2,5	28,918	523,6	13,2	0,6139	83,358	0,695

Appendix 3B: Calibration of phenyl methyl sulfone ($PMSO_2$) on HPLC OD column.

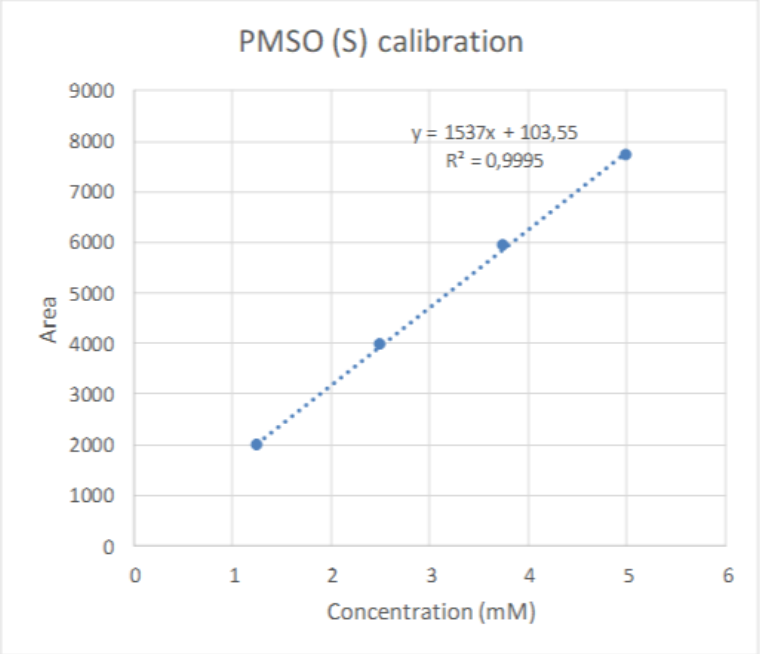

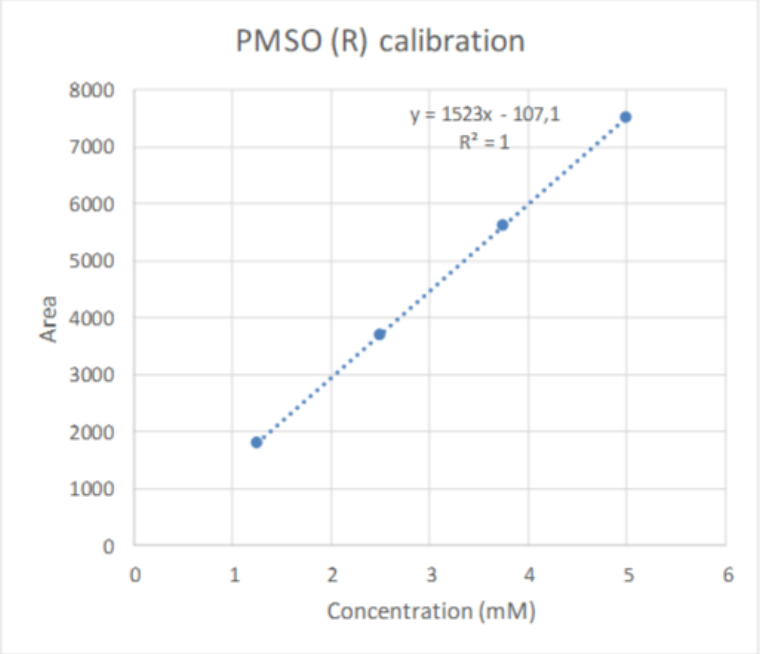

PMSO							
Enan-tiomer	[] (mM)	Time	Area	Height	Width	Area%	Symmetry
(S)	10	23,645	10365,2	288,9	0,5282	49,463	0,58
(R)	10	28,987	10059,6	171,4	0,7902	47,145	0,324
(S)	5	23,54	7736,7	223,5	0,5328	49,353	0,603
(R)	5	28,743	7508,6	137,3	0,8178	47,898	0,376
(S)	3,75	23,675	5932,2	172,9	0,5293	49,984	0,627
(R)	3,75	29,002	5604,7	110	0,7712	47,225	0,432
(S)	2,5	23,72	3972,4	118	0,5198	50,315	0,657
(R)	2,5	29,17	3697,2	78,9	0,7217	46,83	0,502
(S)	1,25	23,765	1985,7	60	0,5102	50,891	0,706
(R)	1,25	29,383	1798,6	42,8	0,6712	46,095	0,655

Appendix 3C: Calibration of phenyl methyl sulfoxide (PMSO) on HPLC OD column.

Appendix 4: Synthetic data for 3-maleimidopropionic acid 37

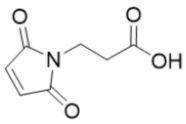

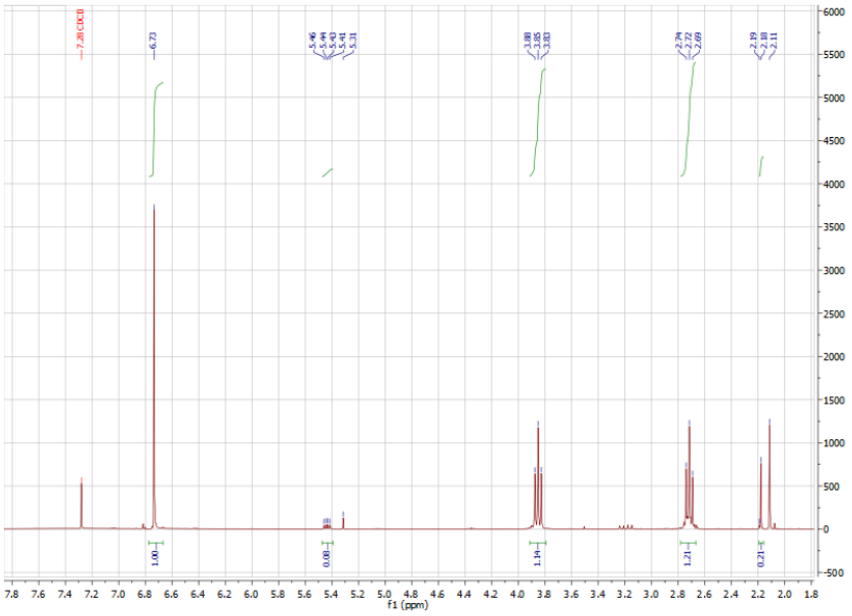

^{1}H NMR ($CDCl_3$)

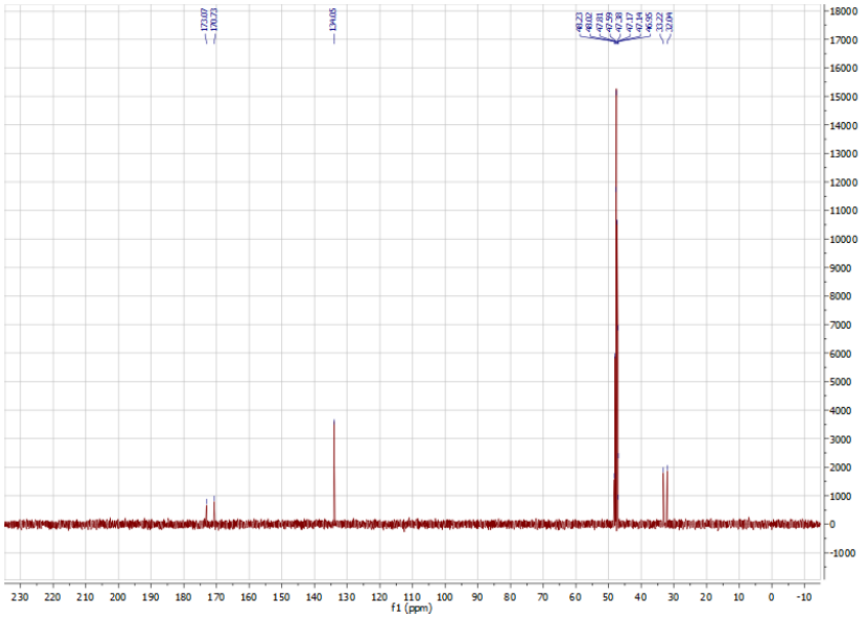

^{13}C NMR ($CDCl_3$)

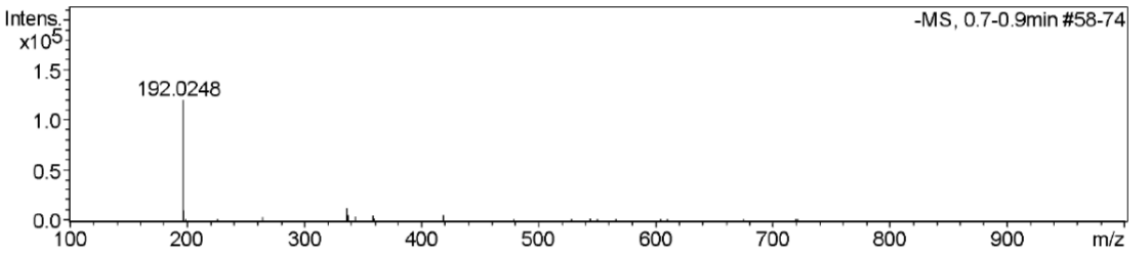

ESI-MS (in CH_3OH)

Appendix 5: 3-maleimidopropionic-*N*-hydroxysuccinimide ester 38

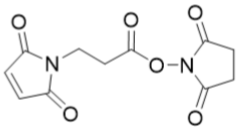

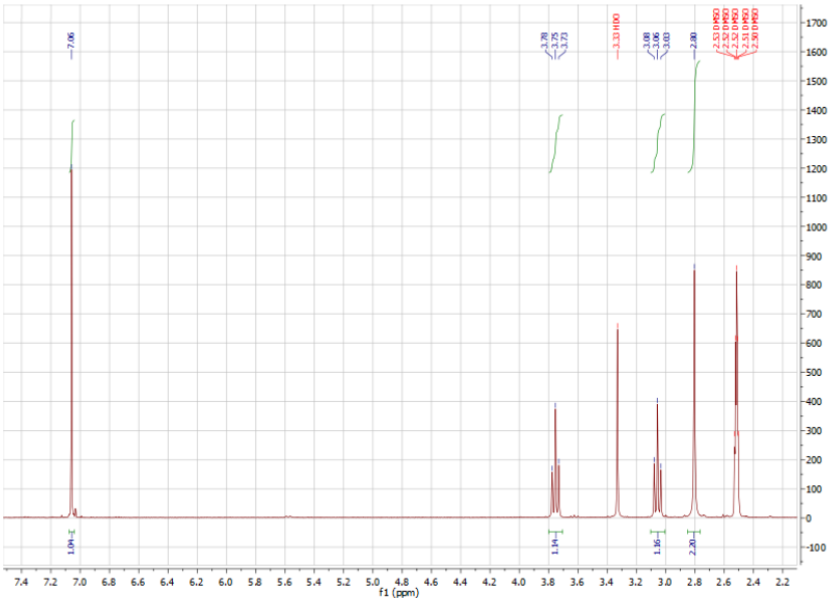

^{1}H NMR (d_6-DMSO)

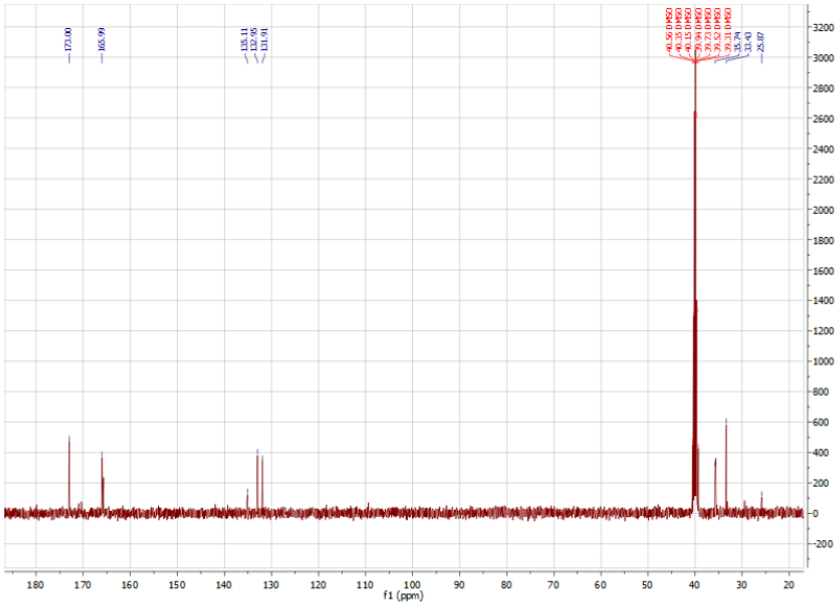

^{13}C NMR (d_6-DMSO)

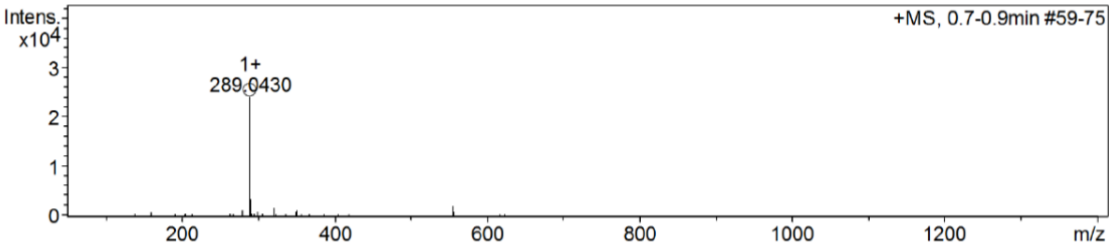

ESI-MS (in CH_3OH)

Appendix 6: 5-(propionic ester)-2-hydroxybenzaldehyde 39

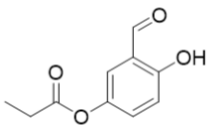

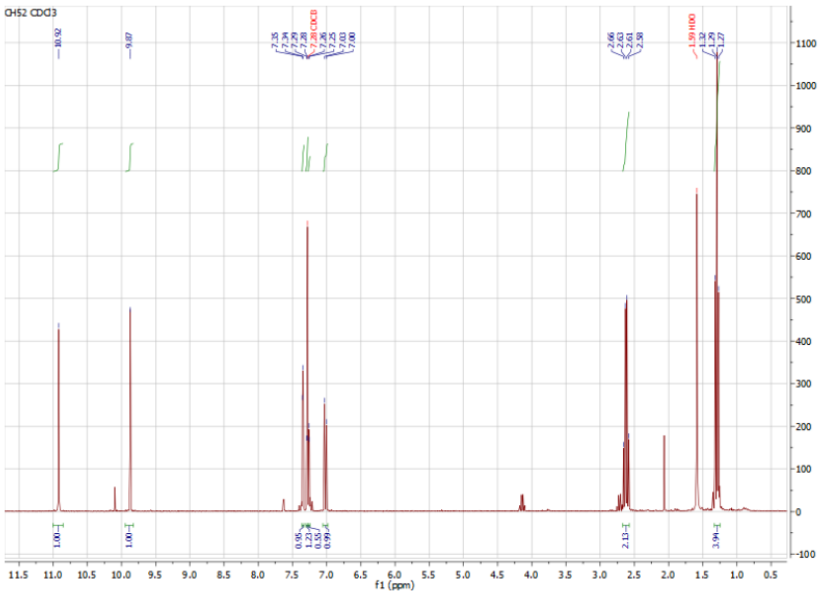

^{1}H NMR ($CDCl_3$)

Appendix 7: 5-(3-maleimidopropionic ester)-2-hydroxybenzaldehyde 40

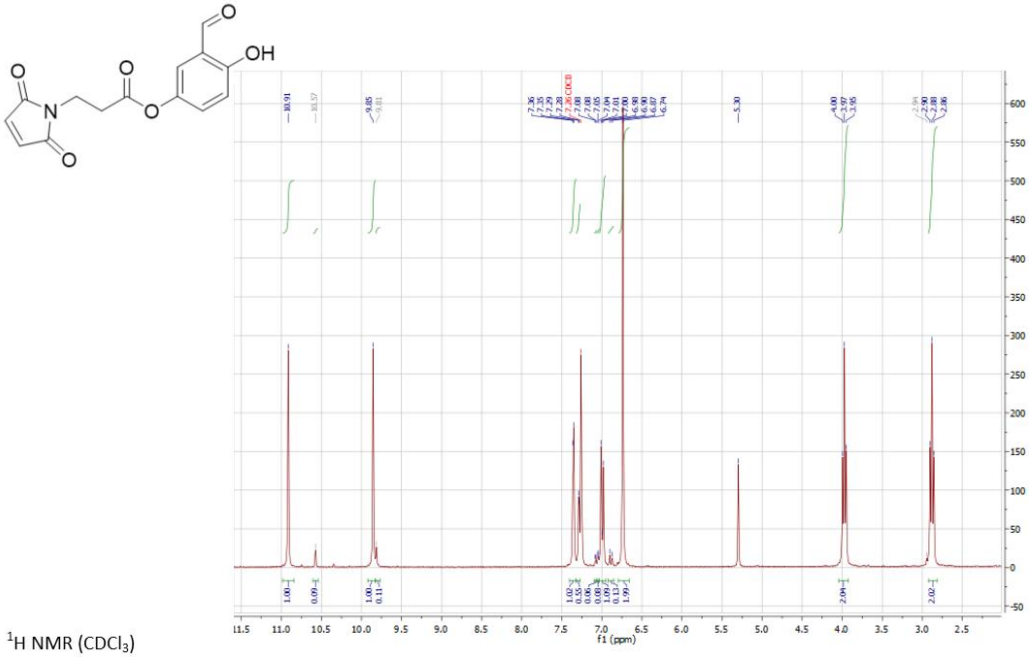

^{1}H NMR ($CDCl_3$)

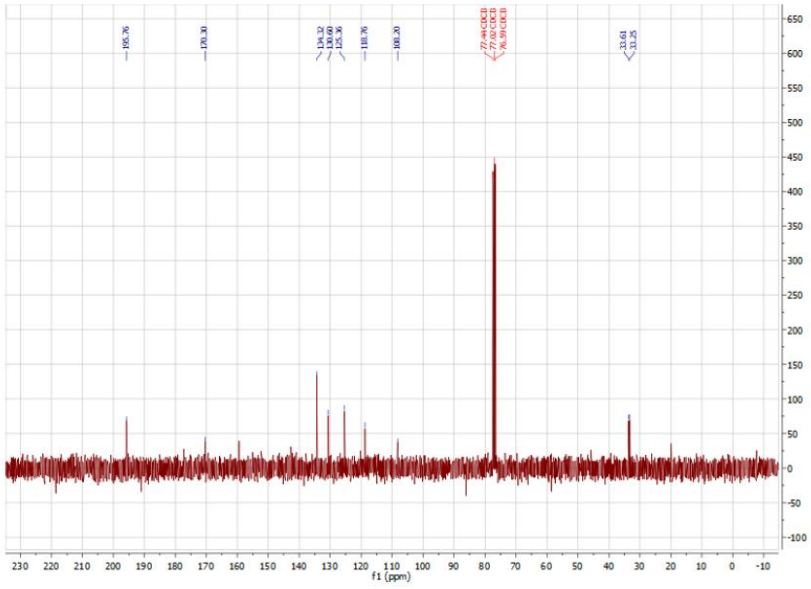

^{13}C NMR ($CDCl_3$)

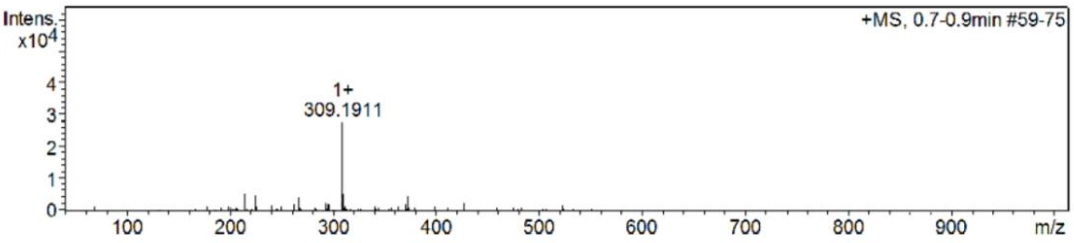

ESI-MS (in CH_3OH)

Appendix 8: *N*-(2,5-dihydroxysalicydene)-*N'*-(3,5-di-*tert*-butyl-2-hydroxysalicydene)ethylenediamine 41

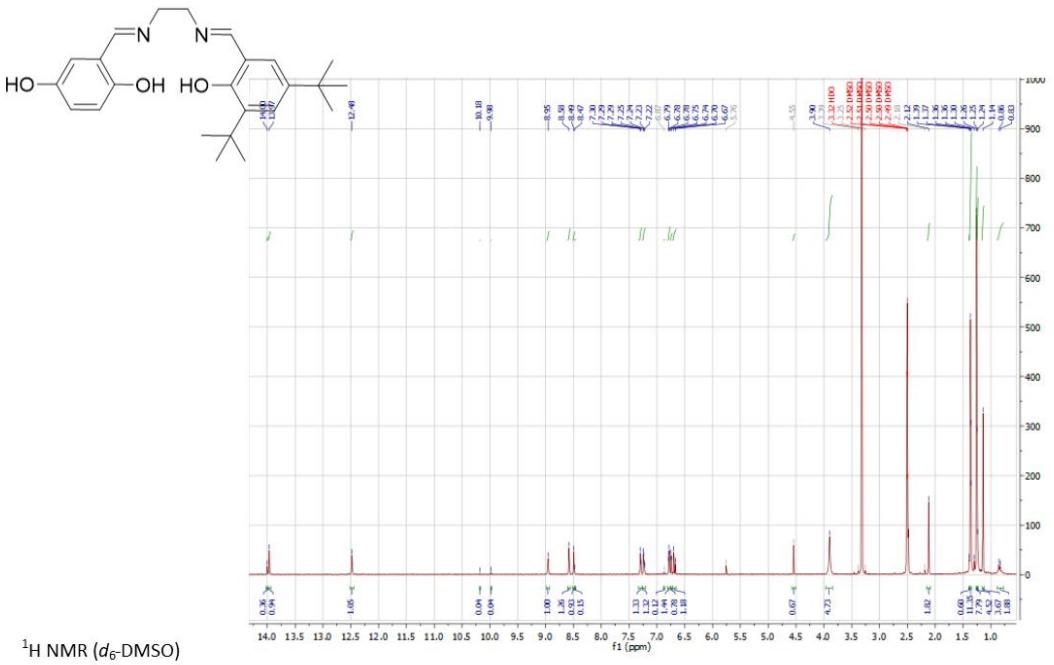

^{1}H NMR (d_6-DMSO)

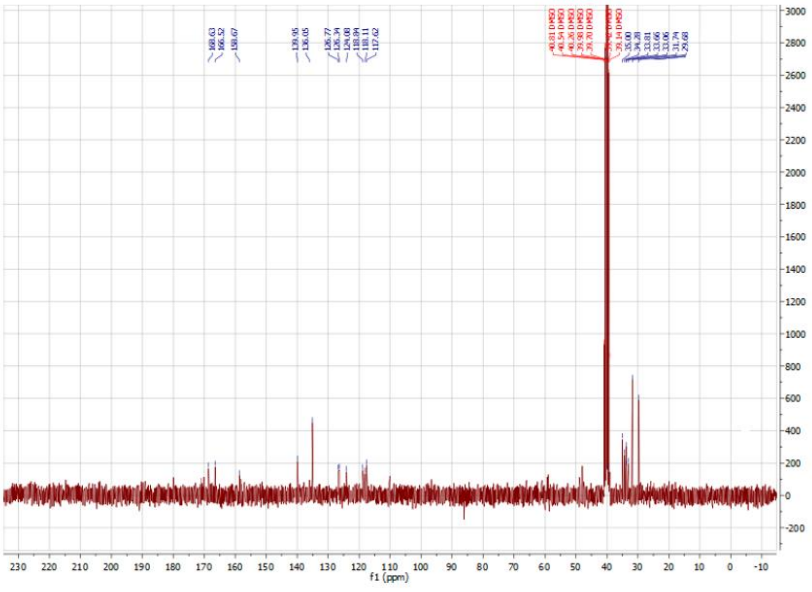

^{13}C NMR (d_6-DMSO)

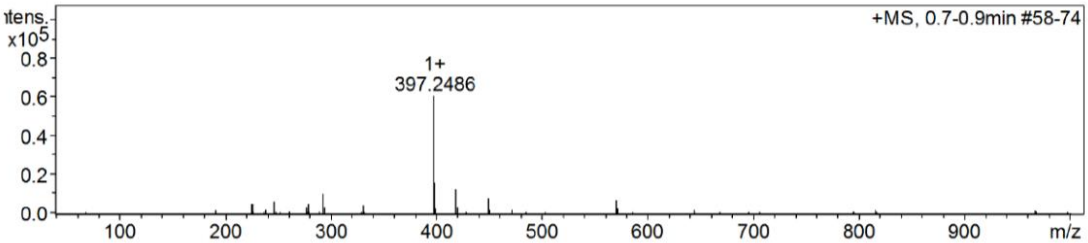

ESI-MS (in CH_3OH)

Appendix 9: *N*,*N*'-(3,5-di-*tert*-butyl-2-hydroxysalicydene)ethylenediamine 42

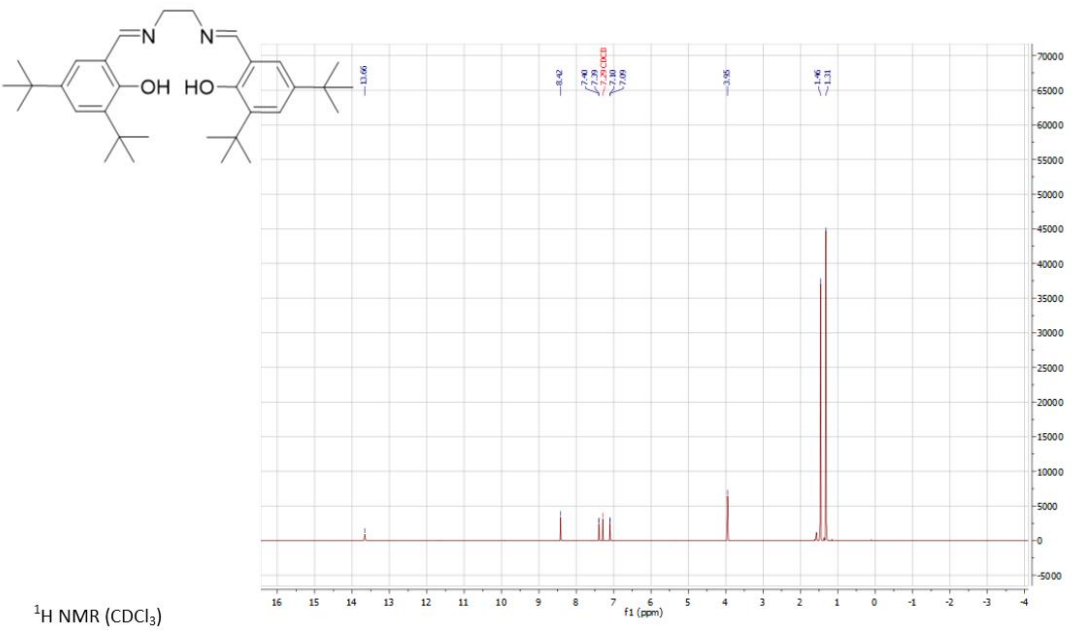

^{1}H NMR ($CDCl_3$)

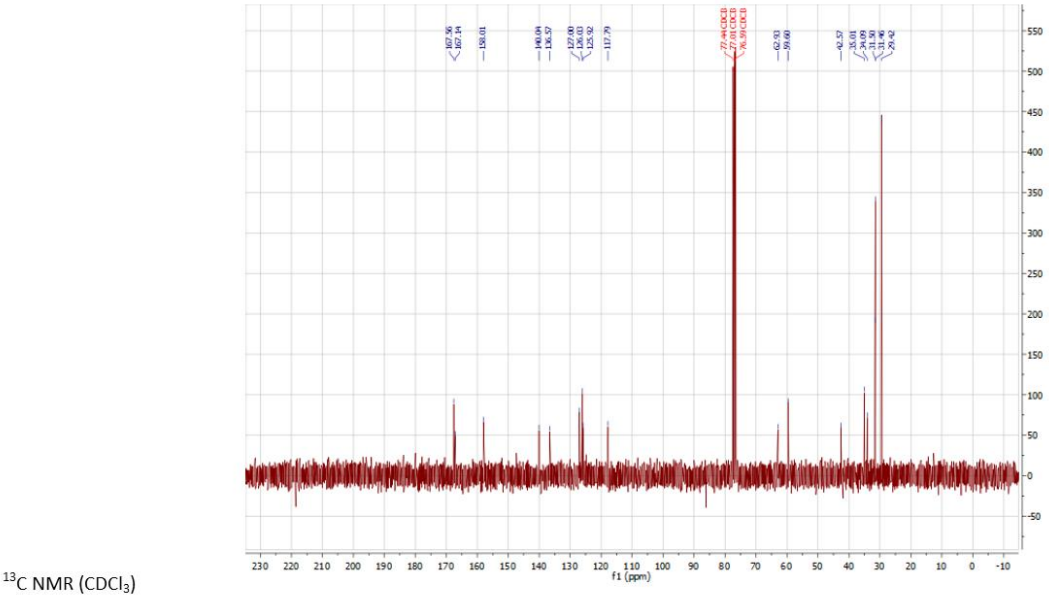

^{13}C NMR ($CDCl_3$)

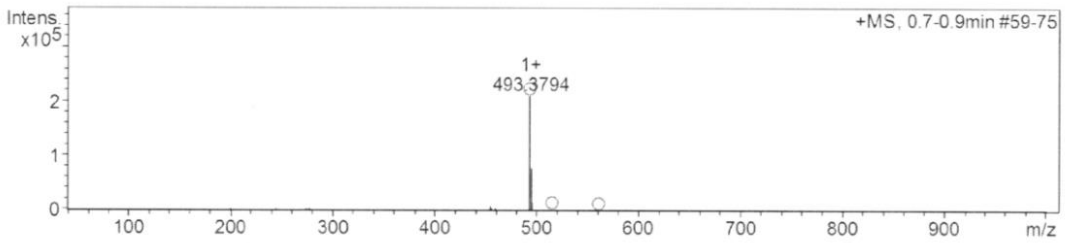

ESI-MS (in CH_3OH)

Appendix 10: *N,N'*-(3,5-di-*tert*-butyl-2-hydroxysalicydene)ethylenediamine manganese chloride 43

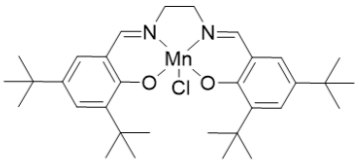

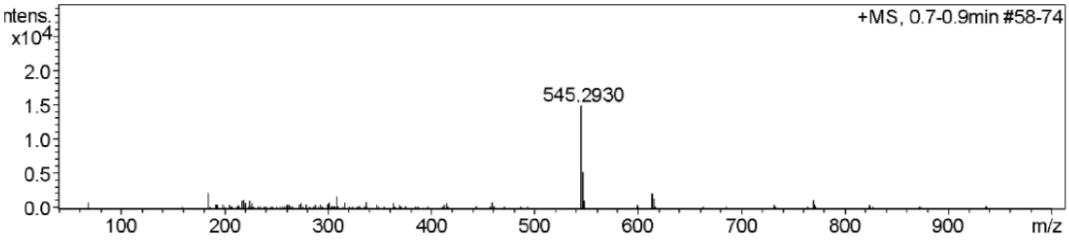

ESI-MS (in CH_3OH)

Appendix 11: *N*,*N*'-(2,5-dihydroxysalicydene)ethylenediamine 44

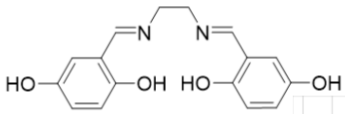

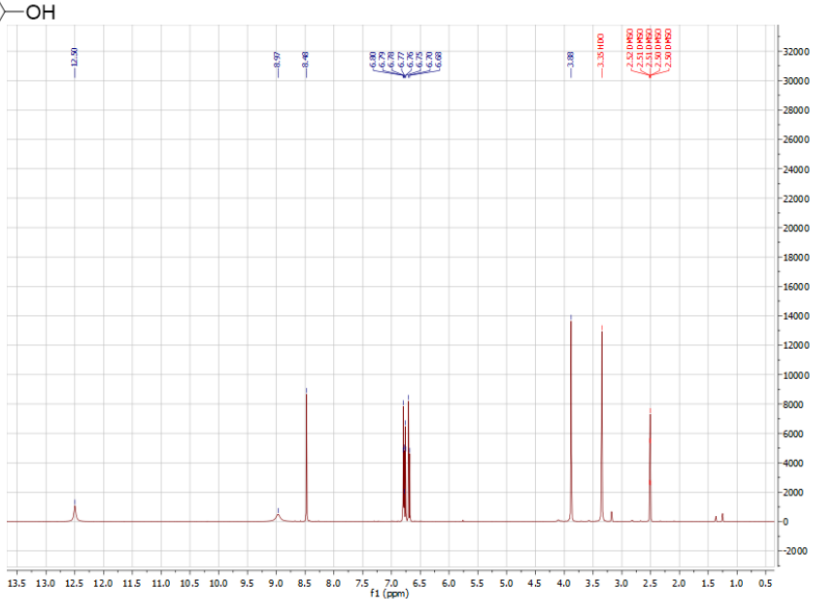

^{1}H NMR (d_6-DMSO)

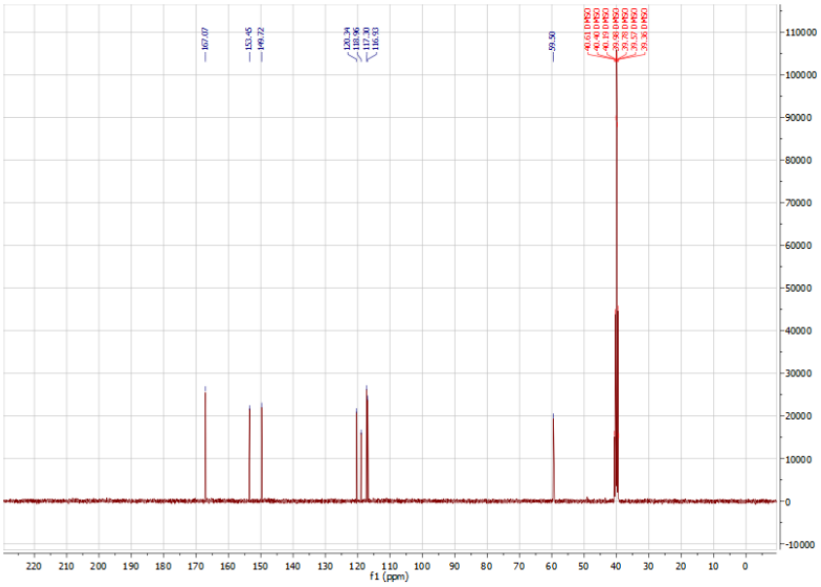

^{13}C NMR (d_6-DMSO)

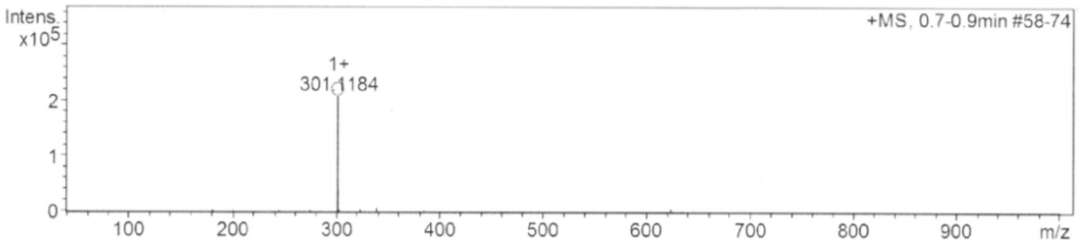

ESI-MS (in CH_3OH)

Appendix 12: *N*,*N*'-(2,5-dihydroxysalicydene)ethylenediamine manganese chloride 45

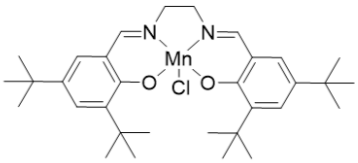

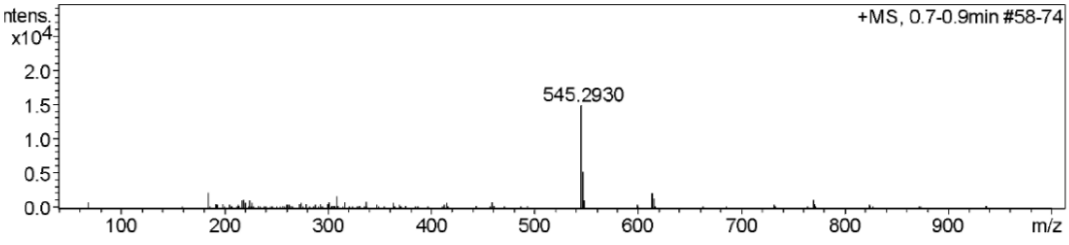

ESI-MS (in CH_3OH)

Appendix 13: *N*-(5-(3-maleimidopropionic ester)-2-hydroxysalicydene)-*N'*-(3,5-di-*tert*-butyl-2-hydroxysalicydene)ethylenediamine 46

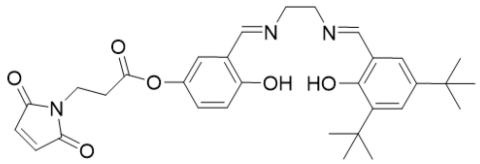

^{1}H NMR (d_6-DMSO)

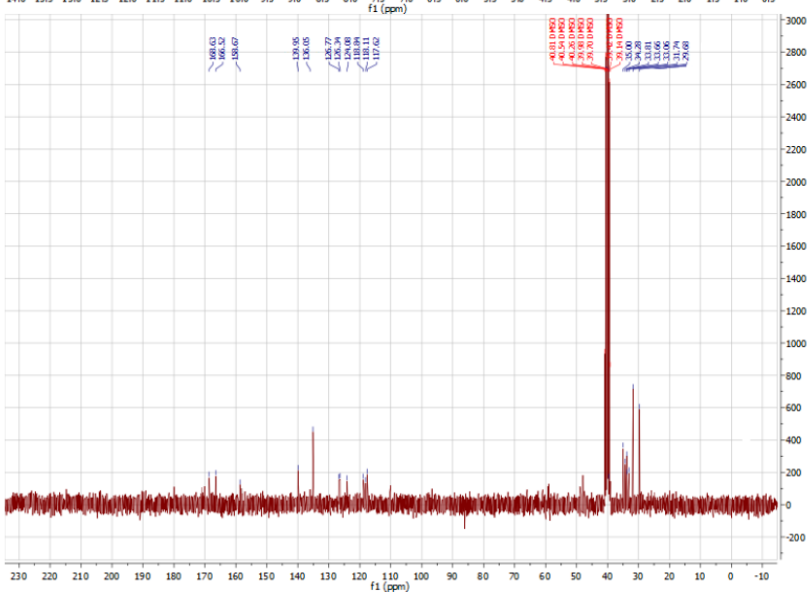

^{13}C NMR (d_6-DMSO)

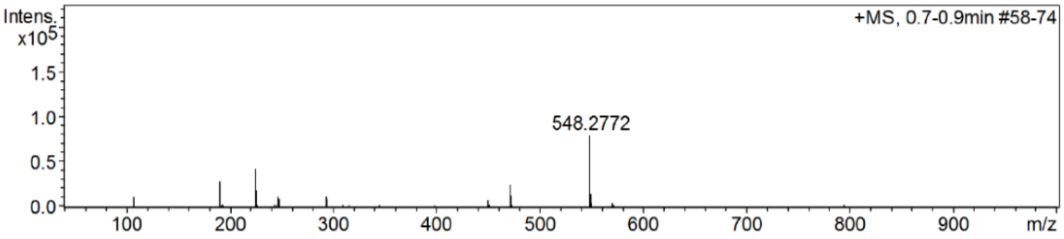

ESI-MS (in CH_3OH)

Appendix 14: *N*-(5-(3-maleimidopropionic ester)-2-hydroxysalicydene)-*N'*- (3,5-di-*tert*-butyl-2-hydroxysalicydene) ethylenediamine manganese chloride 31

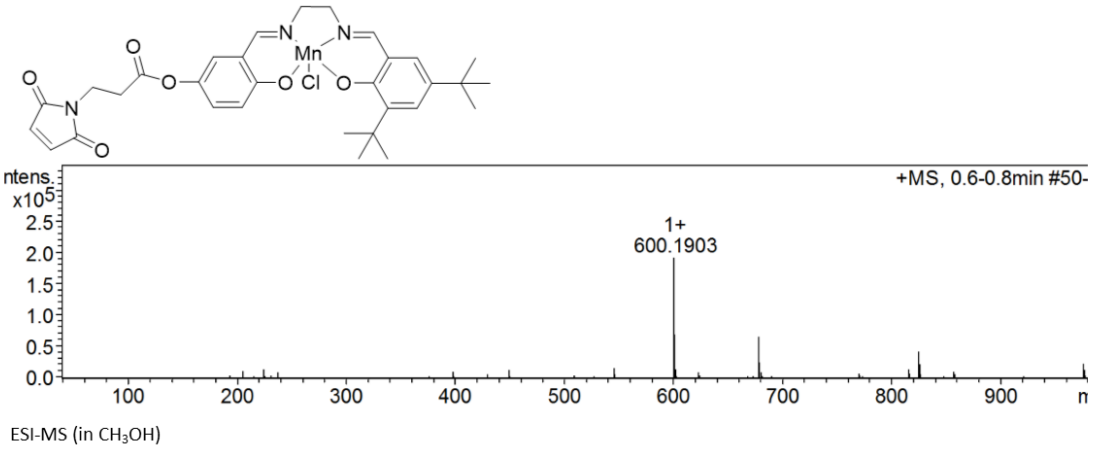

ESI-MS (in CH_3OH)

Appendix 15: Circular dichroism spectra of K68C-Aft and the conjugate

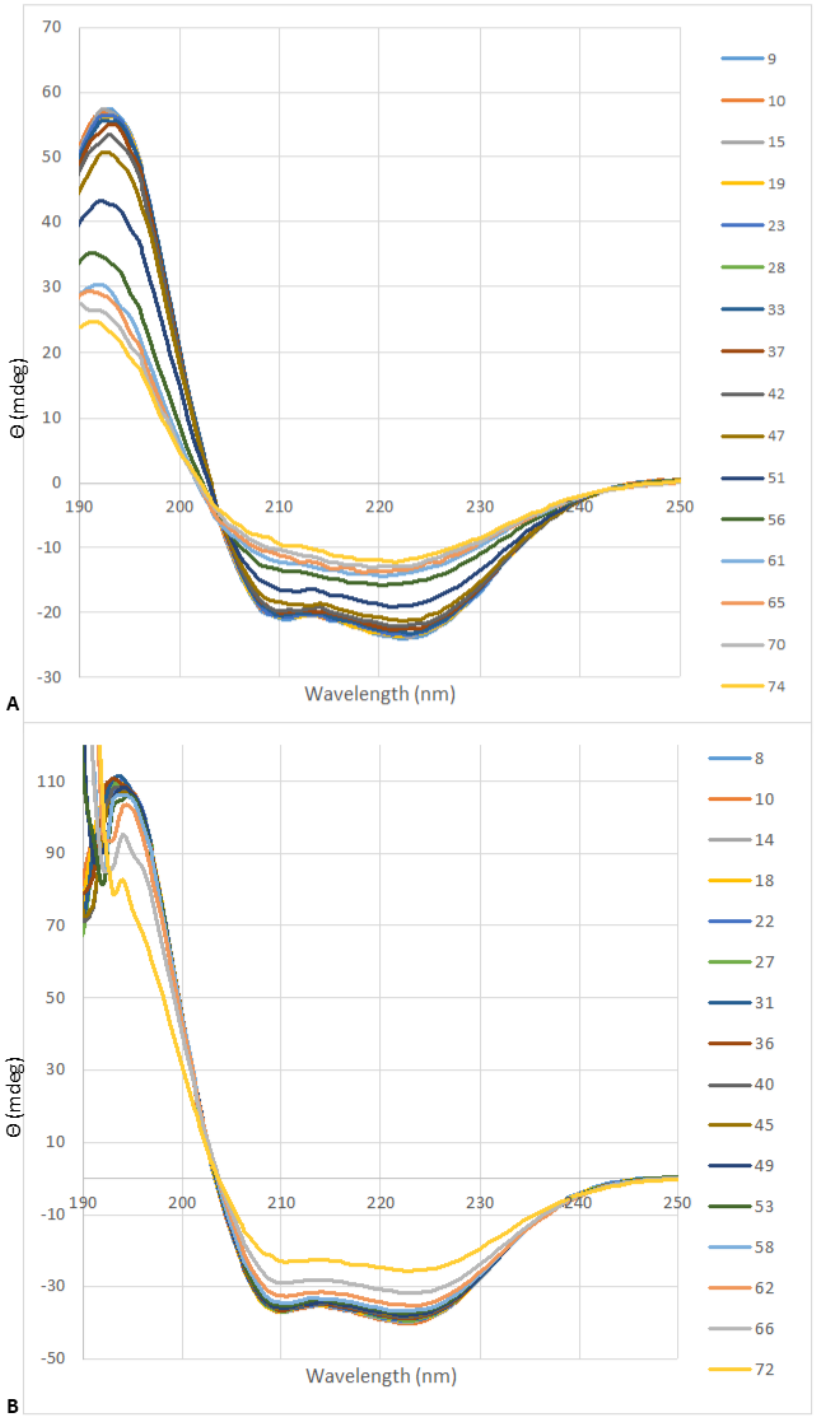

Molar ellipticity, as measured by circular dichroism analysis, of both the conjugate (**A**) and K68C-Aft (**B**) at 25 °C in a sodium phosphate buffer (50 mM, pH 3), exposed to increasing temperature from 5 to 75 °C (displayed temperatures are corrected temperatures from instrument).

Appendix 16: HPLC trace for sulfoxidation catalysis by the conjugate in urea, at pH 3

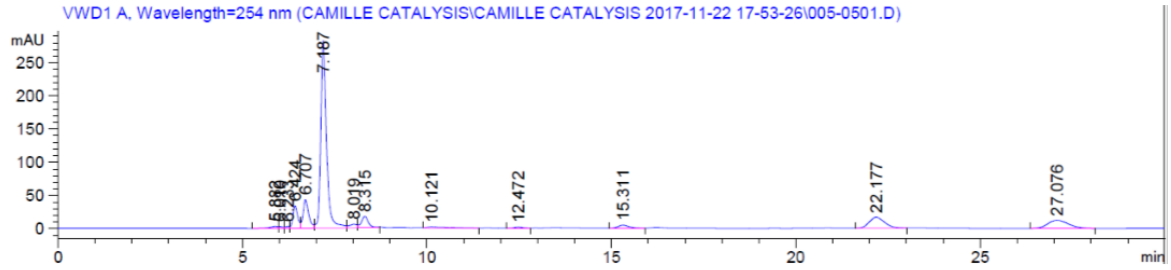

#	Time	Area	Height	Width	Area%	Symmetry	[] (mM)	Proportion %		ee (%)
8	8,315	228,6	17,1	0,1963	4,252	0,851	1,319625	57,81902		8,260101
12	22,177	477,7	16,3	0,4558	8,886	0,813	0,521117	22,83258		
13	27,076	390,4	12,4	0,6179	9,122	0,766	0,441596	19,34839		
							Conv %	42,18098		

HPLC data for the sulfoxidation of thioanisole (2.5 mM) with the conjugate (50 µM – 2 mol %) with 1 equiv. H_2O_2, in water-urea buffer, incubated for 20 h à 20 °C at pH 3. The HPLC analysis was carried on an OD-H chiral column. Peaks relative to thioanisole (8.315 min), (*R*)-phenyl methyl sulfoxide (22.177 min) and (*S*)-phenyl methyl sulfoxide (27.076 min) were observed.

Appendix 17: Notices of permission of reproduction for published material

Scheme 3: Design of peptide-based organometallic catalyst

Republished with permission of John Wiley and Sons Ltd, from Bioinspired Catalyst Design and Artificial Metaloenzymes, Deuss P. J., *et al.*, Chemistry – A European Journal, 17, 17, 2011 ; permission conveyed through Copyright Clearance Center, Inc.

Licence number: 4390941326536

Figure 4: Model encapsulation of diverse compounds of medical interest within apoferritin hollow core through pH-dependent reconstitution

Republished with permission of Future Medicine Ltd, from Apoferritin applications in nanomedicine, Heger Z., *et al.*, Nanomedicine, 9, 14, 2014; permission conveyed through Copyright Clearance Center, Inc.

Licence number: 4418171495793

Figure 5: Coordination of Pd^{II}(allyl) complex with apoferritin's residue within the protein inner cavity

Reprinted with permission from Control of the Coordination Structure of Organometallic Palladium Complexes in an apo-Ferritin Cage, Abe S., *et al.*, Journal of the American Chemical Society, 130, 32, 2008. Copyright 2008 American Chemical Society.

11. REFERENCES

[1] G. Roelfes, B. L. Feringa, *Angew Chem Int Edit* **2005**, *44*, 3230-3232.
[2] T. Masuda, F. Goto, T. Yoshihara, B. Mikami, *Biochem Biophys Res Commun* **2010**, *400*, 94-99.
[3] S. Abe, K. Hirata, T. Ueno, K. Morino, N. Shimizu, M. Yamamoto, M. Takata, E. Yashima, Y. Watanabe, *J Am Chem Soc* **2009**, *131*, 6958-+.
[4] T. Ueno, M. Suzuki, T. Goto, T. Matsumoto, K. Nagayama, Y. Watanabe, *Angew Chem Int Edit* **2004**, *43*, 2527-2530.
[5] Z. Heger, S. Skalickova, O. Zitka, V. Adam, R. Kizek, *Nanomedicine-Uk* **2014**, *9*, 2233-2245.
[6] S. Abe, J. Niemeyer, M. Abe, Y. Takezawa, T. Ueno, T. Hikage, G. Erker, Y. Watanabe, *J Am Chem Soc* **2008**, *130*, 10512-+.
[7] D. M. Lawson, P. J. Artymiuk, S. J. Yewdall, J. M. A. Smith, J. C. Livingstone, A. Treffry, A. Luzzago, S. Levi, P. Arosio, G. Cesareni, C. D. Thomas, W. V. Shaw, P. M. Harrison, *Nature* **1991**, *349*, 541-544.
[8] P. J. Deuss, R. den Heeten, W. Laan, P. C. J. Kamer, *Chem-Eur J* **2011**, *17*, 4680-4698.
[9] S. Kanbak-Aksu, M. N. Hasan, W. R. Hagen, F. Hollmann, D. Sordi, R. A. Sheldon, I. W. C. E. Arends, *Chem Commun (Cambridge, U K)* **2012**, *48*, 5745-5747.
[10] H. Gutfreund, *FEBS Lett* **1976**, *62*, E1-E12.
[11] M. Beller, C. Bolm, *Transition metal for organic synthesis*, Second edition ed., Wiley-VCH, **2004**.
[12] J. P. Taygerly, L. M. Miller, A. Yee, E. A. Peterson, *Green Chem* **2012**, *14*, 3020-3025.
[13] A. Bar-Even, E. Noor, Y. Savir, W. Liebermeister, D. Davidi, D. S. Tawfik, R. Milo, *Biochemistry* **2011**, *50*, 4402-4410.
[14] Y. Lu, N. Yeung, N. Sieracki, N. M. Marshall, *Nature* **2009**, *460*, 855-862.
[15] S. J. Benkovic, S. Hammes-Schiffer, *Science* **2003**, *301*, 1196-1202.
[16] M. R. Ringenberg, T. R. Ward, *Chem Commun (Cambridge, U K)* **2011**, *47*, 8470-8476.
[17] R. L. Shook, A. S. Borovik, *Inorg Chem* **2010**, *49*, 3646-3660.
[18] J. C. Lewis, *Acs Catal* **2013**, *3*, 2954-2975.
[19] W. J. Shaw, M. L. Helm, D. L. DuBois, *Bba-Bioenergetics* **2013**, *1827*, 1123-1139.
[20] C. K. Prier, F. H. Arnold, *J Am Chem Soc* **2015**, *137*, 13992-14006.
[21] P. W. K. Rothemund, *Nature* **2006**, *440*, 297-302.
[22] D. Coquiere, B. L. Feringa, G. Roelfes, *Angew Chem Int Edit* **2007**, *46*, 9308-9311.
[23] A. J. Boersma, B. L. Feringa, G. Roelfes, *Angew Chem Int Edit* **2009**, *48*, 3346-3348.
[24] A. J. Boersma, D. Coquiere, D. Geerdink, F. Rosati, B. L. Feringa, G. Roelfes, *Nature Chem* **2010**, *2*, 991-995.
[25] N. Duchemin, I. Heath-Apostolopoulos, M. Smietana, S. Arseniyadis, *Org Biomol Chem* **2017**, *15*, 7072-7087.
[26] M. P. Cheng, Y. H. Li, J. Zhou, G. Q. Jia, S. M. Lu, Y. Yang, C. Li, *Chem Commun (Cambridge, U K)* **2016**, *52*, 9644-9647.
[27] I. Rivilla, A. de Cozar, T. Schafer, F. J. Hernandez, A. M. Bittner, A. Eleta-Lopez, A. Aboudzadeh, J. I. Santos, J. I. Miranda, F. P. Cossio, *Chem Sci* **2017**, *8*, 7038-7046.
[28] J. Jiang, Y. Meng, L. Zhang, M. H. Liu, *J Am Chem Soc* **2016**, *138*, 15629-15635.
[29] Y. Lu, *Inorg Chem* **2006**, *45*, 9930-9940.
[30] T. Hayashi, K. Kanehira, H. Tsuchiya, M. Kumada, *J Chem Soc Chem Comm* **1982**, 1162-1164.
[31] aA. Agarkov, S. J. Greenfield, T. Ohishi, S. E. Collibee, S. R. Gilbertson, *J Org Chem* **2004**, *69*, 8077-8085; bS. R. Gilbertson, S. E. Collibee, A. Agarkov, *J Am Chem Soc* **2000**, *122*, 6522-6523; cS. R. Gilbertson, X. F. Wang, *Tetrahedron* **1999**, *55*, 11609-11618.
[32] S. T. Jung, R. Lauchli, F. H. Arnold, *Curr Opin Biotechnol* **2011**, *22*, 809-817.
[33] H. Joo, Z. L. Lin, F. H. Arnold, *Nature* **1999**, *399*, 670-673.
[34] M. W. Peters, P. Meinhold, A. Glieder, F. H. Arnold, *J Am Chem Soc* **2003**, *125*, 13442-13450.

[35] J. A. McIntosh, P. S. Coelho, C. C. Farwell, Z. J. Wang, J. C. Lewis, T. R. Brown, F. H. Arnold, *Angew Chem Int Edit* **2013**, *52*, 9309-9312.
[36] O. F. Brandenberg, R. Fasan, F. H. Arnold, *Curr Opin Biotechnol* **2017**, *47*, 102-111.
[37] P. S. Coelho, E. M. Brustad, A. Kannan, F. H. Arnold, *Science* **2013**, *339*, 307-310.
[38] P. Dydio, H. M. Key, A. Nazarenko, J. Y. Rha, V. Seyedkazemi, D. S. Clark, J. F. Hartwig, *Science* **2016**, *354*, 102-106.
[39] P. Dydio, H. M. Key, T. Hayashi, D. S. Clark, J. F. Hartwig, *J Am Chem Soc* **2017**, *139*, 1750-1753.
[40] J. Tang, P. F. Yao, X. L. Xu, H. Y. Li, F. P. Huang, Q. Q. Nie, M. Y. Luo, Q. Yu, H. D. Bian, *Rsc Adv* **2016**, *6*, 44154-44162.
[41] V. Oliveri, G. Vecchio, *Eur J Med Chem* **2011**, *46*, 961-965.
[42] J. Collot, J. Gradinaru, N. Humbert, M. Skander, A. Zocchi, T. R. Ward, *J Am Chem Soc* **2003**, *125*, 9030-9031.
[43] A. Pordea, M. Creus, J. Panek, C. Duboc, D. Mathis, M. Novic, T. R. Ward, *J Am Chem Soc* **2008**, *130*, 8085-8088.
[44] A. Pordea, D. Mathis, T. R. Ward, *J Organomet Chem* **2009**, *694*, 930-936.
[45] K. Okrasa, R. J. Kazlauskas, *Chem-Eur J* **2006**, *12*, 1587-1596.
[46] aP. Piazzetta, T. Marino, N. Russo, D. R. Salahub, *Coord Chem Rev* **2017**, *345*, 73-85; bP. Piazzetta, T. Marino, N. Russo, D. R. Salahub, *ChemCatCshem* **2017**, *9*, 1047-1053.
[47] aD. M. Upp, J. C. Lewis, *Curr Opin Chem Biol* **2017**, *37*, 48-55; bT. R. P. Ward, S.; Jeschek, M., *Trends Biotechnol* **2017**, *36*, 60-72.
[48] K. Yamamura, E. T. Kaiser, *J Chem Soc Chem Comm* **1976**, 830-831.
[49] M. Marchetti, G. Mangano, S. Paganelli, C. Botteghi, *Tetrahedron Lett* **2000**, *41*, 3717-3720.
[50] C. Bertucci, C. Botteghi, D. Giunta, M. Marchetti, S. Paganelli, *Adv Synth Catal* **2002**, *344*, 556-562.
[51] aM. E. Wilson, R. G. Nuzzo, G. M. Whitesides, *J Am Chem Soc* **1978**, *100*, 2269-2270; bM. E. Wilson, G. M. Whitesides, *J Am Chem Soc* **1978**, *100*, 306-307.
[52] A. Mahammed, H. B. Gray, J. J. Weaver, K. Sorasaenee, Z. Gross, *Bioconjugate Chem* **2004**, *15*, 738-746.
[53] A. Mahammed, Z. Gross, *J Am Chem Soc* **2005**, *127*, 2883-2887.
[54] C. A. Kruithof, H. P. Dijkstra, M. Lutz, A. L. Spek, M. R. Egmond, R. J. M. K. Gebbink, G. van Koten, *Eur J Inorg Chem* **2008**, 4425-4432.
[55] H. P. Dijkstra, H. Sprong, B. N. H. Aerts, C. A. Kruithof, M. R. Egmond, R. J. M. K. Gebbink, *Org Biomol Chem* **2008**, *6*, 523-531.
[56] C. H. B. Chen, D. S. Sigman, *Science* **1987**, *237*, 1197-1201.
[57] S. L. Traviglia, S. A. Datwyler, C. F. Meares, *Biochemistry* **1999**, *38*, 4259-4265.
[58] G. T. Hermanson, **2013**, 1-1146.
[59] J. Bos, A. Garcia-Herraiz, G. Roelfes, *Chem Sci* **2013**, *4*, 3578-3582.
[60] J. R. Carey, S. K. Ma, T. D. Pfister, D. K. Garner, H. K. Kim, J. A. Abramite, Z. L. Wang, Z. J. Guo, Y. Lu, *J Am Chem Soc* **2004**, *126*, 10812-10813.
[61] W. Laan, B. K. Munoz, R. den Heeten, P. C. J. Kamer, *ChemBioChem* **2010**, *11*, 1236-1239.
[62] L. Panella, J. Broos, J. F. Jin, M. W. Fraaije, D. B. Janssen, M. Jeronimus-Stratingh, B. L. Feringa, A. J. Minnaard, J. G. de Vries, *Chem Commun (Cambridge, U K)* **2005**, 5656-5658.
[63] J. E. Moore, W. H. Ward, *J Am Chem Soc* **1956**, *78*, 2414-2418.
[64] S. B. Gunnoo, A. Madder, *ChemBioChem* **2016**, *17*, 529-553.
[65] B. Q. Shen, K. Y. Xu, L. N. Liu, H. Raab, S. Bhakta, M. Kenrick, K. L. Parsons-Reponte, J. Tien, S. F. Yu, E. Mai, D. W. Li, J. Tibbitts, J. Baudys, O. M. Saadi, S. J. Scales, P. J. McDonald, P. E. Hass, C. Eigenbrot, T. Nguyen, W. A. Solis, R. N. Fuji, K. M. Flagella, D. Patel, S. D. Spencer, L. A. Khawlil, A. Ebens, W. L. Wong, R. Vandlen, S. Kaur, M. X. Sliwkowski, R. H. Scheller, P. Polakis, J. R. Junutula, *Nat Biotechnol* **2012**, *30*, 184-189.
[66] E. Calce, S. De Luca, *Chem-Eur J* **2017**, *23*, 224-233.

[67] G. Mantovani, F. Lecolley, L. Tao, D. M. Haddleton, J. Clerx, J. J. L. M. Cornelissen, K. Velonia, *J Am Chem Soc* **2005**, *127*, 2966-2973.
[68] I. Dovgan, S. Kolodych, O. Koniev, A. Wagner, *Sci Rep-Uk* **2016**, *6*.
[69] S. D. Fontaine, R. Reid, L. Robinson, G. W. Ashley, D. V. Santi, *Bioconjugate Chem* **2015**, *26*, 145-152.
[70] aM. T. Reetz, M. Rentzsch, A. Pletsch, M. Maywald, *Chimia* **2002**, *56*, 721-723; bM. T. Reetz, M. Rentzsch, A. Pletsch, M. Maywald, P. Maiwald, J. J. P. Peyralans, A. Maichele, Y. Fu, N. Jiao, F. Hollmann, R. Mondiere, A. Taglieber, *Tetrahedron* **2007**, *63*, 6404-6414.
[71] N. Madern, N. Queyriaux, A. Chevalley, M. Ghasemi, O. Nicolotti, I. Ciofini, G. F. Mangiatordi, M. Salmain, *J Mol Catal B-Enzym* **2015**, *122*, 314-322.
[72] C. Zhang, P. Srivastava, K. Ellis-Guardiola, J. C. Lewis, *Tetrahedron* **2014**, *70*, 4245-4249.
[73] R. den Heeten, B. K. Munoz, G. Popa, W. Laan, P. C. J. Kamer, *Dalton Trans* **2010**, *39*, 8477-8483.
[74] P. J. Deuss, G. Popa, C. H. Botting, W. Laan, P. C. J. Kamer, *Angew Chem Int Edit* **2010**, *49*, 5315-5317.
[75] U. Carmona, L. Li, L. B. Zhang, M. Knez, *Chem Commun (Cambridge, U K)* **2014**, *50*, 15358-15361.
[76] P. Santambrogio, S. Levi, P. Arosio, L. Palagi, G. Vecchio, D. M. Lawson, S. J. Yewdall, P. J. Artymiuk, P. M. Harrison, R. Jappelli, G. Cesareni, *J Biol Chem* **1992**, *267*, 14077-14083.
[77] R. Laghaei, D. G. Evans, R. D. Coalson, *Proteins* **2013**, *81*, 1042-1050.
[78] M. Gerl, R. Jaenicke, *Eur Biophys J Biophy* **1987**, *15*, 103-109.
[79] Y. Zhang, B. P. Orner, *Int J Mol Sci* **2011**, *12*, 5406-5421.
[80] F. Bou-Abdallah, G. Zhao, G. Biasiotto, M. Poli, P. Arosio, N. D. Chasteen, *J Am Chem Soc* **2008**, *130*, 17801-17811.
[81] X. K. Yang, P. Arosio, N. D. Chasteen, *Biophys J* **2000**, *78*, 2049-2059.
[82] R. K. Behera, R. Torres, T. Tosha, J. M. Bradley, C. W. Goulding, E. C. Theil, *J Biol Inorg Chem* **2015**, *20*, 957-969.
[83] I. Bertini, D. Lalli, S. Mangani, C. Pozzi, C. Rosa, E. C. Theil, P. Turano, *J Am Chem Soc* **2012**, *134*, 6169-6176.
[84] T. Tosha, H. L. Ng, O. Bhattasali, T. Alber, E. C. Theil, *J Am Chem Soc* **2010**, *132*, 14562-14569.
[85] N. D. Chasteen, P. M. Harrison, J Struc Biol **1999**, *126*, 182-194.
[86] K. K. W. Wong, H. Colfen, N. T. Whilton, T. Douglas, S. Mann, *J Inorg Biochem* **1999**, *76*, 187-195.
[87] D. Boyd, C. Vecoli, D. M. Belcher, S. K. Jain, J. W. Drysdale, *J Biol Chem* **1985**, *260*, 1755-1761.
[88] R. R. Crichton, C. F. A. Bryce, *Biochem J* **1973**, *133*, 289-299.
[89] M. Kim, Y. Rho, K. S. Jin, B. Ahn, S. Jung, H. Kim, M. Ree, *Biomacromolecules* **2011**, *12*, 1629-1640.
[90] M. A. Kilic, E. Ozlu, S. Calis, *J Biomed Nanotechnol* **2012**, *8*, 508-514.
[91] E. Simsek, M. A. Kilic, *J Magn Magn Mater* **2005**, *293*, 509-513.
[92] A. I. Kuruppu, L. Zhang, H. Collins, L. Turyanska, N. R. Thomas, T. D. Bradshaw, *Adv Healthc Mater* **2015**, *4*, 2816-2821.
[93] Z. Yang, X. Y. Wang, H. J. Diao, J. F. Zhang, H. Y. Li, H. Z. Sun, Z. J. Guo, *Chem Commun (Cambridge, U K)* **2007**, 3453-3455.
[94] E. Falvo, E. Tremante, A. Arcovito, M. Papi, N. Elad, A. Boffi, V. Morea, G. Conti, G. Toffoli, G. Fracasso, P. Giacomini, P. Ceci, *Biomacromolecules* **2016**, *17*, 514-522.
[95] Z. P. Zhen, W. Tang, H. M. Chen, X. Lin, T. Todd, G. Wang, T. Cowger, X. Y. Chen, J. Xie, *ACS Nano* **2013**, *7*, 4830-4837.
[96] Z. J. Chen, M. F. Zhai, X. Y. Xie, Y. Zhang, S. Y. Ma, Z. P. Li, F. L. Yu, B. Q. Zhao, M. Zhang, Y. Yang, X. G. Mei, *Mol Pharm* **2017**, *14*, 3087-3097.
[97] L. Li, C. J. Fang, J. C. Ryan, E. C. Niemi, J. A. Lebron, P. J. Bjorkman, H. Arase, F. M. Torti, S. V. Torti, M. C. Nakamura, W. E. Seaman, *Proc Natl Acad Sci U S A* **2010**, *107*, 3505-3510.

[98] J. Y. Li, N. Paragas, R. M. Ned, A. D. Qiu, M. Viltard, T. Leete, I. R. Drexler, X. Chen, S. Sanna-Cherchi, F. Mohammed, D. Williams, C. S. Lin, K. M. Schmidt-Ott, N. C. Andrews, J. Barasch, *Dev Cell* **2009**, *16*, 35-46.
[99] S. Dostalova, T. Cerna, D. Hynek, Z. Koudelkova, T. Vaculovic, P. Kopel, J. Hrabeta, Z. Heger, M. Vaculovicova, T. Eckschlager, M. Stiborova, V. Adam, *ACS Appl Mater Interfaces* **2016**, *8*, 14430-14441.
[100] M. Uchida, M. L. Flenniken, M. Allen, D. A. Willits, B. E. Crowley, S. Brumfield, A. F. Willis, L. Jackiw, M. Jutila, M. J. Young, T. Douglas, *J Am Chem Soc* **2006**, *128*, 16626-16633.
[101] I. Blazkova, H. V. Nguyen, S. Dostalova, P. Kopel, M. Stanisavljevic, M. Vaculovicova, M. Stiborova, T. Eckschlager, R. Kizek, V. Adam, *Int J Mol Sci* **2013**, *14*, 13391-13402.
[102] L. Turyanska, T. D. Bradshaw, J. Sharpe, M. Li, S. Mann, N. R. Thomas, A. Patane, *Small* **2009**, *5*, 1738-1741.
[103] G. Tosi, D. Belletti, F. Pederzoli, B. Ruozi, *Expert Opin Drug Del* **2016**, *13*, 1341-1343.
[104] aS. Aime, L. Frullano, S. G. Crich, *Angew Chem Int Edit* **2002**, *41*, 1017-+; bP. Sanchez, E. Valero, N. Galvez, J. M. Dominguez-Vera, M. Marinone, G. Poletti, M. Corti, A. Lascialfari, *Dalton Trans* **2009**, 800-804.
[105] A. Makino, H. Harada, T. Okada, H. Kimura, H. Amano, H. Saji, M. Hiraoka, S. Kimura, *Nanomed-Nanotechnol* **2011**, *7*, 638-646.
[106] S. G. Crich, J. C. Cutrin, S. Lanzardo, L. Conti, F. K. Kalman, I. Szabo, N. R. Lago, A. Iolascon, S. Aime, *Contrast Media Mol Imaging* **2012**, *7*, 281-288.
[107] I. Szabo, S. G. Crich, D. Alberti, F. K. Kalman, S. Aime, *Chem Commun (Cambridge, U K)* **2012**, *48*, 2436-2438.
[108] B. Hennequin, L. Turyanska, T. Ben, A. M. Beltran, S. I. Molina, M. Li, S. Mann, A. Patane, N. R. Thomas, *Adv Mater (Weinheim, Ger)* **2008**, *20*, 3592-+.
[109] L. Turyanska, T. D. Bradshaw, M. Li, P. Bardelang, W. C. Drewe, M. W. Fay, S. Mann, A. Patane, N. R. Thomas, *J Mater Chem* **2012**, *22*, 660-665.
[110] S. E. Kim, K. Y. Ahn, J. S. Park, K. R. Kim, K. E. Lee, S. S. Han, J. Lee, *Anal Chem* **2011**, *83*, 5834-5843.
[111] G. D. Liu, J. Wang, S. A. Lea, Y. H. Lin, *ChemBioChem* **2006**, *7*, 1315-1319.
[112] G. D. Liu, J. Wang, H. Wu, Y. Y. Lin, Y. H. Lin, *Electroanalysis* **2007**, *19*, 777-785.
[113] Y. Y. Zhang, Z. W. Tang, J. Wang, H. Wu, C. T. Lin, Y. H. Lin, *J Mater Chem* **2011**, *21*, 17468-17475.
[114] P. Liang, C. Y. Kang, E. J. Yang, X. X. Ge, D. Du, Y. H. Lin, *Analyst* **2016**, *141*, 2278-2283.
[115] M. Aubailly, R. Santus, S. Salmon, *Photochem Photobiol* **1991**, *54*, 769-773.
[116] aD. Ensign, M. Young, T. Douglas, *Inorg Chem* **2004**, *43*, 3441-3446; bI. Kim, H. A. Hosein, D. R. Strongin, T. Douglas, *Chem Mater* **2002**, *14*, 4874-4879.
[117] aS. D. Erickson, T. J. Smith, L. M. Moses, R. K. Watt, J. S. Colton, *Nanotechnology* **2015**, *26*; bR. K. Watt, O. D. Petrucci, T. Smith, *Catal Sci Technol* **2013**, *3*, 3103-3110.
[118] B. Maity, K. Fujita, T. Ueno, *Curr Opin Chem Biol* **2015**, *25*, 88-97.
[119] M. Suzuki, M. Abe, T. Ueno, S. Abe, T. Goto, Y. Toda, T. Akita, Y. Yamadae, Y. Watanabe, *Chem Commun (Cambridge, U K)* **2009**, 4871-4873.
[120] W. Zhang, X. Y. Liu, D. Walsh, S. Y. Yao, Y. Kou, D. Ma, *Small* **2012**, *8*, 2948-2953.
[121] S. Abe, T. Hikage, Y. Watanabe, S. Kitagawa, T. Ueno, *Inorg Chem* **2010**, *49*, 6967-6973.
[122] Z. Y. Wang, Y. Takezawa, H. Aoyagi, S. Abe, T. Hikage, Y. Watanabe, S. Kitagawa, T. Ueno, *Chem Commun (Cambridge, U K)* **2011**, *47*, 170-172.
[123] S. Datta, Y. Mori, K. Takagi, K. Kawaguchi, Z. W. Chen, T. Okajima, S. Kuroda, T. Ikeda, K. Kano, K. Tanizawa, F. S. Mathews, *Proc Natl Acad Sci U S A* **2001**, *98*, 14268-14273.
[124] K. Nakajima, K. Kondo, T. Nakane, S. Abe, T. Nakao, Y. Watanabe, T. Ueno, *Chem Commun (Cambridge, U K)* **2015**, *51*, 16609-16612.
[125] S. Abe, B. Maity, T. Ueno, *Chem Commun (Cambridge, U K)* **2016**, *52*, 6496-6512.
[126] G. E. O'Mahony, A. Ford, A. R. Maguire, *J Sulfur Chem* **2013**, *34*, 301-341.

[127] J. Legros, J. R. Dehli, C. Bolm, *Adv Synth Catal* **2005**, *347*, 19-31.
[128] aP. Pitchen, E. Dunach, M. N. Deshmukh, H. B. Kagan, *J Am Chem Soc* **1984**, *106*, 8188-8193; bP. Pitchen, H. B. Kagan, *Tetrahedron Lett* **1984**, *25*, 1049-1052.
[129] N. Komatsu, Y. Nishibayashi, T. Sugita, S. Uemura, *Tetrahedron Lett* **1992**, *33*, 5391-5394.
[130] aL. J. P. Martyn, S. Pandiaraju, A. K. Yudin, *J Organomet Chem* **2000**, *603*, 98-104; bA. K. Yudin, L. J. P. Martyn, S. Pandiaraju, J. Zheng, A. Lough, *Org Lett* **2000**, *2*, 41-44.
[131] C. Bolm, O. A. G. Dabard, *Synlett* **1999**, 360-362.
[132] D. W. Zhang, K. Jamieson, L. Guy, G. H. Gao, J. P. Dutasta, A. Martinez, *Chem Sci* **2017**, *8*, 789-794.
[133] D. Gamenara, G. Seoane, P. Saenz Mendez, P. Dominguez de Maria, *Redox biocatalysis: fundamentals and applications, Vol. 1*, John Wiley & sons, **2012**.
[134] R. A. Sheldon, *Metalloporphyrins in catalytic oxidations*, CRC Press, **1994**.
[135] E. Baciocchi, M. F. Gerini, A. Lapi, *J Org Chem* **2004**, *69*, 3586-3589.
[136] M. K. Stern, J. T. Groves, *J Am Chem Soc* **1987**, *109*, 3812-3814.
[137] C. L. Hill, B. C. Schardt, *J Am Chem Soc* **1980**, *102*, 6374-6375.
[138] J. T. Groves, W. J. Kruper, R. C. Haushalter, *J Am Chem Soc* **1980**, *102*, 6375-6377.
[139] H. Srour, J. Jalkh, P. Le Maux, S. Chevance, M. Kobeissi, G. Simonneaux, *J Mol Cat A-Chem* **2013**, *370*, 75-79.
[140] P. Le Maux, G. Simonneaux, *Chem Commun (Cambridge, U K)* **2011**, *47*, 6957-6959.
[141] K. P. Bryliakov, E. P. Talsi, *J Mol Cat A-Chem* **2007**, *264*, 280-287.
[142] aK. Nakajima, M. Kojima, J. Fujita, *Chem Lett* **1986**, 1483-1486; bK. Nakajima, M. Kojima, K. Toriumi, K. Saito, J. Fujita, *Bull Chem Soc Jpn* **1989**, *62*, 760-767.
[143] C. Bolm, F. Bienewald, K. Harms, *Synlett* **1996**, 775-&.
[144] C. Bolm, F. Bienewald, *Synlett* **1998**, 1327-1328.
[145] aD. A. Cogan, G. C. Liu, K. J. Kim, B. J. Backes, J. A. Ellman, *J Am Chem Soc* **1998**, *120*, 8011-8019; bG. C. Liu, D. A. Cogan, J. A. Ellman, *J Am Chem Soc* **1997**, *119*, 9913-9914.
[146] A. P. Gao, M. Wang, D. P. Wang, L. Zhang, H. B. Liu, W. Tian, L. C. Sun, *Chinese J Catal* **2006**, *27*, 743-748.
[147] C. Drago, L. Caggiano, R. F. W. Jackson, *Angew Chem Int Edit* **2005**, *44*, 7221-7223.
[148] W. Zhang, E. N. Jacobsen, *J Org Chem* **1991**, *56*, 2296-2298.
[149] E. N. Jacobsen, W. Zhang, A. R. Muci, J. R. Ecker, L. Deng, *J Am Chem Soc* **1991**, *113*, 7063-7064.
[150] R. Irie, T. Uchida, K. Matsumoto, *Chem Lett* **2015**, *44*, 1268-1283.
[151] aN. Hosoya, A. Hatayama, R. Irie, H. Sasaki, T. Katsuki, *Tetrahedron* **1994**, *50*, 4311-4322; bH. Sasaki, R. Irie, T. Hamada, K. Suzuki, T. Katsuki, *Tetrahedron* **1994**, *50*, 11827-11838; cH. Sasaki, R. Irie, T. Katsuki, *Synlett* **1994**, 356-358.
[152] H. Tanaka, H. Nishikawa, T. Uchida, T. Katsuki, *J Am Chem Soc* **2010**, *132*, 12034-12041.
[153] S. Koya, Y. Nishioka, H. Mizoguchi, T. Uchida, T. Katsuki, *Angew Chem Int Edit* **2012**, *51*, 8243-8246.
[154] M. Palucki, P. Hanson, E. N. Jacobsen, *Tetrahedron Lett* **1992**, *33*, 7111-7114.
[155] K. Noda, N. Hosoya, K. Yanai, R. Irie, T. Katsuki, *Tetrahedron Lett* **1994**, *35*, 1887-1890.
[156] C. Kokubo, T. Katsuki, *Tetrahedron* **1996**, *52*, 13895-13900.
[157] K. P. Bryliakov, E. P. Talsi, *Eur J Org Chem* **2008**, 3369-3376.
[158] aB. Saito, T. Katsuki, *Tetrahedron Lett* **2001**, *42*, 3873-3876; bB. Saito, T. Katsuki, *Tetrahedron Lett* **2001**, *42*, 8333-8336.
[159] T. Katsuki, *Chem Soc Rev* **2004**, *33*, 437-444.
[160] J. T. Sun, C. J. Zhu, Z. Y. Dai, M. H. Yang, Y. Pan, H. W. Hu, *J Org Chem* **2004**, *69*, 8500-8503.
[161] aL. Duan, F. Bozoglian, S. Mandal, B. Stewart, T. Privalov, A. Llobet, L. Sun, *Nature Chem* **2012**, *4*, 418-423; bS. Barnett, K. Goldberf, J. Mayer, *Nature Chem* **2012**, *4*, 498-502.
[162] H. Egami, T. Katsuki, *J Am Chem Soc* **2007**, *129*, 8940-+.
[163] D. Chakraborty, P. Malik, V. K. Goda, *Appl Organomet Chem* **2012**, *26*, 21-26.

[164] E. Baciocchi, M. F. Gerini, O. Lanzalunga, A. Lapi, M. G. Lo Piparo, *Org Biomol Chem* **2003**, *1*, 422-426.
[165] P. Le Maux, H. Srour, G. Simonneaux, *Tetrahedron* **2012**, *68*, 5824-5828.
[166] I. Nicolas, P. Le Maux, G. Simonneaux, *Tetrahedron Lett* **2008**, *49*, 5893-5795.
[167] Q. Ren, S. Chen, X. Zhou, H. Ji, *Bioorg Med Chem* **2010**, *18*, 8144-8149.
[168] T. Hashihayata, T. Punniyamurthy, R. Irie, T. Katsuki, T. Akita, Y. Moro-oka, *Tetrahedron* **1999**, *55*, 14599-14610.
[169] J. A. Miller, B. A. Gross, M. A. Zhuravel, W. Jin, S. T. Nguyen, *Angew Chem Int Ed* **2005**, *44*, 3885-3889.
[170] P. Subramaniam, T. Vanitha, T. Kodispathi, C. R. S. Sundari, *J Mex Chem Soc* **2014**, *58*, 211-217.
[171] A. Chellamani, N. I. Alhaji, S. Rajagopal, *J Phys Org Chem* **2007**, *20*, 255-263.
[172] Y. Watanabe, A. Namba, N. Umezawa, M. Kawahata, K. Yamaguchi, T. Higuchi, *Chem Commun (Cambridge, U K)* **2006**, 4958-4960.
[173] aM. Ohashi, T. Koshiyama, T. Ueno, M. Yanase, H. Fujii, Y. Watanabe, *Angew Chem Int Edit* **2003**, *42*, 1005-+; bT. Ueno, T. Koshiyama, M. Ohashi, M. Kono, T. Yamane, Y. Watanabe, *Journal of Inorganic Biochemistry* **2003**, *96*, 243-243.
[174] aT. Koshiyama, T. Ueno, M. Ohashi, K. Kondo, M. Kono, A. Suzuki, T. Yamane, Y. Watanabe, *Abstr Pap Am Chem Soc* **2005**, *229*, U1047-U1047; bT. Ueno, T. Koshiyama, M. Ohashi, K. Kondo, M. Kono, A. Suzuki, T. Yamane, Y. Watanabe, *J Am Chem Soc* **2005**, *127*, 6556-6562.
[175] D. K. Garner, L. Liang, D. A. Barrios, J. L. Zhang, Y. Lu, *Acs Catal* **2011**, *1*, 1083-1089.
[176] D. C. M. Albanese, N. Gaggero, *Rsc Adv* **2015**, *5*, 10588-10598.
[177] P. Rousselot-Pailley, C. Bochot, C. Marchi-Delapierre, A. Jorge-Robin, L. Martin, J. C. Fontecilla-Camps, C. Cavazza, S. Menage, *ChemBioChem* **2009**, *10*, 545-552.
[178] M. Cherrier, E. Girgenti, P. Amara, M. Iannello, C. Marchi-Delapierre, J. C. Fontecilla-Camps, S. Menage, C. Cavazza, *J Biol Inorg Chem* **2012**, *17*, 817-829.
[179] C. Esmieu, M. Cherrier, P. Amara, E. Girgenti, C. Marchi-Delapierre, F. Oddon, M. Iannello, A. Jorge-Robin, C. Cavazza, S. Menage, *Angew Chem Int Ed* **2013**, *52*, 3922-3925.
[180] L. Rondot, E. Girgenti, F. Oddon, C. Marchi-Delapierre, A. Jorge-Robin, S. Menage, *J Mol Cat A-Chem* **2016**, *416*, 20-28.
[181] C. Vigier-Carriere, T. Garnier, D. Wagner, P. Lavalle, M. Rabineau, J. Hemmerle, B. Senger, P. Schaaf, F. Boulmedais, L. Jierry, *Angew Chem Int Edit* **2015**, *54*, 10198-10201.
[182] V. T. Kasumov, F. Koksal, *Spectrochimica Acta Part A* **2005**, *61*, 225-231.
[183] A. E. Frost, H. H. Freedman, *J Org Chem* **1959**, *24*, 1905-1907.
[184] L. Zhang, University of Nottingham **2016**.
[185] P. W. Riddles, R. L. Blakeley, B. Zerner, *Methods Enzymol* **1983**, *91*, 49-60.
[186] G. Legler, C. M. Mullerplatz, M. Mentgeshettkamp, G. Pflieger, E. Julich, *Anal Biochem* **1985**, *150*, 278-287.
[187] aY. G. Kim, S. O. Ho, N. R. Gassman, Y. Korlann, E. V. Landorf, F. R. Collart, S. Weiss, *Bioconjugate Chem* **2008**, *19*, 786-791; bM. Henkel, N. Rockendorf, A. Frey, *Bioconjugate Chem* **2016**, *27*, 2260-2265.
[188] D. W. L., (Ed.: S. C. DeLano Scientific, CA, 700), **2002**.
[189] F. Frottin, A. Martinez, P. Peynot, S. Mitra, R. C. Holz, C. Giglione, T. Meinnel, *Mol Cell Proteomics* **2006**, *5*, 2336-2349.
[190] T. Kantner, A. G. Watts, *Bioconjugate Chem* **2016**, *27*, 2400-2406.
[191] J. T. Chin, S. L. Wheeler, A. M. Klibanov, *Biotechnol Bioeng* **1994**, *44*, 140-145.